STUDIES ON POST-SYNTHETIC TREATMENTS OF MICRO- AND MESOPOROUS ZEOLITES:

IMPACT ON THEIR PHYSICOCHEMICAL AND CATALYTIC PROPERTIES

MARÍA J. ORTIZ INIESTA

This work was financially supported by The Netherlands Organisation for Scientific Research (NWO) under the VIDI Project No. 10284.

The work described in this thesis was conducted at the Department of Chemical Engineering, ENTEG, Faculty of Mathematics and Natural Sciences, University of Groningen, The Netherlands.

Cover and layout:  Lovebird design.
www.lovebird-design.com

Printed by: Eikon +

ISBN: 978-90-367-8890-8

ISBN e-book: 978-90-367-8889-2

This thesis is also available in electronic format at: **http://dissertations.rug.nl/**

university of groningen

Studies on post-synthetic treatments of micro- and mesoporous zeolites:

Impact on their physicochemical and catalytic properties

PhD thesis

to obtain the degree of PhD at the
University of Groningen
on the authority of the
Rector Magnificus Prof. E. Sterken
and in accordance with
the decision by the College of Deans

This thesis will be defended in public on

Friday 16 september 2016 at 11.00

By

María J. Ortiz Iniesta

born on 28 March 1985
in Cuenca, Spain

Supervisor

Prof. H.J. Heeres

Co-Supervisor

Dr. P.P. Pescarmona

Assessment committee

Prof. F. Picchioni

Prof. K. Seshan

Prof. D. Murzin

Dedicated to my family and Juan

TABLE OF CONTENTS

1

Introduction

ABSTRACT

Zeolites have a large number of applications and this makes them extensively studied materials. The challenge nowadays is the fine tuning of properties for a specific application by synthetic modifications, either during synthesis or by post synthesis treatments.

1.1. INTRODUCTION TO ZEOLITES: FROM NATURAL TO SYNTHETIC MATERIALS.

Already in 1756, the Swedish mineralogist Cronstedt coined the term zeolite, from the greek *Zeo* "to boil" and *lithos* "a stone", referring to the property of the material to liberate steam from its structure when heated. However, many years passed until the first synthetic preparation of zeolites, reported by Barrer *et al.* in the 1940s. Since then, the field experienced a rapid expansion and this has resulted in the synthesis of 229 structural types of zeolites, with 16 new structures discovered in 2014-2015 (updated on July 2015, IZA [1]). Along that, a wide range of techniques has been developed to characterise zeolites. In addition, relevant properties have been determined and novel applications have been identified and commercialised.

What is a zeolite? Zeolites are crystalline porous solids based on tetrahedral silicate units (SiO_4^{4-}), in which each oxygen atom is shared by two units. However, by far in the most zeolites, part of the Si atoms are replaced by Al atoms. Porous solids are defined as solids with cavities or channels that are deeper than their width. Typically, the tetrahedral units in zeolites are coupled in such a way that a 3D network is formed with pore/cage dimensions between 0.3 and 2.0 nm, which is in the molecular size range. As such, zeolites were classified as molecular sieves in the past by McBain in 1932 [67]. Zeolite cage dimensions are at the microporosity level (< 2 nm according to the IUPAC), which can lead to diffusional limitations. To overcome this potential issue, many investigations have focussed on the synthesis of zeolites with larger pores, and the addition of hierarchical or disordered meso- and macroporosity [2-12].

In terms of atomic substitution, elements such as Be, Ti, V, Cr, Mn, Fe, Co, Cu, Zn, B, Ga, P have been used instead or together with Si and Al to obtain novel structures. Materials with a zeolite type structure but without Si and Al are known as zeotypes. Zeotypes form structures with bond distances, angles and coordination modes that are impossible for regular zeolites. A simplified classification of porous solids is represented in Figure 1.

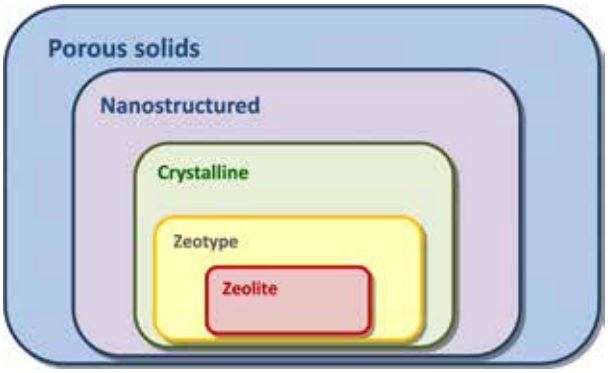

Figure 1. Classification of porous solids. Adapted from Coronas *et al.* (2010) [13].

Aluminium substitution in the silica framework confers an overall negative charge to the structure (Si^{4+} versus Al^{3+}), which has to be compensated with counter-cations linked to O atoms located in the pore voids. When these counter-cations are protons (H^{+}), Brønsted acidity is developed. In some cases, zeolites are also able to host neutral molecules, provided that these are small enough to fit in the cavities. A simplified empirical formula for a zeolite is $M^{n+}_{x/n}Al_xSi_{1-x}O_2.yX$, where x can vary from 0 to 0.5; X is a neutral guest molecules; and represents the counter-cations. The counter-cations can both be inorganic or organic. As-synthesised zeolites usually contain alkali, alkali earth metal or alkyl-ammonium cations. After post-synthesis modifications they can be exchanged to protons or to almost any desired inorganic cations. This property makes that zeolites have the potential to function as adsorbents and ion-exchangers, which during the early stages of their discovery was their main use [14]. Proton exchanged zeolites are strong Brønsted acids with a wide range of (catalytic) applications.

Within the field of porous materials, mesoporous materials, hierarchical systems, metal-organic frameworks (MOFs) and mesoporous organosilicas have been introduced in the last decades. These advanced materials have substantially increased the variety of porous materials and have shown interesting properties and extended the application ranges of porous materials.

1.1.1. WHY ARE ZEOLITES ATTRACTIVE FOR CATALYSIS?

Zeolites have a wide application range. A particularly interesting field is the use of zeolites as catalysts. Actually, zeolites constitute a large portion of the solid catalysts used to date in industry and citing A. Corma: *"Among the heterogeneous catalysts it is safe to say that zeolites are the most widely used materials"* [15,16]. Particularly in the petro-chemical industry and oil refining, zeolites have found widespread applications [17-22]. Recently, zeolites have also been introduced in emerging areas such catalytic biomass conversions, pollution abatement, energy saving devices and sensors [23].

The successful introduction of zeolites in the catalysis arena was due to a number of favourable properties such as [5,24]:

- High stability, translated as slow changes in the material structure in time. Here thermal (during catalyst preparation, in operation, reaction hot-spots); hydrothermal (steam, liquid water); and mechanical stability (low level of attrition) are of relevance.
- Favourable ion-exchange and sorption capacity.
- Shape selective character, in this respect reactant, product, spatio--transition state, and adsorption selectivity are of relevance.
- High catalytic activity, mostly due to the presence of acidic sites. This is favoured to achieve high space time yields for catalytic reactions, and allows for either small reactors or the use of milder operating conditions (e.g. temperature), the latter favouring exothermic equilibrium conversions.
- Potential to act as host for advanced catalysts, and as such act as a microreactor.

1.2. ZEOLITE SYNTHESIS

The first approaches to prepare synthetic zeolites (1845 to 1937) were inspired by nature. Natural zeolites are typically formed by hydrothermal

conversions. The synthesis of some silicates was claimed, however, characterisation was cumbersome at that time and limited to chemical analysis and visual observations. It was not until the 1940s, when R.M. Barrer introduced X-Ray diffraction and used this technique to optimise the conditions to make synthetic zeolites [22]. The procedure involved mixing of minerals and treatment of this mixture under hydrothermal conditions (ca. 170-270 °C). Later, solutions of Si and Al precursors were used for the synthesis [25]. At the same time, Breck, Milton, Kerr and Flaningen pioneered the large scale synthesis and commercial application of zeolites [26]. These activities led to several publications and patents including the discovery of the first two synthetic zeolites, Linde A [27,28] and Linde X (Si/Al=1.0-1.5) [29]. Both zeolites contain new framework structures known as LTA and FAU, respectively. Later, a FAU zeolite with a higher silica content (Si/Al = 1.5-3.0) was synthesised and named as Linde Y [29]. Since the 1980s, a large number of novel zeolites have been synthesised and characterised. This is illustrated by the number of zeolites contained in the various editions of the "Atlas of zeolite structure types" (IZA) [30]. In the first edition (1978) 38 structural types were collected; 64 in the second (1987); 85 in the third (1992) and 176 in the latest (2007). Nowadays, 229 structural types of zeolites have been discovered.

1.2.1. SYNTHETIC PROCEDURES

Synthetic procedures for zeolite synthesis can be divided into two main categories, depending on whether the reaction medium is a liquid or a solid.

For solvent assisted synthesis, solvothermal, hydrothermal and ionothermal approaches are considered. Solvothermal synthesis includes the use of an (organic) solvent [31]. The presence of a solvent during the synthesis reduces the risk of diffusion limitations. Water, by definition, is the solvent for hydrothermal synthesis. This approach is the most commonly used and will be discussed separately (*vide infra*). Ionothermal synthesis involves the

use of ionic liquids (ILs) as solvent, which have favourable properties like a low vapour pressure (and as such, autogenous pressure at high temperature is very low) [32-36]. There are many examples in the literature where ILs are used as reaction medium for the synthesis of inorganic materials [37,38]. Cejka and co-workers were pioneers in the use of ILs as both the solvent and structure directing agent (SDA) [32]. Eutectic mixtures were explored as well, giving similar results as ILs [39] with the benefit of their low cost and biodegradability compared with ILs [32].

Solvothermal non-aqueous zeolite synthesis takes place in the presence of solvents other than water and examples include organic solvents and liquid ammonia [31]. In these systems the solvent can act as a heat transfer agent, a solvent for the reagents or play an active role in the formation of the zeolite structure. The latter is more relevant and occurs to a larger extent when the polarity of the solvent is high, for instance when using a pyridine-HF complex in the presence of stoichiometric amounts of water as the solvent [40,41].

Solid-state synthesis requires typically higher temperatures than liquid phase synthesis. As such, the chances to obtain thermodynamically favoured phases in solid state synthesis is high. This may lead to interesting new zeolites. For instance, the TPA-containing ZSM-5 (5563 Å, 17.6 T/1000 $Å^3$) may be converted to ZSM-11 (5187 Å, 17.9 T/1000 $Å^3$) under very high pressures [42]. In some cases, amorphous materials may be formed [43,44].

1.2.2. HYDROTHERMAL SYNTHESIS

The most common way to synthesise zeolitic materials involves a hydrothermal treatment at relatively low temperatures (100-200 °C) using water as the solvent. Typically the following steps in the preparation procedure can be distinguished [13,45-47]:

1) The amorphous reactants containing the metal ions (Si, Al, P, Ga, Zn, etc.) are mixed, usually in a basic medium, though an acidic

media can be used as well. Upon mixing, a heterogeneous, partly reacted phase is formed, known as the "primary amorphous phase". The nature of this amorphous phase ranges from gel–like to colloidal.

2) Transfer of the reaction mixture to a sealed autoclave and heating of the reaction mixture (above 100 °C) at autogenic pressure (Figure 2). In some cases, this step is preceded by an aging period (from hours to few days).
3) Subsequently, a "secondary amorphous phase" at pseudo-equilibrium with a solution phase is formed. There is evidence that this phase possesses some ordering due to a structuring effect of the cations in the solution.
4) After an ''induction period'', nuclei are formed, the first step to crystalline zeolite formation.
5) Gradually, the amorphous phase is consumed at the expense of zeolite growth.
6) Finally, the crystals are collected by filtration, washed and dried.

During the formation of the crystalline zeolite, the amorphous precursors react in the presence of an alkali metal hydroxides (known as mineralisers) to form Si-O-Al bonds. This process is about energy neutral based on the strong similarities in bonds in the reactants (Si-O and Al-O) and the products (Si-O-Al). The first approaches for zeolite synthesis involved the use of inorganic bases. Later, organic bases were introduced and allowed for better tunability of the structure.

1.2.2.1. MECHANISTIC ASPECTS

A large number of mechanisms have been proposed for the transformation of the amorphous into the crystalline zeolite phase during hydrothermal synthesis. Here the most representative ones will be highlighted. Barrer *et al.*, 1959 [48] proposed a mechanism where secondary building units in the form

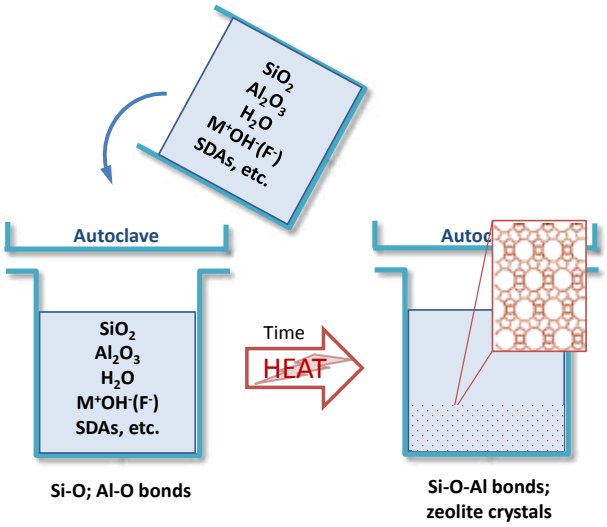

Figure 2. Schematic representation of hydrothermal zeolite synthesis [45].

of tetrahedral or polyhedral rings are formed. Later, he stated that "a plausible process would be the accretion in simple coordination of polygonal or polyhedral anions by condensation polymerisation", giving for instance 4-ring, 6-ring, cube and hexagonal prisms.

In the 1960s, Breck and Flanigen [49] reported an XRD study where they followed the crystallisation process of Na-A and Na-X zeolite over time (at 50 and 100 °C). The profiles are indicative for an induction period followed by a sudden rapid growth. They concluded that the latter was due to the predominant growth of the crystal in the solid state.

In a later review [50], Breck described the zeolite formation mechanism as follows: "the gel structure is depolymerised by hydroxide ions; rearrangement of the aluminosilicate and silicate anions present in the hydrous gel is brought about by the hydrated cation species present; tetrahedra re-group about hydrated sodium ions form the basic polyhedral units (24-hedra) and these then link to form the massive, ordered crystal structure of the zeolite". More specific information about the growth mechanisms can be found in the literature [45].

1.2.2.2. MINERALISERS

As discussed above, conventional zeolite synthesis is performed in highly basic media to assist the mineralisation of silicate and aluminate species. The bases are known as *mineralisers*, the most common ones are alkali metal hydroxides. Their role is to induce the formation of Si-O-Al bonds. A specific concentration of hydroxide ions has to be present, higher or lower concentrations can lead to the solution or precipitation of the zeolite/reactants. Recently, some studies reported that proper control of the OH^- concentration allows for the synthesis of new zeolite structures [51].

Besides hydroxides, fluorides are also effective mineralisers for the synthesis of zeolites and phosphate materials [52]. Fluoride was shown to improve the overall stability of zeolite crystals by decreasing the number of defects. Some examples of materials synthesised in fluorhydric media are cloverite (CLO) [53,54], LTA [55], and ULM [56].

1.2.2.3. ORGANIC STRUCTURE DIRECTING AGENTS

Prior to the 1980s, inorganic cations like Na^+ and K^+ were used as structure directing agents (SDAs). Many industrially relevant zeolites were discovered using these SDAs, examples are zeolites A, X (FAU) and Y (FAU), mordenite (MOR), ferrierite (FER), zeolites L (LTA) and P (KFI), chabazite and Rho. These zeolites are excellent ion exchangers, which is related to the synthetic procedure. Due to the high Al content in the structure, a high amount of counter cations have to be hosted in the zeolite framework to balance the framework charge.

Limitations regarding the synthesis of Si rich zeolites and structural variation in channel dimensions have inspired the scientific community to find alternative SDA molecules. It was found that organic molecules may be used as replacements for inorganic cations like Na^+ and K^+. In the 1980s Barrer *et al.* reported the preparation of zeolites using organic amines

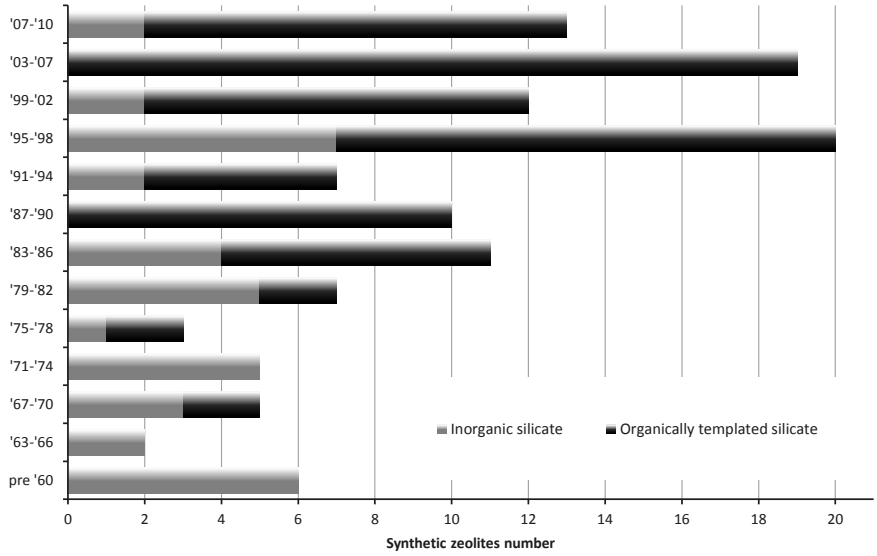

Figure 3. Evolution of the use of organic and inorganic SDAs as a function of time [26].

as SDAs (also known as templates) to obtain zeolites with a high-silica content [57]. The introduction of SDAs has led to discovery of many new zeolites [38,51,58-61]. Examples are ZSM-5 (MFI), ZSM-11 (MEL), Beta (BEA) and alumina-phosphates [1,20,62-64]. Actually, most novel synthetic zeolites prepared the last 2 decades were synthesised using organic templates (Figure 3).

The most commonly used templates are amines and organic quaternary ammonium cations. Like inorganic bases, they are used during synthesis to balance the charge and adjust the pH of the reaction media [45]. However, the organic bases may also be used to tune the pore size and pore size distribution and as such may lead to novel structures with unique properties [62].

Due to the interaction of the organic bases with the zeolite framework, the template is still present in the pores after the zeolite synthesis. The template has to be removed to give the zeolite the desired properties.

1.3. POST-SYNTHESIS TREATMENTS AND MODIFICATIONS

Zeolite properties can be tuned towards the desired (catalytic) application by i) modifications during synthesis and ii) post-synthesis treatments. Synthetic modifications are possible, see previous paragraph for details [1,65-66]. However, when the direct synthesis fails to meet the target properties, modifications by post-synthesis modifications are also feasible [68]. Examples are ion exchange, solid-ion exchange, template removal (when organic SDAs are used during synthesis), metal addition, dealumination/desilication, and the introduction of intra- and extra framework atoms. In the following paragraphs, the main post-treatment procedures are introduced and discussed.

1.3.1. ION EXCHANGE

Ion exchange is an important process for post-synthesis modification of microporous materials to tailor (adsorbents and catalytic) properties. Ion exchange involves substitution of the alkaline counter cations in the zeolites by protons or desired metals, such as Mg^{2+}, Ca^{2+}, La^{3+} or Al^{3+} followed by thermal dehydration [69]. Actually, the ion-exchange capacity of microporous materials, especially of LTA- and P-type zeolites, is the basis for their worldwide application as detergent builders [70]. The exchange reaction is conveniently carried out by the addition of a solution containing the desired cation to the template-free zeolite. Another example involves the exchange with metal cations (e.g. Ni^{2+}, Ru^{3+}). After metal reduction by e.g. hydrogen, zeolites with metal nanoclusters are obtained and these have interesting catalytic properties [24].

When the H-form of the zeolite is desired, the as-synthesised zeolite is first detemplated, commonly by calcination, followed by a mild acidic wash. This combination is highly detrimental for Al rich zeolites, resulting in collapse and dealumination of the structure [70]. Barrer proposed a milder

alternative involving an exchange reaction of the Na^+/K^+ cation by NH_4^+, e.g. by treatment of the zeolite with NH_4NO_3 (Figure 4) [71]. A simplified approach, excluding the initial thermal treatment to reduce thermal stress and energy costs, was proposed by our group [72] and this approach will be discussed in detail in Chapter 2.

An alternative approach involves solid-ion exchange. It involves heating up a mixture of a finely powdered zeolite and metal oxide in a reductive or inert atmosphere at relatively high temperatures (around 800 K).

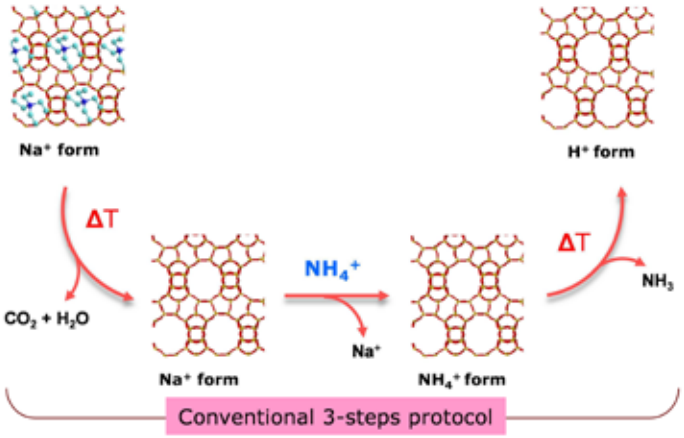

Figure 4. Example of an ion exchange protocol for zeolites [71].

1.3.2. TEMPLATE REMOVAL

For various applications, the removal of the organic templates like alkyl ammonium compounds, amines, alkylphosphonium salts and phosphazenes is essential to open the final porous network (Figure 5) [38,51,58-61].

Template removal strategies can be divided in destructive (thermal and chemical) and non-destructive methods. Advantages and disadvantages for each method are given in Table 1.

Calcination is the most commonly applied detemplating method. It is a destructive method involving heating of the zeolite sample after

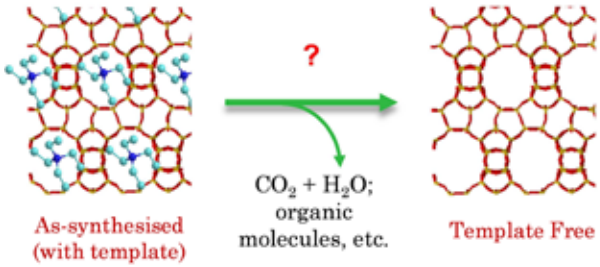

Figure 5. Conceptual representation of organic template removal (BEA as example).

Table 1. Advantages and disadvantages of established detemplation methodologies.

Methods		Advantages	Disadvantages
Destructive			
Thermal (Calcination)		• Creation of specific active sites. • Easy method. • Cheap equipment.	• Reduced crystallinity. • Framework dealumination; reduction in number of Brønsted acid sites. • Special-compositions structures often collapse. • Nanocrystals and ultra-fine zeolites particles: Difficult regeneration due to low thermal and hydrothermal stability.
Chemical	Conventional oxidants	• Preservation of structural-textural integrity.	• Relatively high temperatures are required. • Materials can be hydrolysed. • Hardly applied to microporous materials.
	Fenton detemplation	• Preservation of structural-textural integrity. • Applicable for microchannels. • Use of $OH^{\bullet}$ radicals (small size and high oxidation potential, 2.8 eV). • Full template removal.	• Sample-sensitive, has to be optimised for each material. • Some structures have limited hydrothermal stability.
Non-destructive			
Strategies aiming at **template recovery** (mainly by solvent extraction)		• Template reuse.	• Diffusional limitations in microporous materials. • Strong interactions template-host. • Nearly limited to mesoporous materials.

synthesis and drying in the presence of oxygen at temperatures ranging from 500 up to 650 °C [19,20]. It is a highly exothermal process, resulting in structural damage for sensitive zeolites (special-composition and/or zeolites with crystal sizes below 1 mm).

Mechanistic aspects of the thermal calcination of silicalite-1, silico/alumino-phosphates and heteroatom-containing zeolites have been studied in detail. It is now generally accepted that the decomposition mechanism is based on Hofmann and subsequent radical reactions [73,74]. It was found that the rate of template decomposition strongly depends on the SiO_2/Al_2O_3 ratio [75] and the presence of heteroatoms (Fe or Ti) [76]. For alumino-phosphates and SAPO, template removal is difficult due to the presence of small, 1D channels [77,78]. More severe calcination conditions may lead to structural damage. Therefore, control of the calcination treatment (e.g. atmosphere, heating rate, temperature, time) is of paramount importance to obtain the desired zeolite structure [75,78-80]. An example of the importance of atmospheric control is the calcination of beta zeolite. During calcination, water is formed and the Al-O bonds can be easily hydrolysed [81-83]. The longer distance of the Al-O bond compared to the Si-O reduces the stability of the zeolite framework, especially at high Al-content.

In many cases, the organic template is the most expensive compound used in zeolite synthesis. As such, there is an incentive to recover and reuse the template after zeolite synthesis. Solvent extraction is the most common strategy to recover the template. Davis *et al.* reported that successful extraction is limited to cases where the template has a smaller size than the pore opening of the zeolite. In addition, the interactions of the template with the zeolite framework should be weak. When the latter is not the case, strong diffusional limitations are observed, reducing template recovery efficiencies [84]. As such, solvent extraction is mainly limited to mesoporous materials.

Template recovery by solvent extraction is often far from quantitative and decomposition/fragmentation of the template has been observed (e.g. for SBA-15) [85]. Both factors limit the recyclability of the recovered template. The most efficient extraction approach reported so far [84,86]

involves the use of strong acidic conditions. However, this method seems to have limited applicability. For instance, Jones *et al.* reported that successful extraction is only possible for the recovery of tetra-ethylammonium ions from zeolite beta [84].

Chemical detemplating procedures involve reaction of the template with a chemical reagent under mild conditions, often aimed to reduce the size of the template, facilitating removal from the pores. The most commonly used strategies are i) an ammonia-assisted calcination at 250 ºC to remove tetramethyl ammonium cations [87], ii) the use of acidified solvents (e.g. methanolic HCl [88]), iii) the use of oxidising agents such as ozone [89,90], iv) cold plasma [91], v) ultraviolet irradiation [92], vi) ultraviolet/ozone [93] and vii) hydrogen peroxide. The latter is often employed in combination with a metal catalyst like Fe^{III}/Fe^{II} salts. In this case, the method is known as Fenton detemplation [94-97] and has been applied successfully for both micro- and mesoporous materials [98-103].

1.3.2.A. FENTON DETEMPLATION

Fenton chemistry is widely used for the treatment of waste water and contaminated soils [104-109]. OH radicals, generated by a series of redox reactions between H_2O_2 and Fe^{III}/Fe^{II} ions (eqs 1-2) have a high oxidation potential (2.8 eV) [105] and are capable to oxidise organics, for instance the template in various zeolites [110].

Fenton chemistry involves the decomposition reaction of H_2O_2 in the presence of Fe^{II} to generate hydroxyl radicals ($OH^{\bullet}$), eq. 1; then, the reduction of Fe^{III} with H_2O_2 regenerates Fe^{II} cations (eq. 2) and the cycle is closed:

$$H_2O_2 + Fe^{2+} \rightarrow OH^{\bullet} + OH^{-} + Fe^{3+} \qquad (1)$$

$$H_2O_2 + Fe^{3+} \rightarrow HO_2^{\bullet} + H^{+} + Fe^{2+} \qquad (2)$$

The hydroxyl radical reacts with organic compounds with bimolecular rate constants as high as 10^7 to 10^{10} L/(mol·s) [104-106,111]. The chemistry is non-selective and a large number of reactions have been proposed eq (3-9):

$$RH + OH^{\bullet} \rightarrow H_2O + R^{\bullet} \quad (3)$$

$$OH^{\bullet} + Fe^{2+} \rightarrow OH^{-} + Fe^{3+} \quad (4)$$

$$R^{\bullet} + Fe^{3+} \rightarrow Fe^{2+} + products \quad (5)$$

$$R^{\bullet} + OH^{\bullet} \rightarrow ROH \quad (6)$$

$$R^{\bullet} + H_2O_2 \rightarrow ROH + OH^{\bullet} \quad (7)$$

$$HO_2^{\bullet} + Fe^{3+} \rightarrow O_2 + Fe^{2+} + H^{+} \quad (8)$$

$$OH^{\bullet} + H_2O_2 \rightarrow HO_2^{\bullet} + H_2O \quad (9)$$

In these equations RH represents the substrate to be oxidised, $R^{\bullet}$ is an organic radical (derived from the RH substrate) and $HO_2^{\bullet}$ is a superoxide radical. The rate constant of the equations 2, 5 and 8 are known to be pH dependent [112].

Fenton detemplation was successfully demonstrated for the first time for a microporous material (Beta zeolite) by Melián-Cabrera *et al.* [113]. More recently, the approach was extended to a soft MCM-41 [97] and SBA-15 [114]. Other examples are template removal from mesoporous silicates and aluminosilicates [115,116], RUB-18 [117], aluminophosphates [118,119], silicalite-1 colloids, and organic light emitting diodes (OLED) [120]. The simultaneous detemplation and metal introduction has been reported as well [23,68,121]. A simplified route without the need for a Fe catalyst has been successfully applied for mesoporous silicates such as MCM-56 [122], regeneration of Al-doped ZSM-5 membranes [123], and silicoalumina phosphates (SAPO-34) [119].

Other possibilities to generate $OH^{\bullet}$ radicals from H_2O_2 are based on the use of UV light e.g. to detemplate SBA-15 [98], and the use of microwave irradiation for nano-beta particles [124] and AlPO-5 [125]. An overview of Fenton and Fenton-like detemplation studies are summarised in Table 2. The Table is organised in a chronological order.

Table 2. Summary of Fenton and Fenton-like detemplation studies based on ref. [95].

	Material	Template[a]	H_2O_2 utilisation	Fenton? Y/N
1	Beta zeolite	TEA^+	30 wt.% H_2O_2	Y
2	Mesoporous aluminosilicate	CTA^+	5 mL H_2O + 50 mL (30 wt.% H_2O_2) dropwise for 0.6 g solid	Y
3	SBA-15	P123	60 mL (2 wt.% H_2O_2)/0.6 g solid	N
4	Na-RUB-18 mesophase (silicate)	CTA^+	5 mL H_2O + 50 mL (30 wt.% H_2O_2) dropwise for 0.6 g solid	Y
5	MCM-56	HMI	5 mL(30 wt.% H_2O_2)/g solid	N
6	Mesoporous silica nanoparticles (MCM-41) & colloidal mesoporous silica (CMS)	CTA^+ &TEOS	4 mL H_2O_2 (30 wt.% H_2O_2)/0.2 g solid	Y
7	AlPO-5	TEA^+	25 mL (30 wt.% H_2O_2) + dropwise Fe^{2+}/H_2O_2 solution for 0.5 g solid	Y
8	SBA-15 & MSU-H	-	-	-
9	Al-doped ZSM-5 membranes	Toluene (regeneration)	15 wt.% H_2O_2 solution	N
10	Organic light emitting diodes (OLED)	TEA^+	Equal to entry 1	Y
11	Nano beta	TEA^+	50 mL (35 wt.% H_2O_2), 2 times	Y
12	Mesoporous silica nanoparticles	CTA^+ &TEA^+	10 mL (30 wt.% stabilised H_2O_2)	Y
13	SAPO-34	TEA^+	4 mL (30 wt.% H_2O_2) /10 g solid	N
14	AlPO-5	Tosylate*	Equal to entry 10	Y
15	SBA-15	P123	25 mL H_2O + 50 mL H_2O_2 (30 wt.% H_2O_2)/g solid dropwise at 48 mL/h	Y

[a]*: target organic molecule to be removed; RT = room temperature; MW: microwave irradiation. * Tosylate: 3-(2,3-Dihydroxypropyl)-1,2-dimethylimidazolium tosylate*

	[Fe] / ppm	Reaction time/h	pH	T / K	Assisted?	Ref.
1	500 ppm (298 K) or 20 ppm (353 K)	16	-	298 or 353	No	Melián-Cabrera, I.V.; 2005 [95]
2	12 mg $FeCl_3 \cdot xH_2O$	Overnight, 2 times	-	RT	No	Xia, Y.D.; 2006 [102]
3	-	3-4	3.5	-	UV light	Xiao, L.; 2006 [98]
4	12 mg $FeCl_3 \cdot xH_2O$	Overnight	-	RT	No	Alam, N.; 2008 [101]
5	-	20	-	363	No	Xing, H.J.; 2008 [122]
6	455 ppm (8.8 mg $FeCl_3 \cdot 6H_2O$)	18	-	293	No	Kecht, J.; 2008 [100]
7	Fe^{2+}/H_2O_2 solution (500 ppm Fe^{2+}(Fe-sulphate))	Overnight	-	RT	No	Fan, F.; 2009 [118]
8	-	-	-	-	UV light	Bae, J.A.; 2010 [126]
9	-	2		RT	No	Lu, J.; 2010 [123]
10	Equal to entry 1	3 + 30	1.8		No	Wu, L.S.; 2010 [120]
11	2240	10 min + 50 min	6		MW	Hu, Y.; 2012 [103]
12	10	24	4	343	No	López-Pérez, L.; 2013 [97]
13	0	10	-	343	No	Wang, P.; 2013 [119]
14	2240	10 min + 50 min	6		MW	Khoo, D.Y.; 2014 [125]
15	Aprox. 5 ppm (25 mg Fe^{III}-nitrate)	7		343	No	Zhang, Z.; 2014 [114]

The first study in the field was published in 2005 by Cabrera *et al.* (Table 2, entry 1). It involves the removal of TEA^+ from beta zeolite using catalytic amounts of Fe cations at temperatures between 298 and 353 K, with typical reaction times of 16 h. The template was fully removed. The beta zeolite structure was not changed to a significant extent as shown by XRD, argon physisorption and Al-NMR measurements [95].

The Fenton detemplation protocol was successfully applied by many authors to mesoporous materials. In some case, the use of Fe was avoided as it is incorporated in the zeolite structure and may affect (catalytic) performance. In other cases, radical formation was induced by other means *e.g.* UV light, however, small amounts of other metals present in the structure may also act as a catalyst. For example, SBA-15 with a Pluronic (P123) template was successfully detemplated with diluted H_2O_2 in the presence of UV light (Table 2, entry 3) [98]. The template was fully removed in 3-4 h at room temperature and relevant zeolite properties were improved (larger pore size and surface area). MCM-56 was also detemplated successfully using the Fenton protocol in the absence of Fe cations. Typical conditions are 20 h reaction at 363 K. The resulting materials show larger surface areas, higher pore volumes and more Lewis and Brønsted acid sites compared to the calcined counterparts. The zeolites were subsequently doped and tested for methane aromatisation (Table 2, entry 5) [122].

The silico alumino phosphate (SAPO-34) zeolite with a tetraethylammonium hydroxide (TEA^+) template was also successfully detemplated using a Fenton protocol in the absence of Fe, even at a low hydrogen peroxide to zeolite ratio (4 mL of H_2O_2/10 g solid, 343 K, 10 h) [119] (Table 2, entry 13).

Another application is the regeneration of ZSM-5 membranes (Table 2, entry 9) where trapped toluene was successfully removed at mild conditions (15 wt.% of H_2O_2 for 2 h) [123].

Protocol optimisation has been studied by a number of groups. Xia *et al.* proposed a dropwise addition of H_2O_2 and the use of iron chloride as the Fe source for the detemplation of mesoporous aluminosilicates (Table 2, entry 2). The cetyltrimethylammonium cation (CTA^+) was successfully

removed after two detemplating protocols (16 h, room temperature). Improved textural properties and higher acidity were found for the Fenton detemplated materials compared to the calcined counterparts [102]. A similar procedure was followed by Alam *et al.* to remove CTA^+ from the silicate mesophase RUB-18 (Table 2, entry 4). Only one detemplation sequence was required to fully remove the template and a zeolite with significant crystallinity was obtained [101]. The combined removal of CTA^+ and the residues of tetraethyl orthosilicate (TEOS) from mesoporous silica nanoparticles and MCM-41 by Fenton detemplation was reported by Kecht *et al.* (Table 2, entry 6). These studies were also extrapolated to colloidal suspensions of mesoporous silica nanoparticles aimimg for controlled morphologies and an efficient one-pot reaction [100]. Fenton detemplation was also applied to AlPO-5 by Fan *et al.* to prevent the breakdown of the pores and coke formation during calcination (Table 2, entry 7). In this case, Fe sulphate instead of the chlorine analog was used as the Fe source and the reaction was carried out overnight at room temperature. The AlPO-5 detemplated at different reaction times were characterised by UV Raman spectroscopy to gain molecular insights in the role of the template during framework formation [118]. Two ordered mesoporous silicas, SBA-15 and MSU-H were detemplated with the aid of UV-light by Bae *et al.* and characterised by FT-IR and XPS [126] (Table 2, entry 8). The same procedure as provided in entry 1 of Table 2 was applied by Wu *et al.* (Table 2, entry 10) to quantitatively remove the occluded template of organic light emitting diodes (OLED), though the procedure had to be repeated twice for good performance [120]. The detemplation of nanozeolite Beta was achieved in only 15 minutes using a Fenton protocol assisted by microwave irradiation (Table 2, entry 11). Monodispersity and external surface area were preserved while the formation of extra-framework aluminum was avoided, leading to enhanced catalytic performance for fructose dehydration [103]. López-Pérez *et al.* showed that detemplation of soft silica nanoparticles with preservation of the structure is possible using Fenton reagent at 343 K for 24 h (Table 2, entry 12). Higher pore volume and limited particle agglomeration were evidenced by SAXS

(small-angle X-Ray scattering), Ar-physisorption and TEM [97]. Khoo *et al.* applied the microwave-assisted Fenton protocol for the detemplation of AlPO-5, as recorded at Table 2, entry 14. It was shown that this procedure is more efficient than calcination (IR) and has benefits in terms of microporosity (nitrogen-physisorption measurements) [125]. Recently, Zhang *et al.* reported the successful detemplation of SBA-15 by a Fenton protocol with a modified hydrogen peroxide addition protocol (343 K, 7 h and using Fe--nitrate as Fe source). Adsorption studies with bioactive components showed that Fenton detemplated materials perform better than the calcined counterparts due to a higher silanol density on the SBA-15 surface [114] (Table 2, entry 15).

Thus, we can conclude that the Fenton methodology can be applied successfully for zeolite detemplation. Fenton detemplation preserves the structural and textural integrity of thermo-sensitive materials. The temperature is by far lower than for other chemical detemplation approaches, which is certainly an advantage. However, it is a hydrothermal approach which limits the application to hydrothermally stable materials. As such, Fenton is a favourable approach for detemplation of thermally sensitive, hydrothermal stable micro- and mesoporous materials for which template removal by calcination is not an option.

1.3.3. DEALUMINATION/DESILICATION

In this paragraph, dealumination, a well-known post-synthesis procedure, will be discussed. As already implied by the name, it consists of Al removal from the zeolite framework by chemical reactions. It is well known that the framework Si/Al ratio has a strong influence on zeolite properties such as ion-exchange capacity, thermal and hydrothermal stability, hydrophobicity, and amount and strength of Brønsted and Lewis acid sites. As such, it is a powerful approach to tune catalytic activity and selectivity [127,128]. Dealumination can be done by i) the applications of reagents that

selectively remove Al from the zeolite ii) a hydrothermal treatment and iii) replacement of Al atoms in the framework with Si.

1.3.3.A DEALUMINATION USING CHEMICAL REAGENTS

For chemical dealumination, a number of reagents have been identified. The use of inorganic acids was first reported in 1964 by Barrer et al. [129]. A schematic representation is given in Scheme 1. Typical reaction temperatures are between room temperature and 160 °C. Examples of inorganic acids are strong acids like HNO_3, HCl, HBr and H_2SO_4. The method may be tuned towards quantitative Al removal. However, the thermal stability of the resulting materials decreases considerably at dealumination values higher than 65%. The method was successfully applied to beta zeolite, clinoptilolite, erionite, mordenite, offretite, ZSM-5 and Na-Y [127].

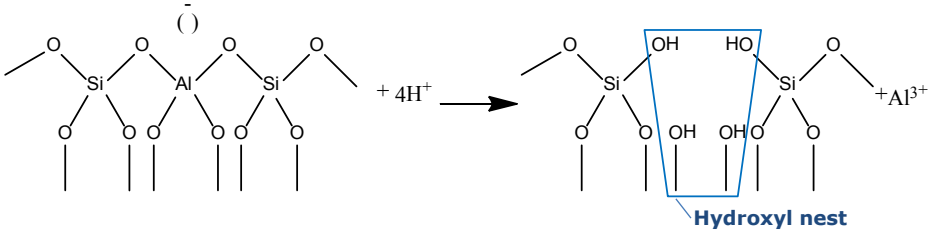

Scheme 1. Chemical dealumination via acid treatment.

In 1968, Kerr showed that dealumination is also possible with H_4-EDTA at room temperature [130]. Experiments with Na-Y showed that 50% of Al was removed while maintaining structural integrity. Actually, the product, Ultra Stable Y (USY), is thermally more stable than the precursor Na-Y. The reaction is proposed to take place in two steps: hydrolysis of Si-O-Al bonds and subsequent solubilisation of Al cations by complexation with EDTA. Other complexing agents have been tested as well, examples are acetylacetone, tartaric acid and oxalic acid [127,128,131,132].

Finally, it also has been shown that gaseous halogen compounds are also able to dealuminate zeolites. The most commonly used agent is Cl_2, sometimes in combination with HCl, or CO (molar ratio 1:1). Typically, the reaction takes place at temperatures higher than 400 °C [70].

1.3.3.B. HYDROTHERMAL DEALUMINATION

Hydrothermal dealumination involves treatment of the zeolite in water or steam. Most of the studies used Zeolite Y and temperatures as high as 5000 °C have been applied. In the case of zeolite Y, the process is divided into two steps i) a fast up to 50% dealumination after around 30 min, and ii) a subsequent slow dealumination leading to enhanced dealumination levels [19].

1.3.3.C. SUBSTITUTION OF FRAMEWORK ALUMINIUM FOR SILICON

This approach is centred on the substitution of framework Al with Si. The first example was reported in 1980 by Beyer and Belenykaya using $SiCl_4$ as the reagent (eq. 10) [19,127]:

$$2\,Al_2O_3 + 3\,SiCl_4 \rightarrow 4\,AlCl_3 + 3\,SiO_2 \quad (10)$$

At proper conditions, framework Al is substituted for Si in a highly exothermic reaction with no substantial lattice damage. These studies were corroborated by ^{29}Si MAS NMR and HR-EM.

1.3.4. DESILICATION

Besides dealumination, desilication has also been studied to obtain zeolites with a higher Al/Si ratio. The first reports stem from 1988 using Y zeolite. It was shown that Si removal is possible by treatment of the zeolite with

alkali solutions (pH > 12) [19]. Another example is the work from Cismek *et al.*, who reported the desilication of silicalite-1 and ZSM-5 with different Si/Al contents using a NaOH solution (5 M) at 80 °C [133,134]. The method was also tested for ZSM-12 at different NaOH concentrations (0.05-0.4 M), reaction time (30-150 min) and temperatures (308-368 K) by Wei *et al.* It was shown that the concentration of the alkali solution is the most critical factor [135]. Groen *et al.* applied similar conditions for the desilication of Beta zeolite [136].

1.4. CHARACTERISATION OF ZEOLITES

A large variety of characterisation techniques have been used to determine zeolite properties on both molecular and meso level with the objective to get a better understanding of aspects like stability, ion-exchange and sorption capacity, shape selectivity towards reactants and products and catalytic activity. A summary of the most significant properties to be determined for solid porous materials with the most common characterisation techniques is presented in Figure 6.

As is evident, a large number of characterisation techniques are available for zeolite characterisation. Detailed descriptions of the various techniques is beyond the scope of this Chapter and the reader is referred to the literature [24,26,137]

1.5. AIM AND SCOPE OF THE THESIS

The major objective of the research described in this thesis is the development of an efficient post-treatment procedure for zeolites to remove the organic template without major structural changes. The major focus is on the use of Fenton chemistry either as a stand-alone methodology or in combination with solvent extraction and/or calcination. Relevant properties of

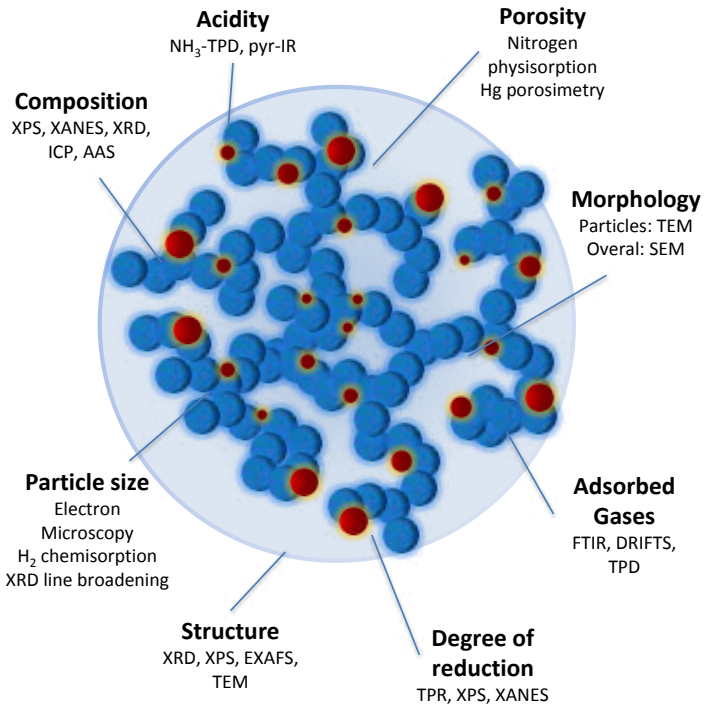

Figure 6. Relevant properties of zeolites and appropriate characterisation techniques.

the selected zeolites were determined and in some cases the performance was assessed in a number of catalytic reactions. Major emphasis was on zeolites such as Beta, ZSM-5, MWW and a mesoporous ZSM-5.

In *Chapter 1,* relevant zeolite properties, synthetic procedures, post--synthesis treatments and characterisation are briefly discussed.

Ion exchange studies on commercial zeolites still containing the organic template are provided in *Chapter 2*. It consists of a liquid exchange of the as-synthesised zeolites followed by a thermal treatment where simultaneously the organic template (as CO_2 and H_2O) and the counterion NH_4^+ (as NH_3) are released. The synthetic methodology was tested for ZSM-5, Beta zeolite and USY.

In *Chapter 3* a detailed study on the mild template removal of a nano--structured beta zeolite based on Fenton chemistry is reported. The effect of process variables on the detemplating efficiency was determined and

resulting products were characterised in detail. The material properties of the products were compared to those obtained using a conventional calcination procedure.

In *Chapter 4*, an extension on the applicability of Fenton detemplation to other materials (BEA, MFI, MesoMFI, MCM-pd, and SnBeta) is reported. The influence of the crystallite size, together with the Si/Al ratio was studied using ZSM-5 zeolite with different Si/Al ratios (25, 40 and 140) and crystallite size.

In *Chapter 5*, mild template removal and activation of microcrystalline Beta zeolite is described. Catalytic performance of the detemplated product was studied with the catalytic cracking of LDPE as a model reaction. The results are compared to well-known commercial zeolites such as MFI, BEA and USY. The experiments were performed in a TGA instrument, as it is a simple, fast and reliable method to determine the kinetics of LDPE cracking at a small scale.

1.6. REFERENCES

[1] IZA Synthesis Commission (2015).

[2] S. van Donk, A. Janssen, J. Bitter, K. de Jong, Catal. Rev. -Sci. Eng. 45 (2003) 297-319.

[3] M. Kustova, K. Egeblad, K. Zhu, C.H. Christensen, Chem. Mater. 19 (2007) 2915-2917.

[4] J. Aguado, D.P. Serrano, J.M. Rodriguez, Micropor. Mesopor. Mat. 115 (2008) 504-513.

[5] J. Perez-Ramirez, C.H. Christensen, K. Egeblad, C.H. Christensen, J.C. Groen, Chem. Soc. Rev. 37 (2008) 2530-2542.

[6] V. Valtchev, S. Mintova, in: V. Valtchev, S. Mintova, M. Tsapatsis (Eds.), Ordered Porous Solids, Elsevier, Amsterdam, 2009, pp. 477-499.

[7] Wang Yang, Ma Liyong, Zhu Ning, Chen Fengqiu, X. Zhan, Prog. Chem. 21 (2009) 1722-1733.

[8] Y. Zhang, N. Ren, Y. Tang, in: V. Valtchev, S. Mintova, M. Tsapatsis (Eds.), Ordered Porous Solids, Elsevier, Amsterdam, 2009, pp. 441-475.

[9] S. Lopez-Orozco, A. Inayat, A. Schwab, T. Selvam, W. Schwieger, Adv Mater. 23 (2011) 2602-2615.

[10] J. Kaerger, R. Valiullin, Chem. Soc. Rev. 42 (2013) 4172-4197.

[11] C.M.A. Parlett, K. Wilson, A.F. Lee, Chem. Soc. Rev. 42 (2013) 3876-3893.

[12] D.P. Serrano, J.M. Escola, P. Pizarro, Chem. Soc. Rev. 42 (2013) 4004-4035.

[13] J. Coronas, Chem. Eng. J. 156 (2010) 236-242.

[14] R.M. Barrer, P R Soc. A-Math Phy. (1938) 392.

[15] A. Corma, J. Catal. 216 (2003) 298-312.

[16] A. Corma, Chem. Rev. 97 (1997) 2373-2419.

[17] D.W. BreckZeolite Molecular Sieves, Structure, Chemistry and Use, John Wiley & Sons, New York, London, Sydney, Toronto, 1974, pp. 636.

[18] J. Weitkamp, L. Puppe, Catalysis and Zeolites, Fundamentals and Applications, Springer, Berlin, 1999.

[19] J. Cejka, H. van Bekkum, A. Corma, F. Schueth, Introduction to Zeolite Science and Practice, 3rd revised edition, Stud. Surf. Catal. 168 ed., Elsevier, Amsterdam, 2007.

[20] R. Xu, W. Pang, J. Yu, Q. Huo, J. Chen, Chemistry of Zeolites and Related Porous Materials. Synthesis and Structures, John Wiley & Sons, (Asia), 2007.

[21] V. Valtchev, S. Mintova, M. Tsapatsis, Ordered Porous Solids: Recent Advances and Prospects, Elsevier, Amsterdam, 2009.

[22] J. Cejka, A. Corma, S. Zones (Eds.), Zeolites and Catalysis: Synthesis, Reactions and Applications, Wiley-VCH, Weinheim, 2010.

[23] J. Coronas, Chem. Eng. J. 156 (2010) 236-242.

[24] Handbook of Heterogeneous Catalysis, (2004) ed., Wiley-VCH, Weinheim, 1999.

[25] R.M. Barrer, J. Chem. Soc. (1948) 2158-2163.

[26] Zeolites and Ordered Porous Solids: Fundamentals and Applications, First edition ed., Editorial Universitat Politècnica de València, 2011.

[27] D. Breck, W. Eversole, R. Milton, T. Reed, T. Thomas, J. Am. Chem. Soc. 78 (1956) 5963-5971.

[28] T. ReeD, D. Breck, J. Am. Chem. Soc. 78 (1956) 5972-5977.

[29] R.M. Milton, ACS Symp. Ser. 398 (1989) 1-10.

[30] C. Baerlocher, L.B. McCusker, D.H. Olson, Atlas of Zeolite Framework Types, Sixth Revised Edition ed., Elsevier, 2007.

[31] R. Morris, S. Weigel, Chem. Soc. Rev. 26 (1997) 309-317.

[32] E. Cooper, C. Andrews, P. Wheatley, P. Webb, P. Wormald, R. Morris, Nature. 430 (2004) 1012-1016.

[33] R. Rogers, K. Seddon, Science. 302 (2003) 792-793.

[34] W.M. Reichert, J.D. Holbrey, K.B. Vigour, T.D. Morgan, G.A. Broker, R.D. Rogers, Chem. Commun. (2006) 4767-4779.

[35] P. Nockemann, B. Thijs, S. Pittois, J. Thoen, C. Glorieux, K. Van Hecke, L. Van Meervelt, B. Kirchner, K. Binnemans, J. Phys. Chem. B. 110 (2006) 20978-20992.

[36] L.A. Blanchard, D. Hancu, E.J. Beckman, J.F. Brennecke, Nature. 399 (1999) 28-29.

[37] S.J. Mugavero III, M. Bharathy, J. McAlum, H. zur Loye, Solid State Sci. 10 (2008) 370-376.

[38] A. Corma, M.J. Diaz-Cabanas, J. Luis Jorda, C. Martinez, M. Moliner, Nature. 443 (2006) 842-845.

[39] M.W. Anderson, O. Terasaki, T. Ohsuna, A. Philippou, S.P. Mackay, A. Ferreira, J. Rocha, S. Lidin, Nature. 367 (1994) 347-351.

[40] A. Kuperman, S. Nadimi, S. Oliver, G.A. Ozin, J.M. Garces, M.M. Olken, Nature. 365 (1993) 239-242.

[41] S. Nadimi, S. Oliver, A. Kuperman, A. Lough, G.A. Ozin, J.M. Garces, M.M. Olken, P. Rudolf, Nonaqueous Synthesis of Large Zeolite and Molecular-Sieve Crystals, 84 (1994) 93-100.

[42] L. Xiaoyang, S. Wenhui, W. Yifeng, Z. Xudong, Chem. Commun. (1992) 902-903.

[43] W.M. Meier, M. Groner, J. Solid State Chem. 37 (1981) 204-218.

[44] S. Cartlidge, E.B. Keller, W.M. Meier, Zeolites. 4 (1984) 226-230.

[45] C.S. Cundy, P.A. Cox, Chem. Rev. 103 (2003) 663-701.

[46] J. THOMAS, Chem. Ind. (1983) 757-758.

[47] R.M. Barrer, P.J. Denny, J. Chem. Soc. (1961) 971-982.

[48] R.M. Barrer, J.W. Baynham, F.W. Bultitude, W.M. Meier, J. Chem. Soc. (1959) 195-208.

[49] E.M. Flanigen, D.W. Breck, 137th Meeting of the ACS, Division of Inorganic Chemistry. (1960).

[50] D.W. Breck, J. Chem. 41 (1964) 678-689.

[51] A. Jackowski, S.I. Zones, S. Hwang, A.W. Burton, J. Am. Chem. Soc. 131 (2009) 1092-1100.

[52] E.M. Flanigen, J.M. Bennett, R.W. Grose, J.P. Cohen, R.L. Patton, R.M. Kirchner, J.V. Smith, Nature. 271 (1978) 512-516.

[53] J.L. Guth, H. Kessler, J.M. Higel, J.M. Lamblin, J. Patarin, A. Seive, J.M. Chezeau, R. Wey, ACS Symp. Ser. 398 (1989) 176-195.

[54] M. Estermann, L.B. Mccusker, C. Baerlocher, A. Merrouche, H. Kessler, Nature. 352 (1991) 320-323.

[55] A. Merrouche, J. Patarin, H. Kessler, M. Soulard, L. Delmotte, J.L. Guth, J.F. Joly, Zeolites. 12 (1992) 226-232.

[56] T. Loiseau, R. Retoux, P. Lacorre, G. Ferey, J. Solid State Chem. 111 (1994) 427-436.

[57] R.M. Barrer, Zeolites. 1 (1981) 130-140.

[58] R. Castaneda, A. Corma, V. Fornes, F. Rey, J. Rius, J. Am. Chem. Soc. 125 (2003) 7820-7821.

[59] A. Corma, F. Rey, J. Rius, M. Sabater, S. Valencia, Nature. 431 (2004) 287-290.

[60] A. Burton, S. Zones, S. Elomari, Curr. Opin. Colloid Interface Sci. 10 (2005) 211-219.

[61] J. Cejka, A. Corma, S. Zones (Eds.), Zeolites and Catalysis: Synthesis, Re-actions and Applications, Wiley-VCH, Weinheim, 2010, pp. 67.

[62] R. Xu, W. Pang, J. Yu, Q. Huo, J. Chen, in: Anonymous Chemistry of Zeolites and Related Porous Materials. Synthesis and Structures, John Wiley & Sons, (Asia), 2007, pp. 39.

[63] N.D. Hould, R.F. Lobo, Chem. Mater. 20 (2008) 5807-5815.

[64] Y. Li, J. Yu, Chem. Rev. 114 (2014) 7268-7316.

[65] L.D. Rollmann, J.L. Schlenker, C.L. Kennedy, G.J. Kennedy, D.J. Doren, J Phys Chem B. 104 (2000) 721-726.

[66] K.J. Balkus, Prog. Inorg. Chem. 50 (2001) 217-268.

[67] J.W. McBain, The Sorption of Gases and Vapours by Solids, Routledge and Sons, 1932, Chapter 5.

[68] V. Valtchev, G. Majano, S. Mintova, J. Perez-Ramirez, Chem. Soc. Rev. 42 (2013) 263-290.

[69] M. Hunger, Catal. Rev. 39 (1997) 345-393.

[70] H.G. Karge, J. Weitkamp, in: Anonymous Molecular Sieves Vol. 3, Post-Synthesis Modifications, Springer, Berlin-Heidelberg, 2002, pp. 205-208.

[71] R.M. Barrer, Nature. 164 (1949) 112-113.

[72] M.J. Ortiz-Iniesta, H.J. Heeres, I. Melian-Cabrera, Micropor. Mesopor. Mat. 171 (2013) 208-214.

[73] L.M. Parker, D.M. Bibby, J.E. Patterson, Zeolites. 4 (1984) 168-174.

[74] E. Bourgeatlami, F. Direnzo, F. Fajula, P.H. Mutin, T.D. Courieres, J. Phys. Chem. 96 (1992) 3807-3811.

[75] X.T. Gao, C.Y. Yeh, P. Angevine, Micropor. Mesopor. Mat. 70 (2004) 27-35.

[76] M. Milanesio, G. Artioli, A.F. Gualtieri, L. Palin, C. Lamberti, J. Am. Chem. Soc. 125 (2003) 14549-14558.

[77] C. Minchev, H. Weyda, V. Minkov, V. Penchev, H. Lechert, J. Therm. Anal. Calorim. 37 (1991) 573-582.

[78] A. Corma, V. Fornes, M. Navarro, J. Pérez-Pariente, J. Catal. 148 (1994) 569-574.

[79] K.H. Gilbert, R.M. Baldwin, J.D. Way, Ind. Eng. Chem. Res. 40 (2001) 4844-4849.

[80] N. Dufau, L. Luciani, F. Rouquerol, P. Llewellyn, J. Mater. Chem. 11 (2001) 1300-1304.

[81] J. Perez-Pariente, J.A. Martens, P.A. Jacobs, Appl. Catal. 31 (1987) 35-64.

[82] M.A. Camblor, A. Mifsud, J. Perezpariente, Zeolites. 11 (1991) 792-797.

[83] M.A. Camblor, A. Corma, S. Valencia, Micropor. Mesopor. Mat. 25 (1998) 59-74.

[84] C.W. Jones, K. Tsuji, T. Takewaki, L.W. Beck, M.E. Davis, Micropor. Mesopor. Mat. 48 (2001) 57-64.

[85] Z. Zhang, J. Yin, H.J. Heeres, I. Melian-Cabrera, Micropor. Mesopor. Mat. 176 (2013) 103-111.

[86] B. Gautier, M. Smaihi, New J. Chem. 28 (2004) 457-461.

[87] O. Kresnawahjuesa, D.H. Olson, R.J. Gorte, G.H. Kuhl, Micropor. Mesopor. Mat. 51 (2002) 175-188.

[88] P.B. Malla, S. Komarneni, Zeolites. 15 (1995) 324-332.

[89] J. Kuhn, M. Motegh, J. Gross, F. Kapteijn, Micropor. Mesopor. Mat. 120 (2009) 35-38.

[90] J. Kuhn, J. Gascon, J. Gross, F. Kapteijn, Micropor. Mesopor. Mat. 120 (2009) 12-18.

[91] M. El Roz, L. Lakiss, V. Valtchev, S. Mintova, F. Thibault-Starzyk, Micropor. Mesopor. Mat. 158 (2012) 148-154.

[92] A.N. Parikh, A. Navrotsky, Q.H. Li, C.K. Yee, M.L. Amweg, A. Corma, Micropor. Mesopor. Mat. 76 (2004) 17-22.

[93] Q.H. Li, M.L. Amweg, C.K. Yee, A. Navrotsky, A.N. Parikh, Micropor. Mesopor. Mat. 87 (2005) 45-51.

[94] I. Melián-Cabrera, F. Kapteijn, J.A. Moulijn, Chem. Commun. (2005) 2178-2180.

[95] I. Melian-Cabrera, F. Kapteijn, J.A. Moulijn, Chem. Commun. (2005) 2744-2746.

[96] I.V. Melián-Cabrera, J.A. Moulijn, in: A. Cybulski, J.A. Moulijn, A. Stankiewicz (Eds.), Novel Concepts in Catalysis and Chemical Reactors: Improving the Efficiency for the Future, Wiley, Weinheim, 2010.

[97] L.L. Perez, M.J. Ortiz-Iniesta, Z. Zhang, I. Agirrezabal-Telleria, M. Santes, H.J. Heeres, I. Melián-Cabrera, J. Mater. Chem. A. 1 (2013) 4747-4753.

[98] L. Xiao, J. Li, H. Jin, R. Xu, Micropor. Mesopor. Mat. 96 (2006).

[99] J. Xu, M. Chen, Y. Liu, Y. Cao, H. He, K. Fan, Micropor. Mesopor. Mat. 118 (2009) 354-360.

[100] J. Kecht, T. Bein, Micropor. Mesopor. Mat. 116 (2008) 123-130.

[101] N. Alam, R. Mokaya, J. Mater. Chem. 18 (2008) 1383-1391.

[102] Y.D. Xia, R. Mokaya, J. Phys. Chem. B. 110 (2006) 18424-18431.

[103] Y. Hu, Y. Zhang, Y. Tang, Rsc. Advances. 2 (2012).

[104] E. Neyens, J. Baeyens, J. Hazard. Mater. 98 (2003) 33-50.

[105] W.Z. Tang, Physicochemical Treatment of Hazardous Wastes, CRC Press LLC, Florida, 2004.

[106] J.J. Pignatello, E. Oliveros, A. MacKay, Crit. Rev. Environ. Sci. Technol. 36 (2006) 1-84.

[107] N.M. Al-Ananzeh, J.A. Bergendahl, R.W. Thompson, Prog. React. Kinet. Mec. 32 (2007) 131-151.

[108] N. Koryabkina, J.A. Bergendahl, R.W. Thompson, A. Giaya, Micropor. Mesopor. Mat. 104 (2007) 77-82.

[109] N. Al Ananzeh, J.A. Bergendahl, R.W. Thompson, Environ. Chem. 3 (2006) 40-47.

[110] I. Melián-Cabrera, S. Espinosa, F.J. Garcia-Montelogo, F. Kapteijn, J.A. Moulijn, Chem. Commun. (2005) 1525-1527.

[111] R.J. Watts, M.D. Udell, P.A. Rauch, S.W. Leung, Hazard. Waste Hazard. Mater. 7 (1990) 335-345.

[112] C. Walling, Acc. Chem. Res. 8 (1975) 125-131.

[113] I. Melian-Cabrera, F. Kapteijn, J.A. Moulijn, Catal. Today. 110 (2005) 255-263.

[114] Z. Zhang, D.L. Santangelo, G. ten Brink, B.J. Kooi, J.A. Moulijn, I. Melian-Cabrera, Mater. Lett. 131 (2014) 186-189.

[115] Y. Xia, R. Mokaya, J. Phys. Chem. B. 110 (2006) 9122-9131.

[116] J. Kecht, T. Bein, Micropor. Mesopor. Mat. 116 (2008) 123-130.

[117] N. Alam, R. Mokaya, J. Mater. Chem. 18 (2008) 1383-1391.

[118] F. Fan, Z. Feng, K. Sun, M. Guo, Q. Guo, Y. Song, W. Li, C. Li, Angew. Chem. Int. Edit. 48 (2009) 8743-8747.

[119] P. Wang, D. Yang, J. Hu, J. Xu, G. Lu, Catal. Today. 212 (2013) 62.

[120] C. Wu, J. Liao, S. Fang, A.S.T. Chiang, Adsorption. 16 (2010) 69-74.

[121] M. Hartmann, S. Kullmann, H. Keller, J. Mater. Chem. 20 (2010) 9002-9017.

[122] H. Xing, Y. Zhang, M. Jia, S. Wu, H. Wang, J. Guan, L. Xu, T. Wu, Q. Kan, Catal. Commun. 9 (2008) 234-238.

[123] J. Lu, N. Liu, L. Li, R. Lee, Sep. Purif. Technol. 72 (2010) 203-207.

[124] Y. Hu, Y. Zhang, Y. Tang, Rsc Advances. 2 (2012) 6036-6041.

[125] D.Y. Khoo, H. Awala, S. Mintova, E. Ng, Micropor. Mesopor. Mat. 194 (2014) 200-207.

[126] J.A. Bae, S.H. Hwang, K. Song, J. Jeon, Y.S. Ko, J. Yim, J. Nanosci. Nanotechno. 10 (2010) 290-296.

[127] H.K. Beyer, in: H.G. Karge, J. Weitkamp, P. Anderson (Eds.), Molecular Sieves Vol. 1, Post-Synthesis Modifications I, Springer, Berlin-Heidelberg, 2002, pp. 203.

[128] M. Muller, G. Harvey, R. Prins, Micropor. Mesopor. Mat. 34 (2000) 135-147.

[129] R.M. Barrer, L.V.C. Rees, J. Phys. Chem. Solids. 25 (1964) 1035-1038.

[130] G. Kerr, G. Shipman, J. Phys. Chem. 72 (1968) 3071-3072.

[131] M.R. Apelian, A.S. Fung, G.J. Kennedy, T.F. Degnan, J. Phys. Chem. 100 (1996) 16577-16583.

[132] G. Kerr, A. Chester, D. Olson, Catal. Lett. 25 (1994) 401-402.

[133] A. Cizmek, B. Subotic, I. Smit, A. Tonejc, R. Aiello, F. Crea, A. Nastro, Microporous Mater. 8 (1997) 159-169.

[134] A. Cizmek, B. Subotic, R. Aiello, F. Crea, A. Nastro, C. Tuoto, Microporous Mater. 4 (1995) 159-168.

[135] X. Wei, P.G. Smirniotis, Micropor. Mesopor. Mat. 97 (2006) 97-106.

[136] J.C. Groen, S. Abello, L.A. Villaescusa, J. Perez-Ramirez, Micropor. Mesopor. Mat. 114 (2008) 93-102.

[137] Catalysis: An Integrated Approach, 2° Edition, Elsevier, Amsterdam (The Netherlands), 2000.

2

Based on:

María Jesús Ortiz Iniesta, Hero J. Heeres and Ignacio V. Melián-Cabrera.

Direct activation of micrcrystalline zeolites.

Microporus and mesoporous Materials, 2013, 171, 208-214

(DOI: 10.1016/j.micromeso.2013.01.006)

Direct Activation of Microcrystalline Zeolites

ABSTRACT

In this work a direct activation route of zeolites is assessed. It consists of NH_4-exchange of the as-synthesised solids before removing the organic template. Calcination afterwards serves to combust the organic template and creates the Brønsted sites directly; thus applying merely a single thermal step. This method simplifies their activation and the material suffers less thermal stress. The approach is particularly effective for microcrystalline beta and ferrierite zeolites. Thorough investigation of the template content and materials' texture points out to three relevant effects that can explain the effective exchange process: partial removal of the template during exchange creates substantial microporosity (ferrierite), the remaining template is reorganised within the pores (ferrierite) and finally, void space can exist due to the non-perfect matching between the network and template (beta). This shorter method appears suited for microcrystalline zeolites; it was ineffective for crystalline MFI types.

Keywords: ion-exchange; H-form zeolites; zeolite activation; calcination; void space.

1. INTRODUCTION

Zeolites, a family of microporous aluminosilicates, are among the most relevant industrial catalysts [1-5]. Numerous commercial processes are based on such structures, from oil-refining to fine chemicals production through petrochemistry [2,3,5]. Their synthesis is generally elaborated involving a relatively large number of discontinuous steps. The synthesis of high-silica Al-containing zeolites generally employs organic templates in a mineralising medium; alkaline hydroxides, M(OH) (M=Na, K) are commonly used in practice. The organic template can have several roles; a true templating effect (e.g. ZSM-18 [6]), structural directing agent (e.g. SSZ-13 [7]), volumetric space filler (e.g. $AlPO_4$-5 [8]) or charge balancing [9]; in all cases it must be fully removed after synthesis to develop the desired porosity. The insertion of trivalent metals in the zeolite framework, mostly Aluminium, generates a charge deficiency that is balanced with surrounding alkaline and the organic template cations. These cations are shielding the desired acidity until the zeolite is activated. In order to yield acidic sites, these cations must be exchanged by H^+; which can come from different sources. Formation of Brønsted sites can be achieved by exchanging the alkali metal with Mg^{2+}, Ca^{2+}, La^{3+} or Al^{3+} followed by thermal dehydration; physisorbed water is dissociated into Brønsted protons [10,11]. Another approach consists of the reduction of noble metals complexes with H_2, which generates metal clusters as well as hydroxyl protons [12]. Occasionally, the organic templates decomposition yields partially activated zeolites with remaining alkaline cations that must be exchanged afterwards.

A generally practiced method consists of calcination, in which the organic template is decomposed, followed by a mild acidic wash. This methodology is suitable for highly-crystalline Si-rich mordenite, ZSM-5 and MCM-22. However, it often leads to collapse for Al-rich zeolites and dealumination [13] for moderately stable structures, accompanied by an acidity decrease and the appearance of AlO_5 and AlO_6 extra-framework species. Barrer [14] introduced an alternative to the acid wash, which is currently

the most applied protocol. It includes an intermediate key step in which Na^+/K^+ are exchanged by NH_4NO_3. In particular, it consists of three steps (Fig. 1, bottom): calcination to degrade the organic template, liquid NH_4-exchange, drying and final thermal decomposition into protonic sites with NH_3 release. Shortening the number of steps is desirable; in particular it can be very advantageous reducing the thermal steps. In this manner, the material is subjected to less thermal stress and self-steaming. This is especially critical for less stable nano-scale, hierarchical, delaminated, unit-cell and thin films zeolites where thermal stress and agglomeration play crucial roles to maintain their original structure [15-18].

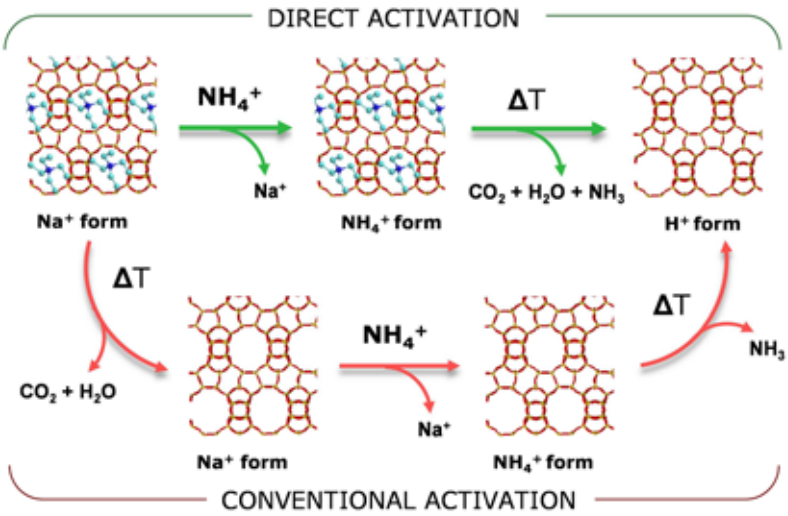

Figure 1. Zeolite activation protocols: conventional (CA, bottom) and proposed direct activation (DA, top) for microcrystalline zeolites.

In this paper, a simplified route for zeolite activation is presented having only a single thermal treatment. The concept is based on exchanging NH_4^+ by Na^+/K^+ in the zeolite that still contains the organic template. This is not an evident phenomenon; its feasibility is inspired by the fact that the matching between organic template and inorganic network is not (always) geometrically perfect. Consequently, we expect the presence of certain void

space in the templated channels of some structures in which the NH_4^+ can diffuse and exchange with Na^+/K^+. The NH_4-exchange can eventually wash out part of the organic template, increasing such void space. If these effects occur, the sample needs to be thermally treated merely once; serving for template removal and activation (Fig. 1, top). This is assessed by comparing two activation methodologies: the Barrer conventional activation (samples name is suffixed with CA) including template removal by calcination, NH_4--exchange and activation, while the proposed direct activation (DA) involves NH_4-exchange of the templated zeolite and a single thermal activation for template burning and activation. Three relevant zeolites were investigated; Beta (BEA, 12MR), Ferrierite (FER, 10MR) and ZSM-5 (MFI, 10MR).

2. EXPERIMENTAL

2.1 MATERIALS

The research materials are ferrierite (pyridine based with SiO_2/Al_2O_3=54), beta (tetraethyl ammonium (TEA) based with SiO_2/Al_2O_3=23) and two ZSM-5 (MFI-I and MFI-II with SiO_2/Al_2O_3=80 and 280 respectively, based on tetrapropylammonium hydroxide); kindly supplied by PQ-Corp. The zeolite structural verification and crystallinity was carried out by XRD (Fig. 2). NH_4NO_3 was purchased from Sigma-Aldrich (purity ≥ 98%). Gases (synthetic air, He, N_2) were of analytical purity (>99.9 %, Alpha gas). Low--density polyethylene was supplied by DSM.

2.2 ACTIVATION PROTOCOLS

The *conventional activation* method (CA) consists of the following sequential steps:

- Calcination: room temperature, 5 °C·min^{-1}, 550 °C for 6 h under atmospheric air.

- NH_4^+ exchange at 353 K using 50 mL·g^{-1} zeolite and a NH_4NO_3 solution (0.5 M) for 48h.
- Thermal activation: room temperature, 5 °C·min^{-1}, 550 °C for 6 h under atmospheric air.

The *direct activation* (DA) implies:

- The as-received material is directly used without any pre-treatment.
- NH_4^+ exchange at 353 K using 50 mL·g^{-1} zeolite and a NH_4NO_3 solution (0.5 M) for 48h.
- Thermal activation: room temperature, 5 °C·min-1, 550 °C for 6 h under atmospheric air.

The materials and treatments are summarised in Table 1. Cations charge is omitted in the text for simplicity.

Table 1. Sample nomenclature and treatments.

Entry	Material	Treatment
1	Na-Bea T	As-synthesised, (organic) templated beta zeolite.
2	NH_4-Bea T	Material **1** (i.e. Na-form, having the organic template) after NH_4NO_3 exchange; first step in DA route.
3	Na-Bea C	Material after calcination of the as-received beta zeolite (**1**) at 550 °C, 6 h.
4	H-Bea CA	H-activated beta zeolite following the conventional activation (CA) route as described below.
5	H-Bea DA	H-activated zeolite beta following the direct activation (DA) route as described below.
6	Na-Fer T	As-synthesised, (organic) templated ferrierite zeolite.
7	NH_4-Fer T	Material **6** (i.e. Na-form, having the organic template) after NH_4NO_3 exchange; first step in DA route.
8	Na-Fer C	Material after calcination of the as-received ferrierite zeolite (**6**) at 550 °C, 6 h.
9	H-Fer CA	H-activated ferrierite zeolite following the conventional activation (CA) route as described below.
10	H-Fer DA	H-activated zeolite ferrierite following the direct activation (DA) route as described below.

2.3 CHARACTERISATION

Thermogravimetric analyses (TGA) were carried out on a Mettler-Toledo analyser (TGA/SDTA851e) using a flow of synthetic air of 100 mL.min^{-1} STP. The temperature was increased from 30 to 900 °C at 10 °C·min^{-1}. Blank curve subtraction using an empty crucible was taken into account. TGA with evolved gas analysis was carried out in the same instrument by continuously analysing the gases in a Hiden Quadrupole analyser. The intensities were normalised to inert gas (Ar^+, m/z=40).

CHN elemental analyses were carried out in a EuroVector 3000 CHNS analyser. All analyses were done in duplicate to verify possible sample heterogeneity. For these zeolites the standard deviation was below 2%. Approximately 2 mg of sample was accurately weighed in a 6-digit analytical balance (Mettler Toledo). The samples were burned at 1800 °C in the presence of an oxidation catalyst, oxygen and decomposed into CO_2, H_2O and N_2. These gases were subsequently separated in a Porapak QS column at 80 °C and quantified with a TCD detector. Acetonitrile (purity 99.9%) was used as external standard.

Powder X-ray diffraction (XRD) spectrum were collected with a Bruker D8 powder X-ray diffractometer using CuKα radiation, λ=1.54056 Å. The spectra were recorded with a step size of 0.02°; 3 seconds (s) accumulation time and in the 2θ angle range of 5-60°.

Low-pressure high-resolution Ar physisorption at 87 K analyses were carried out on a Micromeritics ASAP 2020 analyser. Prior to the measurements the samples were outgassed under vacuum at 300 °C for 10 h for the calcined materials. The materials containing the template were mildly degassed at 180 °C for 10 h. The surface area (S_{BET}) was calculated by BET model. The single point pore volume (V_p) was estimated from the amount of gas adsorbed at a relative pressure of 0.98 in the desorption branch. The micropore size distributions (PSD) were calculated using the Horvath-Kawazoe model [19] applied to the adsorption branch of the isotherm. The full isotherm reconstruction (cumulative pore volume) was done using the

non-local DFT kernel [20]; the NLDFT micropore volume (V_{μ}^{NLDFT}) was estimated for pores ≤ 10 Å.

^{27}Al magic angle spinning nuclear magnetic resonance (MAS-NMR) measurements were conducted on a Bruker Avance-400 spectrometer using a 4 mm zirconium holder, applying spinning frequency of 11 kHz at 298 K. The ^{27}Al MAS NMR spectra were obtained at 104.201 MHz, with acquisition delay of 1 s and acquisition time of 0.08 s. Typically 4000 scans were collected. The spectra were referenced with respect to 1.0 M aqueous solution of $Al(NO_3)_3$ set on 0 ppm.

SEM images were recorded with a JEOL 6320F field emission microscope working at 2 kV. The samples were coated with 20 nm-thickness of Pt/Pd (80/20) to improve contrast.

NH_3-TPD experiments were carried out in a Micromeritics AutoChem II system equipped with a thermal conductivity detector. The sample (*ca.* 50 mg) was pre-treated in a He flow (100 mL.min^{-1} STP) at 500 °C at 10 °C/min heating rate. The sample was cooled to 120 °C at a similar rate, and then exposed to 1.0 *vol.* % NH_3/He (25 mL.min^{-1} STP) for 30 min. Subsequently, the sample was exposed to a flow of He (25 mL.min^{-1} STP) for 60 min to remove weakly adsorbed NH_3. After the baseline stabilisation, desorption of NH_3 was monitored in the range of 120-1000 °C by heating the sample at 10 °C·min^{-1}.

X-Ray fluorescence measurements were performed in a Panalytical Axios FAST spectrometer.

The catalytic cracking of low-density polyethylene in liquid-phase was evaluated by thermogravimetrical analyses in a Mettler-Toledo analyser (TGA/SDTA851e) equipped with a 34-position robot. The ground polymer and the zeolite powder, weight ratio 75:25, were weighted with a 5-digits Mettler Toledo balance, after intimately mixed in an Agatha mortar. Approximately 4 mg of the mixture was loaded in 70 µL α-Al_2O_3 crucibles for analysis. The temperature was ramped from 30 to 600 °C at 5 °C·min^{-1} under nitrogen flow; 80 mL·min^{-1} STP.

2.3. RESULTS AND DISCUSSION

2.3.1. EXCHANGE EFFICIENCY

The proof of this concept is demonstrated on a beta zeolite. It is a micro-crystalline zeolite (Fig. 2-a) formed by nano-sized agglomerates <1 μm (Fig. 4-a) with a template content of *ca.* 15 *wt.*% (Table 2) and *ca.* 0.4 *wt.*% Na (Fig. 3). This Na concentration agrees with the verified synthesis gel composition [21]; this means that 20% of AlO_4^- sites are occupied by Na^+ and 80% by TEA^+, approximately. Application of the conventional approach on this material showed that this method functions well with a residual Na concentration in the final material below the XRF instrumental detection limit, *i.e.* ≤0.05 *wt.* % (data not shown). This corresponds to an exchange efficiency higher than 95%, taking into account the Na level of the directly calcined as-synthesised material (Na-Bea-C). The elemental analysis of the proposed DA protocol proves that this method is effective as well; having a similar concentration as for the CA method, *i.e.* ≤0.05 *wt.*% (Fig. 3).

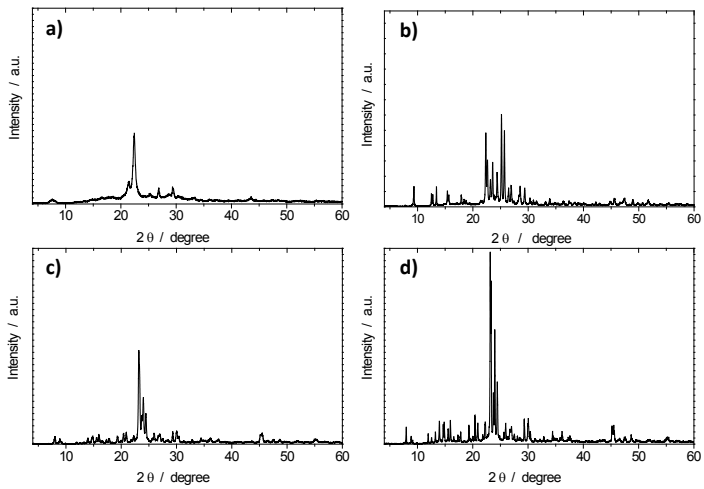

Figure 2. XRD patterns of the templated zeolites: **a)** Beta; **b)** Ferrierite; **c)** MFI-I Si/Al=40 and **d)** MFI-II Si/Al ratio=140.

Table 2. Template content and textural characteristics derived from low-pressure high-resolution Ar physisorption isotherms at 88 K[1].

Material	Template content		S_{BET} [$m^2.g^{-1}$]	V_P [$ml.g^{-1}$]	V_{mp}^{NLDFT} [$ml.g^{-1}$]
	TGA (*wt.*%)[2]	Elemental analysis of C (*wt.*%)			
1 Na-Bea T	15.3[1]	10.48	118	0.478	0.014
2 NH_4-Bea T	16.6[1]	10.61	119	0.561	0.013
3 Na-Bea C	–	–	559	0.697	0.268
6 Na-Fer T	8.7[1]	6.11	14	0.079	0.002
7 NH_4-Fer T	8.4[1]	6.18	135	0.107	0.041
8 Na-Fer C	–	–	286	0.216	0.110

1) TGA analyses for samples 1, 2, 6 and 7 after Argon physisorption show no substantial template removal during the samples' degassing; 2) TGA weight loss between 200-900 °C.

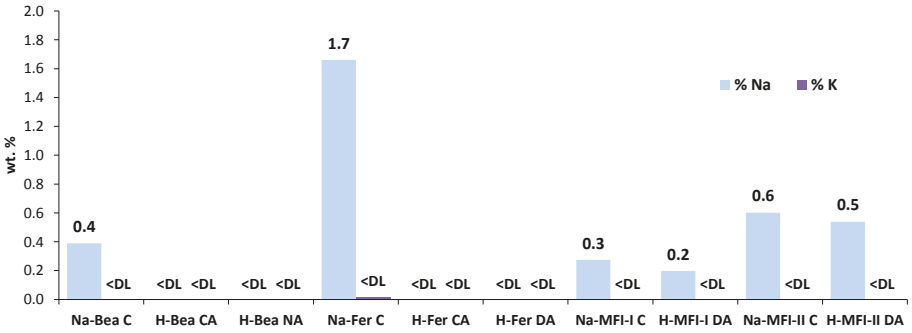

Figure 3. Sodium and potassium weight-based concentration (*wt.*%) for samples activated by the DA method. CA results are omitted as this method works well in all cases with Na <0.05 wt%. Reference materials are those directly calcined: Na-Bea C, Na-Fer C, Na-MFI-I C and Na-MFI-II C. Notation: <DL means below detection limit of XRF.

This approach was extended to another relevant zeolite; a crystalline Ferrierite (Figure 2-b). It is composed by 2D thin platelets of *ca.* 0.5-1 μm lengths (Figure 4-b) with *ca.* 9 *wt.* % of organic template (Table 2). The exchange behaviour of NH_4 in the templated structure is also satisfactory as the Na level for the DA method equals the CA; the Na concentration was below the XRF instrumental detection limit; ≤0.05 *wt.*%. Complete removal of Na was verified by induced coupled plasma analyses for both zeolite structures (data not shown). It is not evident that the DA method could work for a FER structure due to the relatively small pores and related diffusional

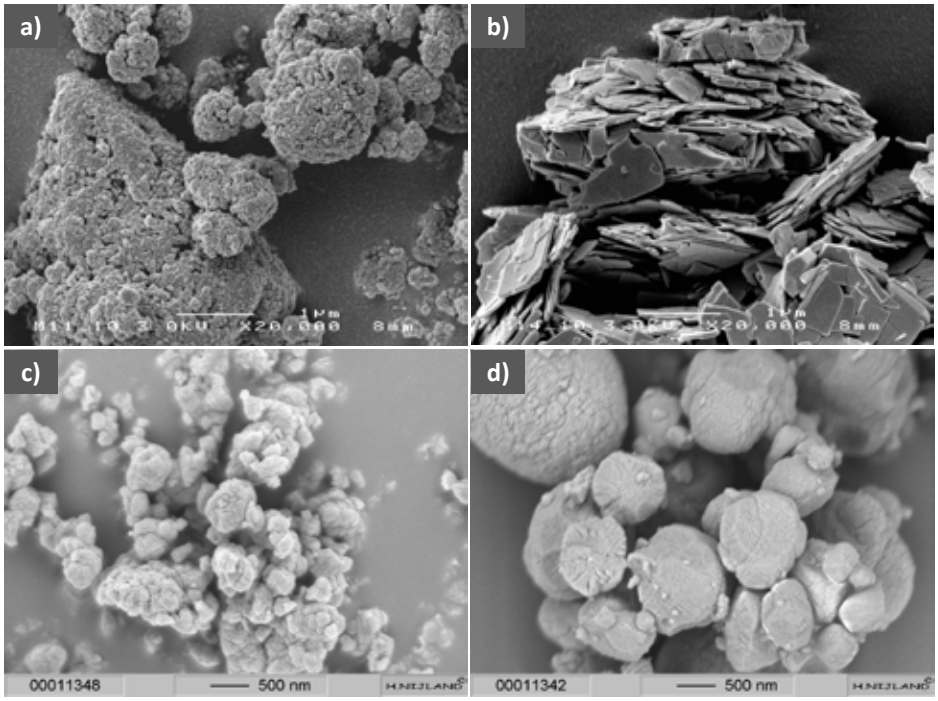

Figure 4. SEM pictures: **a)** Beta; **b)** Ferrierite; **c)** MFI-I and **d)** MFI-II zeolites.

limitations; as will be discussed later, this is related to the partial removal of the template during the NH_4NO_3 exchange.

The DA approach was ineffective concerning two MFI type samples, though having a slightly bigger pore size compared to ferrierite (5.1 × 5.5 ↔ 5.3 × 5.6 versus 4.2 × 5.4 ↔ 3.5 × 4.8, in Å) [22]. The residual Na concentration level in the DA samples remained almost equal to the original counterpart (Fig. 3). Reasons for this behaviour may be attributed to the larger particle size (Fig. 4-c and -d), the 3D conformation of the template in the structure as well as the strong interaction between the template and the framework. The CA method does work well for these two MFI type samples with full Na exchange (data not shown).

In the next sections, we provide a rationalisation of the DA exchange for the successful materials and will discuss their relevant materials properties.

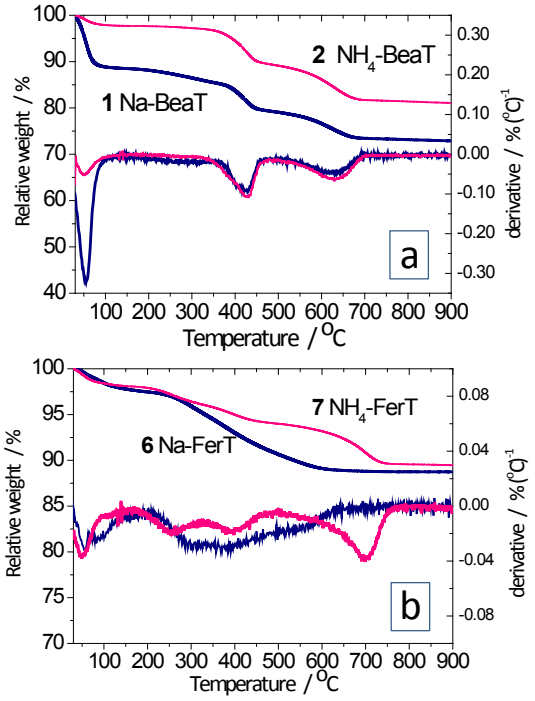

Figure 5. Thermogravimetric patterns for the raw materials before and after NH_4NO_3 exchange: **a)** Beta (samples 1 and 2) and **b)** ferrierite zeolites (samples 6 and 7).

2.3.2. ORGANIC TEMPLATE AND TEXTURAL ANALYSIS

The organic templates and materials' texture before and after DA exchange are analysed in order to understand the successful exchange process for the beta and ferrierite zeolites. The TGA of the as-synthesised beta zeolite is composed by two weight losses centred at 425 and 650 °C (Fig. 5-a); due to the decomposition of the tetraethyl ammonium template (TEA) [23]. Comparison of the TGA before and after NH_4-exchange points out that TEA fully remains during the exchange process. The TGA profiles (Fig. 5-a), TGA weight losses (Table 2) and carbon contents (Table 2) almost coincide. Hence, changes in template content cannot explain the DA exchange process. On the other side, one can consider that the structure may have void space originated from the non-perfect matching between the TEA and the

framework; explaining the effective Na-to-NH_4 exchange under the applied conditions. This hypothesis was investigated by several gas adsorption methods as provided in Figure 6. Nitrogen physisorption derived *t*-plot (Fig. 6-a) was not effective to prove this as it showed solely 0.001 $cm^3.g^{-1}$ of micropore volume, which is within the instrumental error. High-resolution Argon physisorption measurements revealed that the templated beta zeolite adsorbs gas at low relative pressures (Fig. 6-b). This was confirmed by the Horvath-Kawazoe differential pore volume that reveals a certain background level (Fig. 6-c). The presence of void space could be evidenced after applying the NLDFT kernel [20] to the adsorption branch. Figure 6-d gives the cumulative pore volume as a function of the modelled pore width as well as its differential volume increase. The calcined material has a PSD distribution centered at *ca.* 6 Å, which is characteristic of beta zeolite [24] with a micropore volume of 0.268 $cm^3.g^{-1}$ (Table 2). The templated beta material evidences a measurable amount of micropores of 0.014 $cm^3.g^{-1}$ with a maximum also centered at 6 Å. An almost similar quantity was detected after exchange; *i.e.* 0.013 $cm^3.g^{-1}$ (Table 2). This fraction of micropores corresponds to *ca.* 5% of the total micropore volume and it is attributed to the non-perfect matching between the TEA and framework. This fact seems to be very relevant for the exchange process at the conditions applied as it promotes the molecular transport of the cations in- and outwards.

The textural properties of the ferrierite material after NH_4-exchange from Ar physisorption evidences the development of substantial microporosity during the NH_4-exchange process (0.041 $cm^3{\cdot}g^{-1}$, Table 2). This corresponds to almost 37% of the total micropore volume while the starting material has negligible microporosity. The TGA pattern of this material compared to the starting counterpart, indicates a reorganisation of the pyridine template within the structure with the appearance of an additional decomposition step at 650 °C (Fig. 4-b). It must be noted that TGA weight loss and carbon content (CHN analysis) do not show differences in organic total mass among these samples (entries 6 and 7, Table 2). It is suggested that the material can adsorb atmospheric CO_2, which interferes with the pyridine

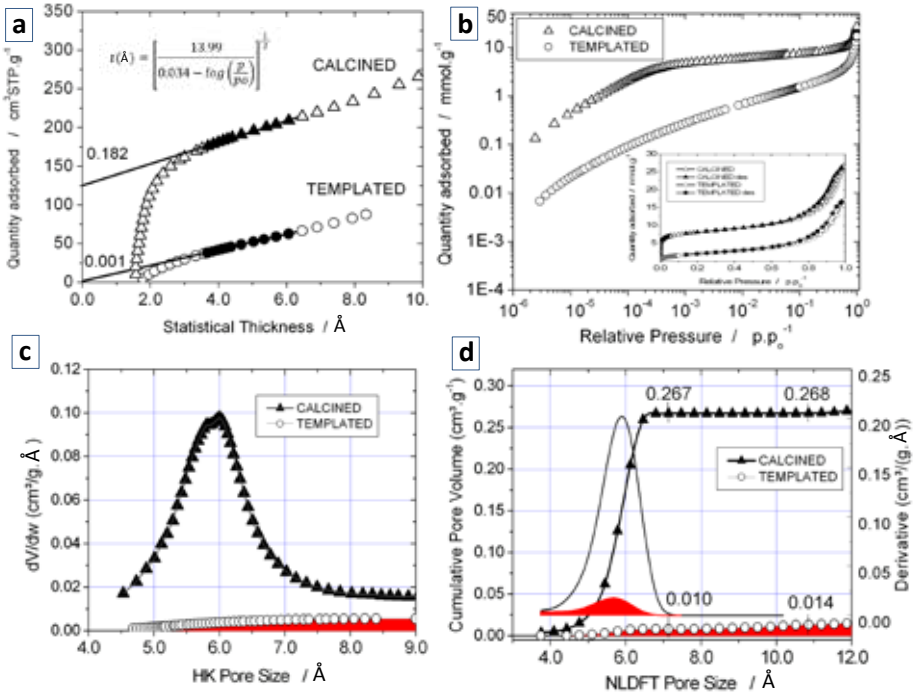

Figure 6. **a)** Harkins-Jura *t*-plot from N_2 gas adsorption (77 K); **b)** low-pressure high-resolution Ar physisorption (88 K) and derived **c)** Horvath-Kawazoe differential pore volume and **d)** NLDFT cumulative pore volume, for the calcined and templated beta materials.

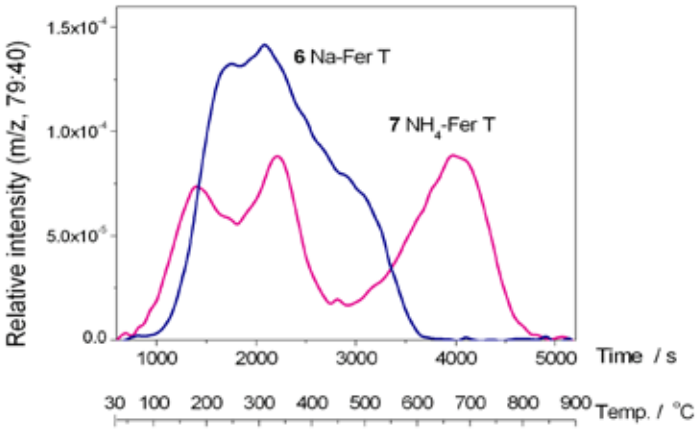

Figure 7. Normalised TGA-EGA-MS patterns (m/z, 79:40, representing pyridine and argon, respectively) for the template decomposition of samples **6** and **7**.

determination by CHN analysis. Alternatively, the amount of pyridine was quantified by evolved gas analysis TGA-MS (Fig. 7). Quantification of the profiles indicates a decrease of *ca.* 6 % of the initial template loading after NH_4-exchange. Hence, two effects are identified during the ferrierite exchange: template removal and its reorganisation. These explain the relatively high microporosity observed for the NH_4-exchanged material; the NH_4-exchange step is able to remove partly the template and rearrange it; this facilitates the Na exchange by NH_4.

2.3.3. RELEVANT MATERIAL PROPERTIES

Relevant properties of the zeolites derived from the DA and CA methods were compared by XRF, ^{27}Al NMR and NH_3-TPD, in order to evaluate the Si/Al ratio, Al coordination and the acidic properties. These are given in Figure 8 and the derived parameters are compiled in Table 3. Concerning the Ferrierite samples, the Si/Al ratios were comparable and both samples display a single Al resonance at *ca.* 54 ppm associated to tetrahedrally coordinated Al; AlO_4 [25,26]. The NH_3-TPD profiles are very similar to each other, presenting weak sites at *ca.* 200 °C and broadly distributed strong acid sites centred at *ca.* 450 °C. Quantification of the acid sites manifests a relatively higher density for the direct activation pathway, *ca.* 7% higher. Such a difference can be attributed to less particle agglomeration, as the DA method makes use of only a single thermal step.

Table 3. Structural Si/Al ratio (XRF), Al coordination (NMR) and acid site density (NH_3-TPD)

Material	Si/Al (at.)	AlO_4/ AlO_6	NH_3 (a.u.)/g
4 H-Bea CA	11.9	2.4	823
5 H-Bea DA	11.1	2.1	906
6 Na-Fer T	26.8	–	–
9 H-Fer CA	25.0	∞	675
10 H-Fer DA	26.0	∞	724

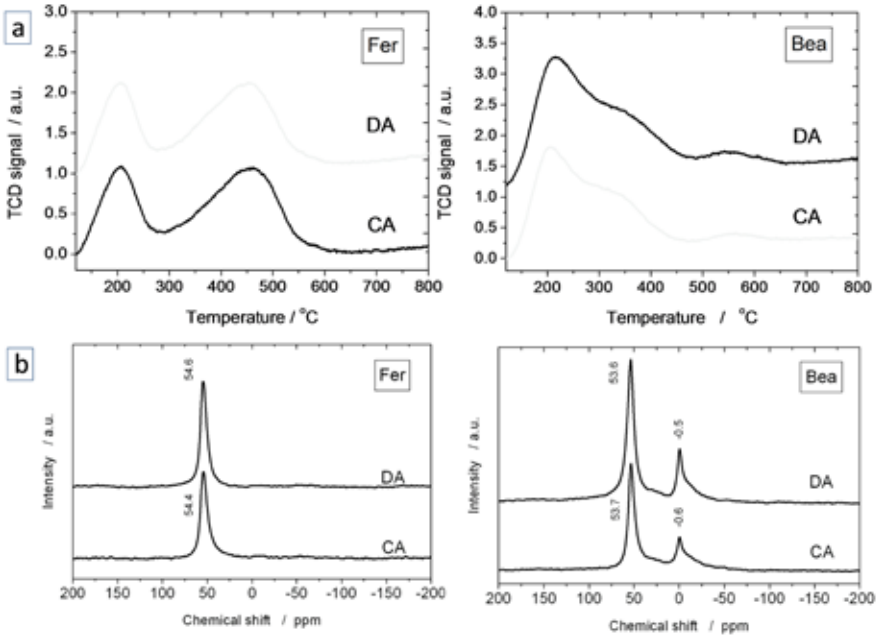

Figure 8. **a)** NH_3-TPD and **b)** ^{27}Al MAS NMR spectra for beta and ferrierite zeolites, via the direct (DA) and conventional (CA) activation.

The properties evaluation of the beta materials derived from the CA and DA routes almost match each other with respect to the Si/Al ratio, acidic properties and Al coordination. The CA material possesses slightly less octahedral Al (species at -0.5 ppm observed in Fig. 8-b right). This is presumably originated from the washing effect of the NH_4NO_3 solution [27] on the fully accessible calcined material; it can remove weakly bonded AlO_6 species. This is consistent with the relatively higher Si/Al ratio. Therefore, the DA method retains more Al and has slightly more in octahedral coordination. The acid site density of the DA method is almost 10% higher than CA (Table 3), that can be ascribed to less particle agglomeration. The acidic properties were furthermore evaluated by means of the liquid-phase catalytic cracking reaction of low-density polyethylene (LDPE), given in Figure 9. The thermal cracking of the free polymer takes place at 467 °C in a single step. The zeolite has a remarkable influence on the decomposition temperature; the CA beta zeolite shows two maxima in the decomposition rate at 314 and

392 °C. The DA beta zeolite presents the first maximum at 291 °C while the second coincides with the CA zeolite. Such a difference in the first step (*ca.* 25°C) suggests that the DA zeolite may be less agglomerated and the liquid polymer can access easier; as soon as the temperature is increased the zeolite particles agglomerate, leading to a similar pyrolysis rate for both zeolites.

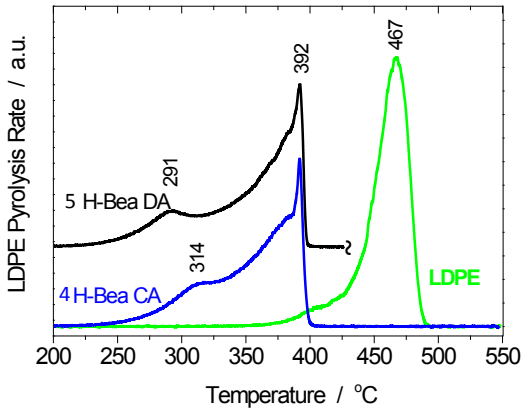

Figure 9. Catalysed decomposition rates in the pyrolysis of low-density polyethylene (LDPE) including the thermal decomposition of LDPE.

2.4. CONCLUSIONS

Two relevant as-synthesised microcrystalline zeolites (beta and ferrierite) can be Na-to-NH_4 exchanged while still containing the pore-filling organic template, while MFI type was intact. A single calcination serves to combust the template and creates the Brønsted sites directly; thus simplifying the activation. Another advantage is that the material suffers less thermal stress. At least three phenomena are relevant to rationalise this route: partial removal of the template (Fer), the remaining template is reorganised within the pores (Fer) and finally, there can be void space due to non-perfect matching between the network and template (Bea). The structural, textural and acidic properties of materials from both methods are in general quite comparable.

2.5. ACKNOWLEDGEMENTS

The authors thank financial support to the Nederlandse Organisatie voor Wetenschappelijk Onderzoek (NWO) under the project VIDI 10284.

2.6. REFERENCES

[1] D.W. Breck, Zeolite Molecular Sieves, Structure, Chemistry and Use, John Wiley & Sons, New York, London, Sydney, Toronto, 1974.

[2] J. Weitkamp and L. Puppe, Catalysis and Zeolites, Fundamentals and Applications, Springer, Berlin, 1999.

[3] J. Cejka, H. van Bekkum, A. Corma, F. Schueth (Eds.), Introduction to Zeolite Science and Practice, 3rd revised edition, Stud. Surf. Sci. Catal.168, Elsevier, Amsterdam, 2007.

[4] R. Xu, W. Pang; J. Yu, Q. Huo and J. Chen, Chemistry of Zeolites and Related Porous Materials. Synthesis and Structure, John Wiley & Sons (Asia), 2007.

[5] J. Cejka, A. Corma, S. Zones (Eds.), Zeolites and Catalysis: Synthesis, Reactions and Applications, Wiley-VCH, Weinheim, 2010.

[6] S.L. Lawton, W.J. Rohrbaugh, Science 247 (1990) 1319-1322.

[7] S.I. Zones, R.A. Vannordstrand, Zeolites 8 (1988) 166-174.

[8] J.C.Jansen, S.T. Wilson, Stud. Surf. Sci. Catal. 137 (2001) 175-227.

[9] X.H. Bu, P.Y. Feng, G.D. Stucky, Science, 278 (1997) 2080-2085.

[10] M. Hunger, Catal. Rev. Sci. Eng. 39 (1997) 345-393.

[11] Section 17.2.2 of reference 5.

[12] G. Ertl, H. Knözinger, F. Schüth, J. Weitkamp (Eds.), Handbook of Heterogeneous Catalysis, Wiley-VCH, Weinheim, 2008, pp. 1955 and 2741.

[13] H.G. Karge and J. Weitkamp, Molecular Sieves Vol. 3, Post-synthesis Modifications. Springer, Berlin-Heidelberg, 2002, pp 205-208.

[14] R. Barrer, Nature 164 (1949) 112-113.

[15] A. Corma, V. Fornes, S.B. Pergher, T.L.M. Maesen, J.G. Buglass, Nature. 396 (1998) 353-356.

[16] K. Na, M. Choi, W. Park, Y. Sakamoto, O. Terasaki, R. Ryoo, J. Am. Chem. Soc. 132 (2010) 4169-4177.

[17] D.P. Serrano, J. Aguado, G. Morales, J.M. Rodriguez, A. Peral, M. Thommes, J.D. Epping, B.F. Chmelka, Chem. Mater. 21 (2009) 641-654.

[18] J. Song, L. Ren, C. Yin, Y. Ji, Z. Wu, J. Li, F. Xiao, J. Phys. Chem. C. 112 (2008) 8609-8613.

[19] A. Saito and H. C. Foley, Micropor. Mater. 3 (1995) 531-542.

[20] Micromeritics V3.04 1994-2008, ASAP 2020.

[21] IZA Synthesis Commission; URL: www.iza-online.org/synthesis.

[22] IZA Structure Commission; URL: www.iza-structure.org.

[23] E. Bourgeat-Lami, F. Di Renzo, F. Fajula, P. Hubert Mutin, T. Des Courieres, J. Phys. Chem., 96 (1992) 3807-3811.

[24] I. Melián-Cabrera, F. Kapteijn, J.A. Moulijn, Chem. Commun., 21 (2005) 2744-2746.

[25] F.R. Chen, J.G. Davis, J.J. Fripiat, J. Catal. 133 (1992) 263-278.

[26] A.P.M. Kentgens, Geoderma 80 (1997) 271-306.

[27] E. Bourgeatlami, P. Massiani, F. Di Renzo, P. Espiau, F. Fajula, T. Courieres, Appl. Catal. 72 (1991) 139-152.

3

Based on:

María J. Ortiz-Iniesta and Ignacio V. Melián-Cabrera .

Fenton chemistry-based detemplation of an industrially relevant microcrystalline beta zeolite. Optimisation and scaling-up studies.

Microporous and Mesoporous Materials, 2014, 206, 58-66

(DOI: 10.1016/j.micromeso.2014.12.019)

Fenton Chemistry-Based Detemplation Of An Industrially Relevant Microcrystalline Beta Zeolite. Optimisation And Scaling-Up Studies

ABSTRACT

A mild template removal of microcrystalline beta zeolite based on Fenton chemistry was optimised. Fenton detemplation was studied in terms of applicability conditions window, reaction rate and scale up. TGA and CHN elemental analysis were used to evaluate of the detemplation efficiency, while ICP, XRD, LPHR-Ar physisorption, and ^{27}Al MAS NMR were applied to characterise the structure and texture of the resulting materials. The material properties were compared to calcination. By understanding the interplay of relevant parameters of the Fenton chemistry, the process can be optimised in order to make the process industrially attractive for scale-up. The utilisation of H_2O_2 can be minimised down to 15 mL H_2O_2/g (88 °C, 30 ppm Fe); implying a high solid concentration and low consumption of H_2O_2. When Fe concentration usage must be minimised, values as low as 5 ppm Fe can be applied (88 °C, 30 mL H_2O_2/g) and still achieve full detemplation. The reaction time to completeness can be reduced to 5 h when combining a Fe-oxalate catalyst with UV radiation. The protocol was scaled up 100 times larger than the original recipe. In terms of the material's properties, the scaled material is structurally comparable to the calcined counterpart (comparable Si/Al and XRD patterns), while it displays benefits in terms of texture and Al-coordination, the latter with full preservation of the tetrahedral Al.

Keywords: zeolites, zeolite beta, calcination, template removal, Fenton chemistry, dealumination.

3.1. INTRODUCTION

Progress in relevant areas of oil-refining, petrochemistry, fine chemicals and pollution abatement can be attributed to zeolites [1-6]. Zeolites are microporous crystalline aluminosilicates that have many exploitable properties such adsorption, separation and catalysis. They are typically synthesised at specific conditions with very precise gel compositions [7]. Often hydrothermal conditions are necessary to provoke the nucleation and crystal growth in the presence of mineralisers, such as NaOH, $NaAlO_4$ or fluoride compounds.

Among the various synthetic approaches, the use of organic structural directing agents (SDA) has been crucial to discovering new zeolites [8-13]. This was possible due to the introduction of quaternary and diquaternary alkyl ammonium compounds, amines, alkylphosphonium salts and phosphazenes, among the most relevant ones. The removal of these SDA molecules is an essential step in order to obtain the final porous network. This step is normally carried out by calcination of the dried gel at temperatures ranging 500 up to 650 °C [3,4]. For the case of ill-crystalline zeolites, having crystal sizes below 1 μm, such type of calcination is problematic. The inorganic network is unstable, in particular when the Al concentration is high. This is caused by the longer distance of the Al-O bonds that makes it easily to be hydrolysed in the presence of the self-generated steam during calcination. This is the case of beta zeolite [14-16]. Recent advances in beta zeolite synthesis are in the direction of template-free routes and some remarkable examples have been reported [17-19]. However, the current industrial manufacturing process of beta zeolite still involves tetraethyl-ammonium hydroxide (TEA) as SDA; the organic template seems to be crucial to control the crystal growth. However, the removal of the TEA by calcination in zeolite beta is known to have serious drawbacks; the most remarkable is the dealumination with the formation of extra framework species [20-23]. Therefore, it has been a challenge to find alternative routes to detemplate beta zeolite at milder conditions.

Studies on solvent extraction of SDAs by Davis and co-workers reported that successful extraction is limited to the case that the SDA has

a smaller size than the pore opening of the zeolite, and secondly, weak interactions with the zeolite framework [24]; in the case of Al-beta zeolite around 50% of the template could be extracted. Solvent extraction applied to a colloidal beta zeolite removed most of the SDA, and ~65% of the microporosity was developed [25]. Cold plasma has been successfully applied to nano-sized beta zeolite, with full template removal and structural preservation. The acidic properties, density and strength, for the plasma-derived route were lowered when compared to the calcined route [26]. In parallel to these studies, a mild detemplation method based on highly-oxidising $OH^{\bullet}$ radicals to decompose the SDA of a microcrystalline beta zeolite was proposed by Melián-Cabrera *et al.* [27-29]. More recently, the approach was extended to a soft MCM-41 [30] and SBA-15 [31]. This methodology has been successfully applied to mesoporous silicates and aluminosilicates [32,33], RUB-18 [34], aluminophosphates [35,36], silicalite-1 colloids, and transparent composite film containing zeolite nanoparticles for organic light emitting devises (OLED) [37]. A simultaneous detemplation and metal introduction method has been reported as well [38-40]. A simplified route using H_2O_2 in the absence of Fe has been successfully applied to mesoporous silicates such as MCM-56 [41], regeneration of Al-doped ZSM-5 membranes [42], and silicoalumina phosphates (SAPO-34) [36]. Other attempts to generate $OH^{\bullet}$ radicals from H_2O_2 were assisted by UV light radiation to detemplate SBA-15 [43], and microwave irradiation over nano-beta particles [44] and AlPO-5 [45].

Fenton chemistry-based detemplation consists of using $OH^{\bullet}$ radicals as oxidising agents to remove the organic templates in zeolites, zeotypes and mesopororous materials. These radicals are normally originated from the catalytic decomposition of H_2O_2 at low temperature, using a Fe salt as catalyst at ppm level, though it can be assisted by UV radiation. In order to make this approach industrially attractive for zeolite activation, there are a number of aspects that require careful consideration. In this work we have carried out systematic studies considering those practical aspects, such as: the influence of relevant parameters on detemplation (temperature, Fe concentration and H_2O_2 utilisation), optimisation about reducing

the utilisation of H_2O_2 and Fe concentration, reduction of the reaction time aided by UV irradiation, and scaling-up investigation and the evaluation of relevant properties for the derived scaled-up material. These investigations have been carried out on an industrially relevant zeolite beta.

3.2. EXPERIMENTAL

3.2.1. MATERIALS

Stabilised hydrogen peroxide (30 *wt.*% H_2O_2 in H_2O), nitric acid, (65 *wt.*%, pro analysi) and ammonia solution (25 *wt.*%, pro analysi) were purchased from Merck. Non-stabilised hydrogen peroxide (30 *wt.*% H_2O_2 in H_2O) was purchased from Sigma-Aldrich. $Fe(NO_3)_3 \cdot 9H_2O$ (98 %, metal basis, denoted as Fe^{III}-nitrate) and $(NH_4)_3[Fe(C_2O_4)_3] \cdot 3H_2O$ (pure, denoted as Fe^{III}-oxalate) were supplied by Riedel-de-Haën. NH_4-templated beta zeolite (HSZ-930A) was purchased from TOSOH Corporation.

3.2.2. DETEMPLATION PROTOCOLS

3.2.2.1. CALCINATION

The general calcination procedure was carried out in a LT9/11 Nabertherm box furnace. The samples were loaded in porcelain crucibles in shallow bed configuration, heated from 30 to 550 °C at 5 °C/min and held at 550 °C for 6 h.

3.2.2.2. FENTON CHEMISTRY-BASED DETEMPLATION

Standard experiment: 0.5 g of raw zeolite was mixed with the desired amount (15 mL) of 30% H_2O_2 (stabilised or non-stabilised; non-stabilised was used for temperatures ≤70 °C) and stirred until the mixture was homogeneous. Then,

the chosen concentration of Fe was adjusted. In the standard experiment 30 mg Fe/Kg (referred as ppm) was used. This concentration was obtained by adding 65 µL of a stock solution (5 g Fe^{III}-nitrate or 5.28 g Fe^{III}-oxalate in 100 mL of deionised water). The pH was adjusted to 4 using diluted HNO_3. The flask containing the reaction mixture was submerged in a pre-heated oil bath at the desired temperature (79 °C in this case) and it was maintained for 24 h under stirring and refluxing to prevent evaporation. The solid was separated by centrifugation, washed with deionised water and dried overnight at 80 °C in a stove oven. In other cases, the pH of the resulting mixture was below 4 and it was adjusted using a diluted NH_3 solution.

Optimisation studies: For the optimisation studies, temperature was evaluated from room temperature to 90 °C, the Fe concentration from 0 to 60 ppm, and H_2O_2 utilisation from 10 to 90 mL/g. The influence of the H_2O_2 type was investigated using stabilised and non-stabilised H_2O_2. The pH was adjusted with either diluted HNO_3 or NH_3 depending on the applied Fe ppm and H_2O_2 utilisation. For the evaluation of the dominant parameters, boundary conditions were selected according to Table 1.

Kinetic study: In the time-dependency pseudo-kinetic study, Fe^{III}--nitrate and Fe^{III}-oxalate were used as precursors; the concentration was fixed at 30 and 60 ppm and reaction times ranged from 1 to 20 h. Individual experiments were performed for each reaction time. A water-bath was used to keep the reaction temperature constant at 70 °C.

Photo-Fenton: The experiments assisted with UV-light (5.5 W Hg lamp) were performed in a commercial set-up (Aceglass, 7880-60) which was modified for this purpose. The preparation of the reaction mixture follows the same procedure than the standard protocol detailed above. In this case, two Fe sources were employed: Fe^{III}-nitrate and Fe^{III}-oxalate. The reaction time ranged between 1 and 8 hours.

Scale-up experiment: 16.67 g of zeolite was mixed with 500 mL of stabilised H_2O_2 and 2.166 mL of Fe^{III}-nitrate stock solution (5 g Fe^{III}-nitrate in 100 mL of deionised water), and the standard protocol described above was followed.

3.2.3. CHARACTERISATION

Thermogravimetric analyses (TGA) were carried out in a Mettler-Toledo (TGA/SDTA851e) analyser using a flow of synthetic air of 80 mL/min (NTP). Typically, 5-10 mg of sample was loaded in a 70 μL γ-Al_2O_3 crucible and the temperature was increased from 30 to 900 °C at 10 °C/min. Blank curve correction using an empty crucible was subtracted.

CHN elemental analyses were carried out in a EuroVector 3000 CHNS analyser. All analyses were done in duplicate to check sample heterogeneity; the standard deviation was below 2 *wt.*%. Approximately 2 mg of sample was accurately weighed in a 6-digit analytic balance (Mettler-Toledo). The samples were burned at 1800 ºC in the presence of an oxidation catalyst and decomposed into CO_2, H_2O and N_2. These gases were then separated in a Porapak QS column at 80 °C and quantified with a TCD detector. Acetanilide (99.9 %, Heka Tech) was used as external standard.

Inductively coupled plasma atomic emission spectroscopy (ICP-AES) analyses were carried to determine the Si/Al ratio and the concentration of residual Fe in the samples. To that effect, a known amount of solid sample was dissolved in a 6 *wt.* % HF solution overnight to ensure complete dissolution. The liquid concentration was determined in a Perkin-Elmer (Optima 7000 DV) instrument.

Powder X-ray diffraction (XRD) spectra were collected with a Bruker D8 powder X-ray diffractometer using CuKα radiation, λ=1.54056 Å. The spectra were recorded with a step size of 0.02°; 3 seconds (s) accumulation time and in the 2θ angle range of 5-60°.

Textural analyses were carried out by Ar physisorption at -186 °C, in a Micromeritics ASAP 2020. Prior to the measurements, the samples were outgassed under vacuum at 300 ºC for 12 h. The Fenton-derived materials were degassed at 150 ºC. The surface area was calculated by BET method (S_{BET}). The single point pore volume (V_T) was estimated from the amount adsorbed at a relative pressure of ~0.98 in the desorption branch. The micropore parameters were determined from the *t*-plot model, cumulative pore

volume and surface area. The pore size distribution was determined from the Horvath-Kawazoe differential model.

^{27}Al magic angle spinning nuclear magnetic resonance (MAS-NMR) measurements were conducted on a Bruker Avance-400 spectrometer using a 4 mm zirconium holder, applying spinning frequency of 11 kHz at 25 °C. The ^{27}Al MAS NMR spectra were obtained at 104.201 MHz, with acquisition delay of 1 s and acquisition time of 0.08 s. Typically 4000 scans were collected. The spectra were referenced with respect to 1.0 M aqueous solution of $Al(NO_3)_3$ set on 0 ppm.

3.2.4. DEFINITIONS

TGA-BASED DETEMPLATION EFFICIENCY:

$$\eta^{TGA}\ (\%) = \left[1 - \frac{TGA_{200-900}(\text{sample}) - Wo}{TGA_{200-900}(\text{raw}) - Wo}\right] \times 100 \qquad (1)$$

Where $TGA_{200\text{-}900}$(sample) is the TGA weight loss between 200 and 900 °C for any sample, $TGA_{200\text{-}900}$(raw) is the TGA weight loss for the zeolite containing the template and *Wo* is the TGA weight loss of a reference material consisting of a fully detemplated beta zeolite where full detemplation was confirmed by carbon elemental analysis. *Wo* corresponds to the experiment using 30 mL H_2O_2/g, 30 Fe ppm at 70 °C for 24 h (scale-up experiment). This weight loss has two contributions; first, the condensation of the silanol groups, which condensate at temperatures higher than 300 °C. And secondly, residual NH_4 groups after detemplation, available in the original zeolite (NH_4-form). During TGA experiments, these groups release at temperatures > 300 °C, contributing to *Wo* as well. Thus, this parameter will account for the release of dehydroxylation water and residual NH_4-groups.

CHN-BASED DETEMPLATION EFFICIENCY:

$$\eta^{C}(\%) = \left[1 - \frac{C_{CHN}(\text{sample})}{C_{CHN}(\text{raw})}\right] \times 100 \qquad (2)$$

Where C_{CHN}(sample) is the carbon content determined by elemental analysis of the material under study and C_{CHN}(raw) is the carbon content of the raw material (BT-*raw*) determined in the same way.

MESOPORE VOLUME:

$$V_{MESO}^{t-plot}\ (cm^3/\text{g}) = V_T\ -\ V_{\mu}^{t-plot} \qquad (3)$$

Where V_T (cm^3/g) is the total pore volume and is the corresponding micropore volume according to the *t*-plot model:

$$r(\text{Å}) = \left[\frac{13.99}{0.034 - log\left(\frac{p}{p_0}\right)}\right]^{1/2} \qquad (4)$$

MESOPORE SURFACE AREA:

$$S_{MESO}^{t-plot}\ (m^2/\text{g}) = S_{BET} -\ S_{\mu}^{t-plot} \qquad (5)$$

Where S_{BET} (m^2/g) is the specific surface area determined by the BET model and is the corresponding micropore surface area for pores ≤ 20 Å, determined by the *t-plot* model (eq. 4).

IRON ADSORPTION:

$$\text{Fe}^{ADS}(\%) = \left[\frac{\text{Fe}^{ICP}(\text{material}) - \text{Fe}^{ICP}(\text{calcined})}{\text{Fe (applied Fenton solution)}}\right] \times 100 \qquad (6)$$

Where Fe^{ICP}(material) is the concentration of Fe measured on the dried material after Fenton detemplation by ICP, Fe^{ICP}(calcined) is the measured ICP value for the BT-*C* calcined material, which contains Fe impurities, and

Fe (applied Fenton solution) is the applied Fe concentration of the solution used to catalyse the Fenton reaction.

3.3. RESULTS AND DISCUSSION

3.3.1. INFLUENCE OF RELEVANT DETEMPLATION PARAMETERS

The kinetics of Fenton reaction are known to be dependent on several parameters [46-48]: reactor geometry and scale, temperature, concentration of Fe and H_2O_2, pH, stirring and addition modes. The first step in the optimisation of this procedure was to determine which variables are relevant for zeolite detemplation. Thus, the influence of the temperature, Fe concentration and H_2O_2 utilisation was investigated. Preliminary experiments were performed to test the reaction scale (between 5 and 15 mL) and reactor geometry (cylinder or bulb); and no substantial differences on the detemplation level were found, as long as the temperature was well controlled. The pH was adjusted at the beginning of the reaction for all the experiments, and the parameters related to the experimental protocol such as stirring rate and addition mode were kept constant. Subsequently, the additional experimental parameters for optimisation were chosen: reaction temperature, H_2O_2 utilisation (mL per gram of zeolite) and Fe concentration.

Table 1. Detemplation conditions corresponding to the experimental design.

Parameters	**H1**	**H2**	**H3**	**H4**
P1: Detemplation temperature (°C)[a]	88	88	70	70
P2: H_2O_2 utilisation (mL/g)	30	10	30	10
P3: Iron concentration (ppm)	60	0	0	60
Detemplation level (η^{TGA}, %)	99	19	25	37

[a]: The resolution of the Hadamard matrix is carried out using absolute temperature.

In order to determine how these parameters affect the detemplation level, a model based on the Hadamard design was applied [49,50]. This model is based on experimental values and it provides the level of influence of each parameter. Since it is a relatively simple model, the dependency between parameters is not considered. Once the variables were defined, the range (i.e. minima and maxima) has to be determined experimentally. These values will determine the barriers where the model works. The experimental conditions of the four experiments (denoted as H1, H2, H3 and H4) are given in Table 1. In this Hadamard design, the influence of three chosen variables was studied on the level of zeolite detemplation. The following equations (7-10) were solved:

$$y_1 = \theta_0 + \theta_1 + \theta_2 + \theta_3 + e_1 \qquad (7)$$

$$y_2 = \theta_0 + \theta_1 - \theta_2 - \theta_3 + e_2 \qquad (8)$$

$$y_3 = \theta_0 - \theta_1 + \theta_2 - \theta_3 + e_3 \qquad (9)$$

$$y_4 = \theta_0 - \theta_1 - \theta_2 + \theta_3 + e_4 \qquad (10)$$

where y_1, y_2, y_3 and y_4 are the experimental values of the parameter to be optimised; θ_1, θ_2 and θ_3 are the values of the parameters P_1, P_2 and P_3, respectively; and θ_o is their average value. The associated errors are e_1, e_2, e_3 and e_4. The estimated values θ_o, θ_1, θ_2 and θ_3 are applied in Eq. (11) being Y the parameter to be optimised (degree of detemplation).

$$Y = \theta_0 + \theta_1 P_1 + \theta_2 P_2 + \theta_3 P_3 \qquad (11)$$

For this set of experiments, the 4×4 Hadamard matrix was defined according to equations (12-15):

$$99 = \theta_0 + \theta_1 + \theta_2 + \theta_3 + e_1 \qquad (12)$$

$$19 = \theta_0 + \theta_1 - \theta_2 - \theta_3 + e_2 \quad (13)$$

$$25 = \theta_0 - \theta_1 + \theta_2 - \theta_3 + e_3 \quad (14)$$

$$37 = \theta_0 - \theta_1 - \theta_2 + \theta_3 + e_4 \quad (15)$$

that were solved as:

$$Y = 48.8 + 17.3P_1 + 16.8P_2 + 23.3P_3 \quad (16)$$

All the parameters have positive coefficients, meaning that their increase would imply a detemplation improvement. Quantitatively, very similar influence was found for the reaction temperature (P_1) and H_2O_2 utilisation (P_2): 17.3 and 16.8, respectively. Remarkably, the Fe concentration (P_3) showed the largest influence, 23.3. However, from the practical point of view, increasing the Fe concentration excessively would be negative in terms of the purity of the final material and acidity, since Fe ions will replace H^+ on the Brønsted sites. Incrementing the amount of H_2O_2 is also detrimental to the final process costs. Temperature seems to be the way to enhance further the detemplation level. This approach was applied systematically in the forthcoming study.

3.2. EXPERIMENTAL OPTIMISATION

The fundamentals of Fenton chemistry have been studied for the treatment of residual water and soils. It consists of the decomposition reaction of H_2O_2 in the presence of Fe^{II} to generate hydroxyl radical ($OH^{\bullet}$), eq. 17; then, the reduction of Fe^{III} with H_2O_2 produces new Fe^{II} (eq. 18) that closes the cycle:

$$H_2O_2 + Fe^{2+} \rightarrow OH^{\bullet} + OH^- + Fe^{3+} \quad (17)$$

$$H_2O_2 + Fe^{3+} \rightarrow HO_2^{\bullet} + H^+ + Fe^{2+} \quad (18)$$

The hydroxyl radical reacts with organic compounds with bimolecular rate constants as high as 10^7 to 10^{10} L/mole·s [46-48,51]. Besides the main reactions, other competing reactions occur as well:

$$RH + OH^{\bullet} \rightarrow H_2O + R^{\bullet} \quad (19)$$

$$OH^{\bullet} + Fe^{2+} \rightarrow OH^- + Fe^{3+} \quad (20)$$

$$R^{\bullet} + Fe^{3+} \rightarrow Fe^{2+} + products \quad (21)$$

$$R^{\bullet} + OH^{\bullet} \rightarrow ROH \quad (22)$$

$$R^{\bullet} + H_2O_2 \rightarrow ROH + OH^{\bullet} \quad (23)$$

$$HO_2^{\bullet} + Fe^{3+} \rightarrow O_2 + Fe^{2+} + H^+ \quad (24)$$

$$OH^{\bullet} + H_2O_2 \rightarrow HO_2^{\bullet} + H_2O \quad (25)$$

Where RH represents the substrate to be oxidised, is an organic radical (derived from the RH substrate) and HO_2 is a superoxide radical. The rate constants of the equations 18, 21 and 24 are also pH dependent [52]. As a result of the high reaction kinetic constants, second order and complexity of side reactions, temperature, Fe concentration and H_2O_2 utilisation require optimisation.

The focus of this optimisation is to find suitable conditions to enable the application of this process on a larger scale. It means using the lowest possible H_2O_2 utilisation and Fe concentration, the latter for proper temperature control due to the exothermic and radical reaction, and to prevent acid site density depletion. Therefore, an experimental screening study varying the H_2O_2 utilisation, Fe concentration, temperature and reaction time was carried out; using two types of H_2O_2, stabilised and non-stabilised.

The determination of the detemplation level was carried out by TGA as analysis technique of choice. In order to confirm the TGA results, control experiments by CHN elemental analysis were performed as well, in the raw and selected resulting materials. For detemplation levels >95% there was no correlation between TGA (η^{TGA}) and CHN (η^{CHN}), Fig. S-1. Possibly because the techniques are near the detection limit, since the materials under analysis possess a low organic content. It was assumed that for η^{CHN} or η^{TGA} ≥ 95% full template removal can be considered.

The results from this study are compiled in Table 2, where some general trends can be observed. Reaction temperature, H_2O_2 utilisation and Fe concentration have a positive effect on the detemplation level. These results are consistent with the theoretical findings derived from the Hadamard design.

At low temperatures, RT and 40 °C, stabilised H_2O_2 did not show much detemplation (data no shown). For comparison, non-stabilised H_2O_2 was employed in this range and it showed detemplation values up to 37%. At higher temperatures such as 70 °C, the use of *non*-stabilised H_2O_2 brought also some benefits such as the reduction of H_2O_2 utilisation from 30 to 20 mL (30 h reaction, 30 ppm of Fe), and the Fe concentration from 30 to 10 ppm (30 mL H_2O_2/g, 24 h reaction), achieving a 97% and 98% detemplation respectively. The attained benefits of the use of *non*-stabilised H_2O_2 likely come from the absence of stabilizers, usually phosphates, which prevent the decomposition of H_2O_2. Moreover, the stabilizers can precipitate Fe cations ($FePO_4.2H_2O$, pK_s = 15 [53]) and consequently, Fe will suffer a reduction on its effective concentration in solution.

It was generally found that temperature can compensate Fe concentration. At 30 mL/g H_2O_2 utilisation when temperature is increased from 70 to 79 °C, the Fe concentration can be lowered to half (30 to 15 ppm) to achieve a 91 % detemplation. While at 88 °C, only 5 ppm were needed to achieve full detemplation. A similar trend was observed at 15 mL/g H_2O_2 utilisation and 30 ppm of Fe: the detemplation improved from 40% at 70 °C to 95% at 88 °C.

Table 2. Summary of the detemplation levels (η^{TGA}, %) as a function of temperature, Fe concentration (ppm), H_2O_2 utilisation (mL/g) and reaction time (hours). Two types of commercial H_2O_2 were employed: stabilised, and non-stabilised (values in italic). Underlined values correspond to the detemplation efficiency based on CHN (η^{C}).

Temperature (°C)	H_2O_2 (mL/g)	Reaction time (h)	Iron concentration (ppm)					
			0	5	10	15	30	60
RT	**10**	**24**	-	-	-	-	*25*	-
40	**30**	**8**	-	-	-	-	-	*32*
	30	**24**	*36*	-	*32*	-	*32*	*37*
	30	**48**	*22*	-	*30*	-	-	-
70	**10**	**24**	-	-	*31*	-	*31*	37
		30	-	-	-	-	*46*	-
	15	**24**	-	-	-	-	40	-
		30	-	-	*41*	-	*64*	-
	20	**24**	-	-	-	-	47/*56*	-
		30	-	-	*63*	-	*97*	-
	30	**11**	-	-	-	-	-	*99*
		24	25/*30*	-	*98*	45	100/*99*/<u>96</u>	100/*99*/<u>98</u>
		41	*32*	-	-	-	-	-
79	**10**	**24**	-	-	-	22	-	32
	15	**24**	-	-	-	73	40	65
	20	**24**	-	26	31	76	92	92
	30	**24**	22	32	89	91	95/<u>99</u>	96/<u>96</u>
88	**10**	**24**	19	-	-	-	-	-
	15	**24**	-	-	-	86	95/<u>93</u>	-
	20	**24**	29	93	93	97/<u>92</u>	-	-
	30	**24**	48	98/<u>97</u>	-	-	-	99

A trend between H_2O_2 utilisation and temperature was observed as well. At 70 and 79 °C 30 mL of H_2O_2/g are required for full detemplation (30 ppm Fe), while at 88 °C it can be reduced to 20 mL/g (97%, 15 ppm Fe) and 15 mL/g (95%, 30 ppm Fe). It indicates also that under isothermal conditions, there is interplay between H_2O_2 and Fe concentration: a reduction in H_2O_2 requires an increase in Fe concentration. This was just discussed at 88 °C. At 70 °C, the H_2O_2 utilisation can be reduced from 30 to 20 mL/g by increasing the Fe concentration from 10 to 30 ppm.

A similar effect occurs at 79 °C, 30 to 20 mL H_2O_2/g with an increase of 15 to 30 ppm Fe, though in this case the detemplation was partial (~90%).

Control experiments, where no Fe was added, were performed for comparison. The same temperature dependency was observed but reaching a maximum of 48% detemplation at the highest applied temperature, 88 °C. The presence of partial detemplation in these cases may be due to the combination of two factors: H_2O_2 is an oxidant by itself (E^o=1.77 eV) [53], and the possible catalytic effect of Fe impurities present in the zeolite [54,55]. These blank experiments show that the addition of Fe as catalyst is crucial to achieve full detemplation on zeolite beta.

An important parameter for the final sample purity is the applied Fe concentration. Fe could be reduced from 30 to 10 ppm at 70 °C, using non-stabilised H_2O_2, with full detemplation using 30 mL H_2O_2/g of zeolite. At 79 °C, the Fe concentration could not be reduced, while at 88 °C the Fe concentration could be decreased to 15 ppm (20 mL/g) or 5 ppm (30 mL/g).

In summary, from the optimisation study two set of conditions seem to be appealing for large-scale application of this methodology. When the H_2O_2 needs to be reduced, the optimal conditions were found at 88 °C using 15 mL/g and 30 ppm Fe. It means a relatively high solid concentration (6.25 wt.%) and low consumption of H_2O_2. If Fe should be limited in the final zeolite product composition, optimal conditions are found at 88 °C, 30 mL/g and 5 ppm Fe.

3.3. KINETIC STUDY

Additional studies using Fe concentrations of 30 and 60 ppm at different reaction times but at fix temperature (70 °C) and pH (4) were performed in order to understand the kinetic influence of the concentration, Fe source and UV-assistance. The results are given as detemplation level (η^{TGA}) as a function of the reaction time in Figure 1. A clear effect was observed when the Fe concentration was increased; the reaction time to achieve full detemplation was shortened from 20 to 8 hours.

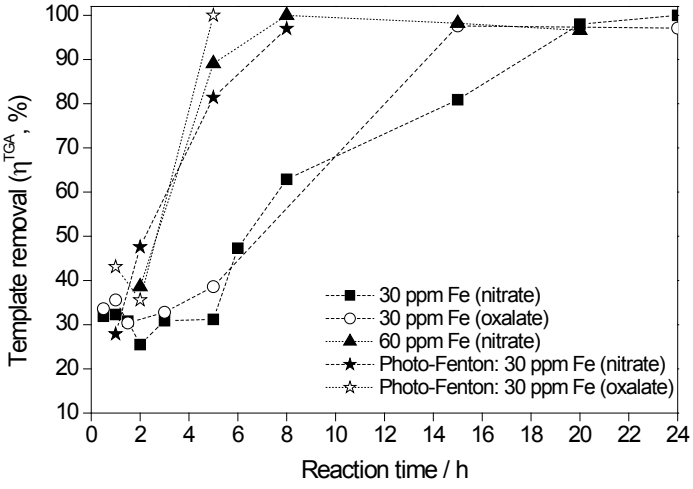

Figure 1. Kinetic study under dark and UV-light conditions. Template removal (η^{TGA}, %) as a function of the reaction time using 30 and 60 ppm of Fe. Fe^{III}-nitrate and Fe^{III}-oxalate were used as iron sources and the reaction temperature was kept constant at 70 °C. The use of UV-Vis light (5.5 W) was applied for 30 ppm Fe^{III}-nitrate and Fe^{III}-oxalate.

Looking at the TGA patterns of partially detemplated materials (Fig. 2), an additional decomposition peak (step IV) centred at *ca.* 130 °C was observed, that is absent in the raw zeolite decomposition. This temperature is lower than the template decomposition peaks (steps II and III) of the raw material (BT-*raw*) and higher than adsorbed water (step I). According to reported thermal analysis studies [56], step IV can be assigned to oxalate group decomposition. Oxalates are commonly formed during Fenton oxidation of aliphatic-based compounds [48]. Under the presence of Fe, the formation of Fe-oxalate complexes during the process would be favourable thermodynamically, due to their high stability constants (log K_1 (Fe^{II}-oxalate) > 4.7; log K_1 (Fe^{III}-oxalate) = 9.4 [53]). Therefore, the TGA observation suggests the presence of Fe-oxalates. In order to understand if Fe-oxalate complexes play a role, Fe^{III}-oxalate was directly used as Fe-source. The results are shown in Figure 1. A reduction in the reaction time to achieve full detemplation was observed, from 20 to 15 hours. This enhancement is an indication on the favourable role of stabilizing Fe by complexation during the detemplation.

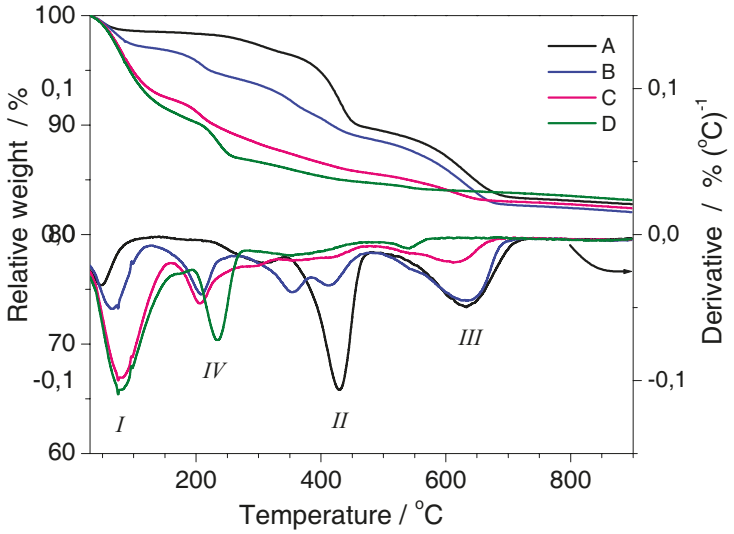

Figure 2. TGA and DTGA patterns of the partially Fenton detemplated materials at different H_2O_2 utilisation: (**B**) 10 mL/g; (**C**) 15 mL/g; and (**D**) 30 mL/g at 79 °C and 60 ppm of Fe. BT-*raw* was added for comparison (**A**).

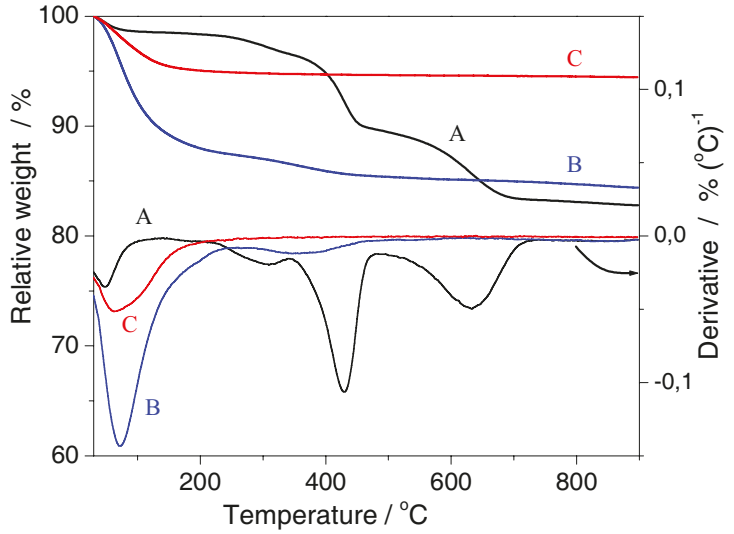

Figure 3. TGA/DTGA patterns of the raw beta zeolite (A, BT-*raw*), scaled-up Fenton detemplated (B, BT-*fsu*) and calcined (C, BT-C).

According to the literature [48,57-60], UV light radiation assists the Fenton reagent in the decomposition of aromatic and aliphatic compounds, leading to higher yields and faster reaction rates. Furthermore, Sulzberger *et al.* reported that UV light in combination with Fe-oxalate complexes give a higher efficiency than using other Fe salts [59,60]. Considering this background information, light-assisted reactions were carried out using Fe-oxalate and Fe-nitrate (30 ppm in both cases). The results are shown in Figure 1. According to our expectations, the reaction time to achieve full detemplation was notably reduced from 15 to 5 hours by combining UV-light and Fe-oxalate; and from 24 to 8 hours combining UV-light and Fe-nitrate as the Fe source.

3.3.4. SCALE UP

After investigation on the experimental window where the Fenton chemistry works optimally for the detemplation of such an industrially-relevant beta zeolite, the experiment was scaled up. For that purpose, the following conditions were applied: 30 mL H_2O_2/g, temperature 70 °C and 30 ppm of Fe.

The scale was progressively increased from 5 mL to 500 mL, through 30 and 200 mL. Full detemplation was achieved in all the cases. As example, the TGA pattern for the 500 mL-scale is shown in Fig. 3. It consists of pronounced weight loss at *ca.* 100 °C due to water desorption and a secondary weight loss at *ca.* 350 °C due to the release of NH_4 groups [28], that is absent in the calcined material. The template removal was confirmed via CHN elemental analysis, where less than a 0.05% of elemental C was found, see BT-*fsu* in Table 3 for the 500 mL-scale experiment, indicating a detemplation efficiency > 99%.

Table 3. Summary of the detemplation conditions, CHN elemental analysis (*wt.*%), Si/Al and Fe composition for the optimal and reference materials.

Material	Si/Al ratio	Fenton conditions			Elemental analysis / *wt.* %					
		H_2O_2 / mL/g zeolite	T / °C	[Fe] / ppm	C	H	N	Fe	Fe^{ADS} / %	η^C / %
BT-*raw*	13.5[a]	-	-	-	10.4	2.1	1.6	-	-	0
BT-*C*	13.1	-	-	-	0.0	0.3	0.0	0.01	-	100
BT-*f*	12.4	30	70	30	0.4	1.1	1.5	0.08	64	96
BT-*fsu*	12.8	30	70	30	<0.1	1.3	1.3	0.10	83	>99

[a]: Commercial specifications.

3.3.5 MATERIAL PROPERTIES

3.3.5.1. STRUCTURE AND COMPOSITION

The structural characteristics of the Fenton-scaled beta zeolite was analysed by XRD and compared to the calcined counterpart (Fig. 4). The XRD profile of Beta zeolite is a combination of sharp and broad diffractions as a result of the intergrowth of the polymorphs A and B. Both materials show the typical diffractions for BEA structure. Based on the XRD patterns, no substantial structural differences were observed after the Fenton-based treatment compared to calcination.

ICP elemental analysis was performed in order to quantify a possible dealumination due to the acidic medium applied during the Fenton detemplation process (Table 3). Analyses show negligible variation of the Si/Al ratio for BT-*C,* BT-*f* and BT-*fsu,* with a Si/Al ratio ranging 12.4 to 13.5. The Fe content in the final dried solids was measured, in order to evaluate the Fe adsorption during the Fenton detemplation. For that purpose, equation (6) described in the experimental section was employed. In the calcined BT-*C*, Fe traces were found (0.01 *wt.*%). During the Fenton treatment, a substantial part of the applied Fe was adsorbed, ranging 64 and 83% of the applied Fe in solution, rising the absolute values up to 0.1 *wt.*%.

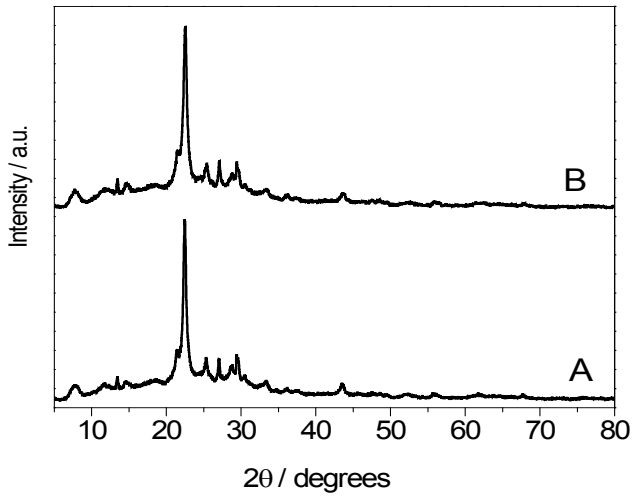

Figure 4. XRD patterns for the scaled-up Fenton detemplated (A, BT-*fsu*) compared to the calcined counterpart (B, BT-*C*).

3.3.5.2. TEXTURAL PROPERTIES

Low-pressure high-resolution Ar physisorption (LPHR-Ar) measurements were performed in order to determine the porosity of the materials under study. The shape of the isotherms (Fig. 5) shows the interaction between adsorbent (Ar) and zeolite surface [16,61]. The adsorption/desorption isotherms correspond to a typical nano-sized Beta zeolite isotherm [16,62-64]. Both materials exhibit a shape of type IV with a type H3 hysteresis loop in the mesopores region according to the IUPAC classification [65]. This isotherm profile is characteristic of multilayer adsorption with capillary condensation in the mesopores. H3 type loop is observed when small particles aggregate giving rise to slit-shaped pores [65]. At the micropores region (p/p_o<0.3) BT-*fsu* shows higher adsorption; it agrees with the *t*-plot calculations as discussed later. A slight rise of adsorption was observed in the mesopores range 0.3<p/p_o<0.4 followed by two capillary rises: one broad in the range 0.4<p/p_o<0.85 and another near 0.9. The range covered by the desorption hysteresis loop of BT-*fsu* is comparable to BT-*C*.

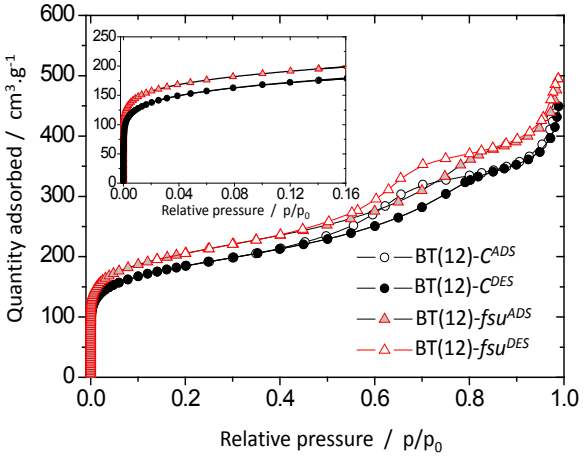

Figure 5. High-resolution Argon physisorption isotherms at –186.2 °C for the calcined and scaled-up Fenton detemplated counterpart. The superscript in the sample codes indicates whether it is an adsorption or desorption branch.

Argon physisorption derived *t*-plot (Figure 6) shows an increase in the intercept on the *y* ordinate. A positive intercept corresponds to the presence of micropores. Consequently, the micropore volume was enhanced by using mild detemplation (BT-*fsu*) instead of calcination (BT-*C*). The overall textural parameters are collected in Table 4. BT-*fsu* has a higher BET surface area; the rise comes from an increase in the micro- and mesoporous contributions, with a higher contribution of the micropores to the increase (~15% increase in the micropore area versus ~8% increase in mesopore area). The calculated mesoporous parameters were 24 m^2/g and 0.04 cm^3/g higher for BT-*fsu*, with absolute values of 342 m^2/g and 0.448 cm^3/g. At the macroscopic level, the BT-*fsu* showed a total pore volume 11% higher than BT-*C*, *cf.* 0.562 and 0.508 cm^3/g.

Table 4. Summary of the porosity parameters calculated from the high-resolution argon physisorption isotherms at –186.2 °C.

Material	S_{BET} m^2/g	S_{μ}^{t-plot} m^2/g	S_{MESO}^{t-plot} m^2/g	V_T cm^3/g	V_{μ}^{t-plot} cm^3/g	V_{MESO}^{t-plot} cm^3/g
BT-C	566	248	318	0.508	0.097	0.411
BT-*fsu*	628	286	342	0.562	0.114	0.448

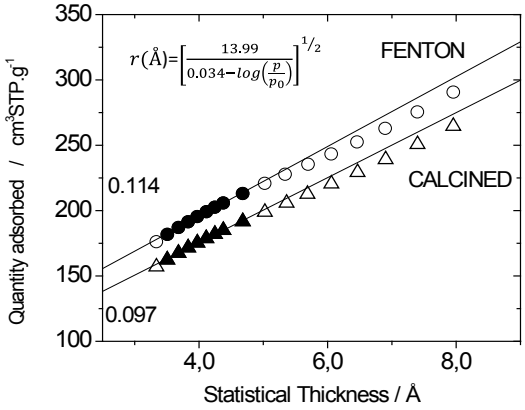

Figure 6. Harkins and Jura *t*-plot derived from the LPHR-Argon adsorption (–186.2 °C) of Fenton detemplated (BT-*fsu*) and calcined Beta zeolite (BT-*C*).

In Figure 7 the differential pore volume versus the pore diameter calculated with the Horvath-Kawazoe model for BT-*C* and BT-*fsu* is plotted. BT-*fsu* displays a sharper pore diameter distribution and shifted to smaller pore diameters (*ca.* 0.05 Å) compared to BT-*C*. Thermal stress and sintering may be the cause of the peak broadening. The shift towards smaller pore

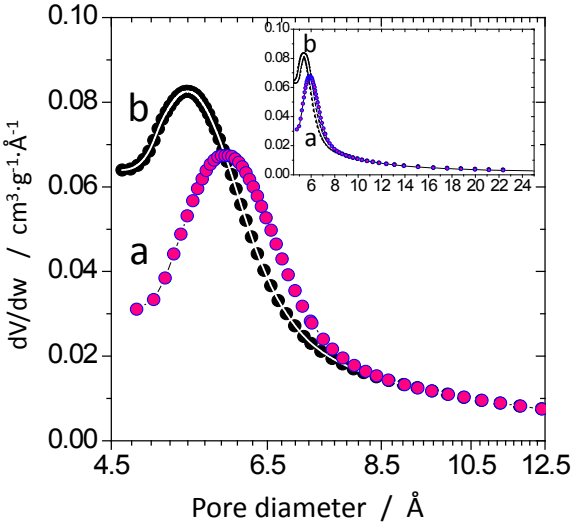

Figure 7. Horvath-Kawazoe differential pore volume for the calcined (a) and scaled-up Fenton detemplated (b), applied to the LPHR isotherms (Ar, –186.2 °C).

sizes of the BT-*fsu* can be attributed to the different nature of the materials. BT-*fsu* remains in the NH_4-form [28] while BT-*C* is on the H-form; therefore the effective pore size for the Fenton-based material is smaller than for the calcined one.

3.3.5.3. AL-COORDINATION

The Al-coordination was studied by ^{27}Al-MAS NMR. The spectra for various materials are displayed in Figure 8. The raw material shows a single resonance centred at *ca.* 50 ppm related to tetrahedrically coordinated framework-aluminium atoms [20]. BT-*fsu* shows no distortion in the Al atoms distribution after template removal, showing an identical pattern compared to the starting material (BT-*raw*). Contrariwise, BT-*C* displays, additionally to the framework Al, a shoulder (*ca.* 25 ppm) related to pentahedrically coordinated–Al [66] and a resonance at around 0 ppm ascribed to octahedrically-coordinated Al (AlO_6) [20]. Approximately 16% of the Al was driven off the structure (calculated as AlO_6) due to the thermal stress suffered during calcination.

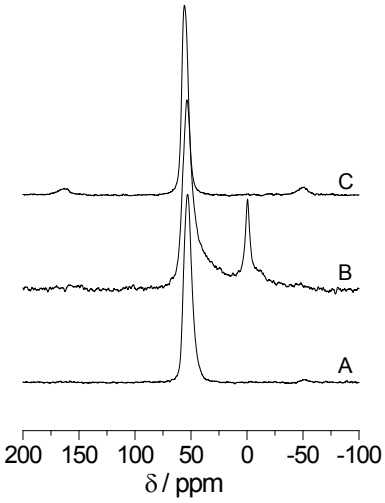

Figure 8. ^{27}Al MAS NMR spectra for the raw material (A), calcined (B) and scaled-up Fenton detemplated (C).

3.4. CONCLUSIONS

The Hadamard design shows preliminary trends, with Fe concentration having the largest effect in the detemplation efficiency followed by H_2O_2 utilisation and temperature. A thorough optimisation study reveals that to achieve full detemplation, higher temperatures can compensate Fe concentration and H_2O_2 utilisation. An interplay between H_2O_2 utilisation and Fe concentration was also observed.

By understanding the interplay between relevant parameters, attractive reaction conditions for large-scale implementation were identified. If H_2O_2 needs to be minimised, optimal conditions are found at 88 °C, 30 ppm Fe and 15 mL H_2O_2/g which means a relatively high solid concentration and low consumption of H_2O_2. When Fe should be limited in the final product composition, optimal conditions are obtained at 88 °C, 5 ppm Fe and 30 mL H_2O_2/g.

A kinetic study demonstrates that reaction time to get full detemplation can be reduced in several fashions: applying a higher Fe concentration, Fe-oxalates are more effective than Fe-nitrate, especially under UV radiation, having the shortest reaction time of 5 h, at the applied conditions.

The protocol was scaled up to 100 times, with >99% detemplation efficiency. The resulting scaled material was structurally similar to the calcined counterpart based on similar Si/Al ratio and XRD pattern. Textural and Al coordination properties are more favourable compared to the calcined counterpart.

3.5. ACKNOWLEDGEMENTS

The 'Nederlandse Organisatie voor Wetenschappelijk Onderzoek' (NWO) is thanked for the financial support of the VIDI grant no. 10284. The industrial steering committee (Shell, DSM and Norit Nederland, now Cabot) and the Dutch Technology Foundation (STW) are acknowledged.

3.6. REFERENCES

[1] D.W. Breck, Zeolite Molecular Sieves, Structure, Chemistry and Use, John Wiley & Sons, New York, 1974.

[2] J. Weitkamp, L. Puppe, Catalysis and Zeolites, Fundamentals and Applications, Springer, Berlin, 1999.

[3] J. Cejka, H. van Bekkum, A. Corma, F. Schueth (Eds.), Introduction to Zeolite Science and Practice, 3rd revised edition, Stud. Surf. Catal. 168, Elsevier, Amsterdam, 2007.

[4] R. Xu, W. Pang, J. Yu, Q. Huo, J. Chen, Chemistry of Zeolites and Related Porous Materials. Synthesis and Structure, John Wiley & Sons, Singapore, 2007.

[5] V. Valtchev, S. Mintova, M. Tsapatsis, Ordered Porous Solids: Recent Advances and Prospects, Elsevier, Amsterdam, 2009.

[6] J. Cejka, A. Corma, S. Zones (Eds.), Zeolites and Catalysis: Synthesis, Reactions and Applications, Wiley-VCH, Weinheim, 2010.

[7] C.S. Cundy, P.A. Cox, Chem. Rev. 103 (2003) 663-701.

[8] J. Cejka, A. Corma, S. Zones (Eds.), Zeolites and Catalysis: Synthesis, Reactions and Applications, Wiley-VCH, Weinheim, 2010, pp. 67.

[9] A. Burton, S. Zones, S. Elomari, Curr. Opin. Colloid In. 10 (2005) 211-219.

[10] A. Jackowski, S.I. Zones, S. Hwang, A.W. Burton, J. Am. Chem. Soc. 131 (2009) 1092-1100.

[11] R. Castaneda, A. Corma, V. Fornes, F. Rey, J. Rius, J. Am. Chem. Soc. 125 (2003) 7820-7821.

[12] A. Corma, F. Rey, J. Rius, M. Sabater, S. Valencia, Nature. 431 (2004) 287-290.

[13] A. Corma, M.J. Diaz-Cabanas, J. Luis Jorda, C. Martinez, M. Moliner, Nature. 443 (2006) 842-845.

[14] J. Pérez-Pariente, J.A. Martens, P.A. Jacobs, Appl. Catal. 31 (1987) 35-64.

[15] M.A. Camblor, A. Mifsud, J. Pérez-Pariente, Zeolites. 11 (1991) 792-797.

[16] M.A. Camblor, A. Corma, S. Valencia, Micropor. Mesopor. Mater. 25 (1998) 59-74.

[17] T. De Baerdemaeker, B. Yilmaz, U. Mueller, M. Feyen, F. Xiao, W. Zhang, T. Tatsumi, H. Gies, X. Bao, D. De Vos, J. Catal. 308 (2013) 73-81.

[18] H. Zhang, B. Xie, X. Meng, U. Mueller, B. Yilmaz, M. Feyen, S. Maurer, H. Gies, T. Tatsumi, X. Bao, W. Zhang, D. De Vos, F. Xiao, Micropor. Mesopor. Mater. 180 (2013) 123-129.

[19] B. Yilmaz, U. Mueller, M. Feyen, S. Maurer, H. Zhang, X. Meng, F. Xiao, X. Bao, W. Zhang, H. Imai, T. Yokoi, T. Tatsumi, H. Gies, T. De Baerdemaeker, D. De Vos, Catal. Sci. Technol. 3 (2013) 2580-2586.

[20] E. Bourgeat Lami, P. Massiani, F. Di Renzo, P. Espiau, F. Fajula, T. Courieres, Appl. Catal. 72 (1991) 139-152.

[21] I. Kiricsi, C. Flego, G. Pazzuconi, W.O. Jr. Parker, R. Millini, C. Perego, G. Bellussi, J. Phys. Chem. 98 (1994) 4627-4634.

[22] P.J. Kunkeler, B.J. Zuurdeeg, J.C. van der Waal, J.A. van Bokhoven, D.C. Koningsberger, H. van Bekkum, J. Catal. 180 (1998) 234-244.

[23] J.A. van Bokhoven, D.C. Koningsberger, P. Kunkeler, H. van Bekkum, A.P.M. Kentgens, J. Am. Chem. Soc. 122 (2000) 12842-12847.

[24] C.W. Jones, K. Tsuji, T. Takewaki, L.W. Beck, M.E. Davis, Micropor. Mesopor. Mater. 48 (2001) 57-64.

[25] B. Gautier, M. Smaihi, New J. Chem. 28 (2004) 457-461.

[26] M. El Roz, L. Lakiss, V. Valtchev, S. Mintova, F. Thibault-Starzyk, Micropor. Mesopor. Mater. 158 (2012) 148-154.

[27] I. Melian-Cabrera, S. Espinosa, F.J. Garcia-Montelogo, F. Kapteijn, J.A. Moulijn, Chem. Commun. (2005) 1525-1527.

[28] I. Melian-Cabrera, F. Kapteijn, J.A. Moulijn, Chem. Commun. (2005) 2744-2746.

[29] I. Melian-Cabrera, F. Kapteijn, J.A. Moulijn, Catal. Today. 110 (2005) 255-263.

[30] L.L. Perez, M.J. Ortiz-Iniesta, Z. Zhang, I. Agirrezabal-Telleria, M. Santes, H.J. Heeres, I. Melian-Cabrera, J. Mater. Chem. A. 1 (2013) 4747-4753.

[31] Z. Zhang, D.L. Santangelo, G. ten Brink, B.J. Kooi, J.A. Moulijn, I. Melian-Cabrera, Mater Lett. 131 (2014) 186-189.

[32] Y. Xia, R. Mokaya, J. Phys. Chem B. 110 (2006) 9122-9131.

[33] J. Kecht, T. Bein, Micropor. Mesopor. Mater. 116 (2008) 123-130.

[34] N. Alam, R. Mokaya, J. Mater. Chem. 18 (2008) 1383-1391.

[35] F. Fan, Z. Feng, K. Sun, M. Guo, Q. Guo, Y. Song, W. Li, C. Li, Angew. Chem. Int. Edit. 48 (2009) 8743-8747.

[36] P. Wang, D. Yang, J. Hu, J. Xu, G. Lu, Catal. Today. 212 (2013) 142-148.

[37] C. Wu, J. Liao, S. Fang, A.S.T. Chiang, Adsorption. 16 (2010) 69-74.

[38] J. Coronas, Chem. Eng. J. 156 (2010) 236-242.

[39] M. Hartmann, S. Kullmann, H. Keller, J. Mater. Chem. 20 (2010) 9002-9017.

[40] V. Valtchev, G. Majano, S. Mintova, J. Pérez-Ramirez, Chem. Soc. Rev. 42 (2013) 263-290.

[41] H. Xing, Y. Zhang, M. Jia, S. Wu, H. Wang, J. Guan, L. Xu, T. Wu, Q. Kan, Catal. Commun. 9 (2008) 1060-1065.

[42] J. Lu, N. Liu, L. Li, R. Lee, Sep. Purif. Technol. 72 (2010) 203-207.

[43] L. Xiao, J. Li, H. Jin, R. Xu, Micropor. Mesopor. Mater. 96 (2006) 413-418.

[44] Y. Hu, Y. Zhang, Y. Tang, RSC Adv. 2 (2012) 6036-6041.

[45] D.Y. Khoo, H. Awala, S. Mintova, E. Ng, Micropor. Mesopor. Mater. 194 (2014) 200-207.

[46] E. Neyens, J. Baeyens, J. Hazard. Mater. 98 (2003) 33-50.

[47] W.Z. Tang, Physicochemical Treatment of Hazardous Wastes, CRC Press LLC, Florida, 2004.

[48] J.J. Pignatello, E. Oliveros, A. MacKay, Crit. Rev. Environ. Sci. Technol. 36 (2006) 1-84.

[49] A. Hedayat, W. Wallis, Ann. Stat. 6 (1978) 1184-1238.

[50] M. Baro, E. Sánchez, A. Delgado, A. Perera, C. Evora, J. Control. Release. 83 (2002) 353-364.

[51] R.J. Watts, M.D. Udell, P.A. Rauch, S.W. Leung, Hazard. Waste Hazard. 7 (1990) 335-345.

[52] C. Walling, Acc. Chem. Res. 8 (1975) 125-131.

[53] The CRC Handbook of Chemistry and Physics, 89th edition. ed., CRC Press, 2011.

[54] J. Perez-Ramirez, F. Kapteijn, J. Groen, A. Domenech, G. Mul, J. Moulijn, J. Catal. 214 (2003) 33-45.

[55] A.H. Oygarden, J. Perez-Ramirez, Appl. Catal. B-Environ. 65 (2006) 163-167.

[56] P. Hermankova, M. Hermanek, R. Zboril, Eur. J. Inorg. Chem. (2010) 1110-1118.

[57] D. Hermosilla, M. Cortijo, C.P. Huang, Chem. Eng. J. 155 (2009) 637-646.

[58] D. Zhou, F. Wu, N. Deng, Chemosphere. 57 (2004) 283-291.

[59] M. Balmer, B. Sulzberger, Environ. Sci. Technol. 33 (1999) 2418-2424.

[60] P. Mazellier, B. Sulzberger, Environ. Sci. Technol. 35 (2001) 3314-3320.

[61] M. Thommes, Chem-Ing-Tech. 82 (2010) 1059-1073.

[62] P. Prokesova-Fojokova, S. Mintova, J. Cejka, N. Zilkova, A. Zukal, Micropor. Mesopor. Mater. 92 (2006) 154-160.

[63] L. Wang, Z. Zhang, C. Yin, Z. Shan, F. Xiao, Micropor. Mesopor. Mater. 131 (2010) 58-67.

[64] J.C. Groen, L.A.A. Peffer, J. Perez-Ramirez, Micropor. Mesopor. Mater. 60 (2003) 1-17.

[65] K.S.W. Sing, D.H. Everet, R.A.W. Haul, L. Moscou, R.A. Pieroti, J. Rouquerol, T. Siemieniewska, Pure Appl. Chem. 57 (1985) 603-619.

[66] A. Duevel, E. Romanova, M. Sharifi, D. Freude, M. Wark, P. Heitjans, M. Wilkening, J. Phys. Chem. C. 115 (2011) 22770-22780.

Fenton detemplation of zeolites: scope, advantages and limitations on the way to industrial application

ABSTRACT

We report the suitability and scope of an environmental friendly detemplation method using Fenton chemistry for relevant microporous and mesoporous zeolites: BEA, MFI, mesoporous MFI, MWW derivatives, and Sn-containing BEA. The influence of the Si/Al ratio and crystallite size was studied for MFI and BEA zeolites (Si/Al = 25, 40 and 140 for MFI; Si/Al = 12.5 and 19 for BEA). Although high Si/Al ratio hinders the template removal, high detemplation degree (> 90%) was achieved for BEA zeolites including a Sn-containing BEA (Sn-Beta). In the case of carbon-templated mesoporous ZSM-5 (MesoMFI), the meso-template was fully removed with the Fenton technique. In the case of MWW derivatives (partially delaminated MCM-22), Fenton detemplation had to be combined with mild thermal treatments to remove the template completely. The detemplation degree was monitored by TGA and the results were corroborated by CHN elemental analysis. Structural and textural properties were analysed by XRD, N_2 and Ar physisorption, while solid state ^{27}Al MAS NMR was used to investigate the Al coordination. The obtained results and their comparison to template removal with a conventional calcination approach indicate that Fenton chemistry displays significant potential as an environmental friendly detemplation method for the industrial manufacture of zeolites.

Keywords: Zeolite; detemplation; calcination; template removal; Fenton chemistry.

4.1. INTRODUCTION

Zeolites have a wide range of applications in industrial catalytic processes, environmental protection, medicine, nanotechnology, and bioengineering [1-4]. The industrial relevance and versatility of zeolites stems from their tunable properties including high-surface area, acidity, crystallinity, selectivity and ion-exchange capacity [5,6]. Therefore, their synthesis and post-synthetic treatments are under continuous development, with a total of 229 zeolitic structures reported to date [7]. In the 1980s, the introduction of organic bases that regulate the pH of the synthesis mixture and simultaneously can act as templates in the synthesis of zeolites opened a wide variety of possibilities for tailoring the composition, structure and textural properties of these materials towards the desired final application. Many zeolitic structures have been synthesised with the help of organic bases, including ZSM-5 (MFI), ZSM-11 (MEL), ZSM-12 (MTW), ZSM-22 (TON), ZSM-23 (MTT), ZSM-48 (*MRE), ZSM-57 (MFS), EU-1 (EUO), NU-87 (NES) and Beta (BEA) [8,9]. Many studies revealed the complex character of the synthesis mechanism involving the template/structure directing agent (SDA) and other ions and molecules present in the solution during the zeolite synthesis [10]. The most commonly used templates are amines and organic quaternary ammonium cations. The removal of these organic compounds without damaging the zeolite framework is of great importance to obtain the desired porosity and acidity. Different protocols for template removal have been described in the literature [11-13]. However, an optimal protocol has not been fully developed yet.

Template removal protocols can be divided in: thermal treatments, template extraction (with the aim of reusing the template), and chemical approaches. Thermal treatment usually involves the application of high temperatures under air or oxygen to achieve combustion of the organic template, and is referred to as calcination. This process is highly exothermal and leads to structural damage in numerous zeolites, especially in the case of special-composition structures (i.e. containing other metals

than Al), nanocrystals, membranes and ultra-fine zeolite particles [14,15]. Moreover, the removal of the template is also affected by the presence and content of Al (or of other metal atoms) partially substituting Si in the zeolite framework [16]. It has been observed that the presence of Al leads to stronger interaction with the template [17,18].

The strategies aiming template recovery are motivated by the idea of reusing it, as this is often the most expensive compound employed in zeolite synthesis. However, this approach is mostly limited to mesoporous materials and is less suitable for zeolites, in which the templates are typically ionic species trapped within the pores. Indeed, a successful template extraction was reported only in a few cases, e.g. for tetraethylammonium ions from zeolite Beta [17]. Moreover, it should be noted that acid treatments, together with the detemplation, can lead to partial deterioration of the structure by dealumination [19].

The last type of template removal involves reaction with a chemical reagent under mild conditions. The chemical reagent is chosen depending on the nature of the template molecule to be oxidised/degraded, together with the temperature requirements to avoid structural damage. The most commonly used routes are the ammonia-assisted thermal treatment at 250 °C to remove tetramethylammonium cations [20], oxidation using ozone [21,22], cold plasma [23], ultraviolet irradiation [24], ultraviolet/ozone [25] and Fenton detemplation [26-30]. Fenton chemistry has been widely employed for the treatment of residual waste water and soils [31-33]. The OH radicals generated by a series of redox reactions between H_2O_2 and Fe^{III}/Fe^{II}, have a high oxidation potential (2.8 eV) [32], which was shown to be suitable for oxidising the template in beta zeolite [34]. The combination of affordable reactants and the low temperature required make Fenton chemistry a favourable approach for detemplation of micro- and mesoporous materials, which are sensitive to calcination. For example, microcrystalline zeolites such as beta zeolite are known for their sensitivity to calcination, which leads to the formation of extra-framework aluminium (EFAL) with consequent decrease of the number of Brønsted acid sites [18,35-38]. This dealumination of the

framework is caused by the high inner pressure generated by the steam produced during the template decomposition and subsequent hydrolysis of the Si-O-Al bonds [36,39,40].

In this study we aim at extending the Fenton detemplation protocol to zeolites with relevant catalytic applications and namely: BEA (Beta with different Si/Al and Sn-Beta), MFI (conventional and mesoporous ZSM-5) and partially delaminated MWW. The three-dimensional network of large micropores [formed by 12 member-rings (MR) of 6.6 × 6.7 Å (2D) and 5.6 × 5.6 Å (1D)] of zeolite Beta combined with its strong acidity [41-43] make this material of great interest in catalytic processes such as hydro-cracking and isomerisation of alkanes [44,45], methylation of phenols [46], alkylation [47-50] and acylation [51,52]. Sn-Beta is characterised by a BEA framework in which Sn atoms partially substitute Si atoms. These Sn sites act as Lewis acids for various important catalytic applications ranging from the Baeyer-Villiger oxidation to biomass conversion [53,54]. The 3D structure of MFI shows narrower micropore size (10 MR with dimension; 5.1 × 5.5 Å and 5.3 × 5.6 Å) compared to Beta, which endows it with shape selectivity in isomerisation and alkylation of hydrocarbons [55-57]. On the other hand, this implies diffusional constrains. Various approaches have been considered to overcome this limitation, such as the introduction of mesoporosity via carbon-templating during the synthesis [58]. This material is referred to as MesoMFI in this work. With a similar purpose, the delamination of MWW frameworks was proposed [59,60]. The enhanced accessibility to MWW´s strong acid sites has been of use in many catalytic reactions such as the conversion of alkanes to aromatics, acylations, isomerisations, alkylations and cracking [61-66]. The efficiency of the Fenton detemplation of these zeolites was monitored by thermal techniques and elemental analysis, while the structure and texture of the materials were evaluated by XRD, SEM, Ar-physisorption and ^{27}Al NMR, and compared to the calcined counterparts.

4.2. EXPERIMENTAL

4.2.1. MATERIALS

Stabilised hydrogen peroxide (30 *wt.*% H_2O_2 in H_2O), nitric acid (65 *wt.*%), and ammonia solution (25 *wt.* %) were purchased from Merck. Non-stabilised hydrogen peroxide (30 *wt.*% H_2O_2 in H_2O), sodium hydroxide (NaOH) pellets (99%), fumed silica, hexamethyleneimine, tetrapropylammonium hydroxide (1 M aqueous solution, TPAOH), hexadecyltrimethylammonium bromide solution (29 *wt.*% in Demineralized water, C_{16}TEABr), and HCl (36%) were purchased from Sigma-Aldrich. $Fe(NO_3)_3 \cdot 9H_2O$ (98 % on metal basis, denoted as Fe^{III}-nitrate), sodium aluminate powder (technical grade) and $(NH_4)_3[Fe(C_2O_4)_3] \cdot 3H_2O$ (pure, denoted as Fe^{III}-oxalate) were supplied by Riedel-de-Haën.

NH_4-templated zeolite Beta (HSZ930A (BT1) and HSZ940 (BT2)) was purchased from TOSOH Corporation; Na-templated zeolite Beta (CP806E (BZ1) and CP806C (BZ2)) was supplied by Shell. ZSM-5 (NH_4-templated) was obtained from Zeolyst International (CBV5524G (MFI1), CBV8014 (MFI2), and CBV28014 (MFI3)). Carbon-templated ZSM-5 (MesoMFI) and Sn-Beta (SnBeta) were obtained from TOPSOE [54,58]. The suppliers and types of the zeolitic materials are summarised in Table 1.

4.2.2. MATERIALS PREPARATION

4.2.2.1. SYNTHESIS OF MCM-22(P) AND MCM-22-PD

The MCM-22(P) zeolite [MWW] was prepared following a procedure reported elsewhere [62,67]. In a typical synthesis, 0.161 g of sodium aluminate and 1.09 g of 4M NaOH aqueous solution were dispersed in 31.7 g of demineralized water. To this solution, 2.40 g of fumed silica were added while the mixture was magnetically stirred until a gel was formed. Then, 1.98 g of hexamethyleneimine

(HMI) was added to complete the synthesis gel. The molar composition of the gel was: SiO_2 : 0.028 Al_2O_3 : 0.075 Na_2O : 0.5 HMI : 44 H_2O. The gel was autoclaved at 150°C for 7 days; the resulting product was washed with demineralized water until neutral pH, and dried overnight at 80°C in an oven. To swell MCM-22(P), 0.216 g of MCM-22(P) was suspended in 8.64 g of demineralized water. Then, 4.2 g of C_{16}TEABr (29 *wt.*% in demineralized water) and 2.64 g of 1M TPAOH were refluxed for 16 h at 80°C. The swollen MCM-22(P) was stripped apart by placing the slurry in an ultrasound bath for 1 h. During the ultrasound treatment, the pH was kept at around 12.5. Finally, the solid phase was separated by: first, adding a few drops of concentrated hydrochloric acid to help the precipitation of the layers (pH of the slurry slightly below 2), and then by centrifugation. Afterwards, the solid phase was dried at 80°C overnight in a stove oven. The partially delaminated MCM-22 obtained, named as MCM-22-pd, was a material in between the calcined MCM-22 and the optimal delaminated material reported in the literature [59], on the basis of its moderate external surface area.

4.2.2.2. CALCINATION

The general calcination procedure was carried out in a box furnace in shallow bed using porcelain crucibles. The raw samples were heated from 30 to 550 °C at 10 °C/min and held at this temperature for 6 h, except for the MWW material, which was calcined at 550°C during 6h with a heating rate 1 °C/min in a muffle oven. The materials that were detemplated by calcination are denoted as "–*C*", preceded by the code of the material (e.g. BT1-*C*, BT2-*C*, etc.).

4.2.2.3. FENTON CHEMISTRY-BASED DETEMPLATION

A standard protocol is described here (Table 1, entry 3), from which the other methods can be easily inferred. The raw zeolite BT1-raw (0.5 g) was mixed

with 30 *wt.*% aqueous H_2O_2 (15 mL) and stirred until the mixture was homogeneous. Then, 65 µL of an aqueous solution of Fe(III)-nitrate (5 g in 100 ml of demineralized water) was added to obtain a Fe concentration of 30 ppm. The pH of the slurry was adjusted to 4 by adding a dilute HNO_3 solution (0.4 M). The flask containing the reaction mixture was immersed in a pre-heated oil bath at 70 °C for 24 h under continuous stirring and refluxing to prevent evaporation. The solid was separated by centrifugation, washed with demineralized water twice and dried overnight at 80°C in an oven.

For the experiments in which Fe-oxalate was employed as Fe source, the mother solution was made by mixing 2.64 g Fe-oxalate in 100 mL of demineralized water.

The BZ1 and BZ2 materials were previously exchanged with 0.5 M NH_4NO_3 solution at 80 °C during 48 hours.

The obtained materials by Fenton detemplation are denoted as "*–f*" preceded by the code of the material (BT1-*f*, BT2-*f*, etc.).

4.2.2.4. ION EXCHANGE

For the standard procedure, 90 mL of ammonium nitrate solution (1M) was used per gram of template-free zeolite. The exchange was carried out at room temperature in two steps. In the first step the pH was adjusted to neutral values using a diluted ammonia solution and it took place for 16 hours. During the second exchange step the pH was not controlled and the time was shortened to 6 hours. Then, the samples were washed 3 times with demineralized water and dried overnight at 80 °C in a stove oven.

4.2.2.5 MILD THERMAL TREATMENT POST-FENTON DETEMPLATION

The thermal treatment was held at 400 °C during 6 h, heating rate of 5 °C/min. Applied to MesoMFI-*f* and MCM-22-pd to fully remove the template.

4.2.3. CHARACTERISATION

The template content was calculated based on the weight-loss of the heat treated materials under air. For that purpose, thermogravimetric analyses (TGA) were performed using a Mettler-Toledo (TGA/SDTA851e) analyser with a flow of synthetic air of 80 mL/min (STP) equipped with a 34-position sample robot in an opened chamber. Typically, 5-10 mg of sample was loaded in a 70 μL α-Al_2O_3 crucible and the temperature was increased from 30 to 900 °C at 10 °C/min under air. Blank curve correction using an empty crucible was subtracted.

For confirmation of the detemplation levels, carbon elemental analyses were carried out on selected samples. CHN elemental analyses were performed in a EuroVector 3000 CHNS analyser. All analyses were done in duplicate to check sample heterogeneity; the standard deviation was below 2 *wt.*%. 2.00±0.20 mg of sample were weighed in a 6-digit analytic balance (Mettler-Toledo). The samples were burned at 1800 °C in the presence of an oxidation catalyst and decomposed into CO_2, H_2O and N_2. These gases were then separated in a Porapak QS column at 80 °C and quantified with a TCD detector. Acetanilide (99.9 *wt.*%) was used as external standard. For calculations, the carbon amount of the raw material was taken as reference for 0% detemplation. CHN-based detemplation efficiency (η^C(%)) was calculated as follows (eq. 1):

$$\eta^C(\%) = \left[1 - \frac{C_{CHN}(\text{sample})}{C_{CHN}(\text{raw})}\right] \times 100\% \qquad (1)$$

Where C_{CHN}(sample) is the carbon content determined by elemental analysis of the material under study and C_{CHN}(raw) is the carbon content of the raw material determined in the same way. A higher amount of H was systematically found in the Fenton detemplated materials compared to the calcined counterparts. This is due to the higher amount of water absorbed (more hydrophilic structure) and NH_4^+ released from the decomposition of the template (substituted ammonium ions such as TPA^+ and TEA^+).

Inductively coupled plasma atomic emission spectroscopy (ICP-AES) analyses were carried out to determine the Si/Al ratio and the concentration of residual Fe in the samples (eq. 2). To that effect, a known amount of solid sample was dissolved in a 6 *wt.*% HF solution overnight to ensure complete dissolution. In the cases in which Fenton detemplation did not fully remove the template, the analyses were performed after additional thermal treatment to ensure no interferences during the measurements due to the presence of organic compounds. The liquid concentration was determined in a Perkin-Elmer (Optima 7000 DV) instrument.

The amount of Fe adsorbed was calculated as follows (eq. 2):

$$Fe^{ADS}(\%) = \left[\frac{Fe^{ICP}(\text{material}) - Fe^{ICP}(\text{calcined})}{Fe\ (\text{applied Fenton solution})}\right] \times 100\% \qquad (2)$$

where Fe^{ICP}(*material*) is the concentration of Fe measured by ICP-AES in the dried material after Fenton detemplation, Fe^{ICP}(*calcined*) is the measured ICP-AES value for the calcined material, which contains Fe impurities, and Fe(applied Fenton solution) is the applied Fe concentration of the solution used to catalyse the Fenton reaction. For the Fe^{ICP}(calcined/material) calculation, the weightlosses due to the template removal had been taken into account.

Powder X-ray diffraction (XRD) patterns were collected with a Bruker D8 powder X-ray diffractometer using CuKα radiation (λ=1.54056 Å). The spectra were recorded with a step size of 0.02°, 3 s accumulation time and in the 2θ angle range 5-60°.

Textural analyses were carried out by Ar physisorption at -186 °C, in a Micromeritics ASAP 2420 or 2020. Prior to the measurements the samples were degassed at 300 °C for 12 h; Fenton-derived materials were degassed at 150 °C. The surface area was calculated by the BET approach (S_{BET}). The single point pore volume (V_T) was estimated from the amount adsorbed at a relative pressure of 0.972 in the desorption branch [68]. The micropore volume was derived from the t-plot model ($V\mu$). The pore size distribution was determined from the Horvath-Kawazoe differential model.

^{27}Al magic angle spinning nuclear magnetic resonance (MAS NMR) measurements were conducted on a Bruker Avance-400 spectrometer using a 4 mm zirconium holder, applying spinning frequency of 11 kHz at 25 °C. The ^{27}Al MAS NMR spectra were obtained at 104.201 MHz, with acquisition delay of 1 s, acquisition time of 0.08 s, and typically 4000 scans were collected. The spectra were referenced with respect to 1.0 M aqueous solution of $Al(NO_3)_3$ set at 0 ppm.

SEM images were recorded with a Philips XL 20 microscope at 10 kV. Samples were coated with Pd to improve contrast. The quantification of the particle size was carried out using 2D SEM images and the manual tool of the software IMAGE PRO PLUS V4.5 (Media Cybernetics®).

4.3. RESULTS AND DISCUSSION

4.3.1. FENTON DETEMPLATION

This work investigates the scope, advantages and limitations of the detemplation of zeolites by Fenton chemistry. It aims at extending the Fenton detemplation protocol to zeolites with industrially relevant catalytic applications and namely: Beta, SnBeta, ZSM-5, and partially delaminated MWW (MCM-22-pd).

The fundamental aspects of Fenton chemistry have been widely studied for the treatment of residual water and soils [33]. In the absence of any organic compound, hydrogen peroxide reacts with Fe^{II} to generate hydroxyl radicals ($OH^{\bullet}$), while the subsequent reaction of the formed Fe^{III} with H_2O_2 restores Fe^{II}. In the presence of organic compounds, the hydroxyl radicals react at rate constants as high as 10^7-10^{10} L/(mol·s) [69]. The hydroxyl radicals mainly abstract H atoms from the organic molecules, but they can also be involved in other competing reactions. The rate constants of some of these competing reactions are pH dependent [70,71]. Because of the high reaction constants, second order and complexity of the mechanism (side reactions),

the temperature, Fe and H_2O concentration must be interplayed carefully in order to control the outcome of the process. This study focuses on finding suitable conditions to reach the maximum (ideally full) detemplation on the target zeolites by means of Fenton chemistry. The choice of the investigated zeolites enabled to study the effects of Si/Al ratio, template, and zeolitic channel morphology on the suitability of Fenton detemplation approach. The most suitable conditions from a previous study [71] were used as starting point to investigate the effect of varying the H_2O_2 amount and the Fe concentration at different temperatures. However, increasing the Fe^{n+} concentration can have a negative impact on the purity of the final sample and on its Brønsted acidity, because Fe^{n+} tends to partially replace H^+ in the zeolite structure. Increasing the amount of H_2O_2 would be detrimental to the final process costs, particularly in the perspective of an industrial scale application. Therefore, temperature is considered the preferable way to further enhance the detemplation level, and this methodology was the first choice if the standard protocol (Table 1, entry 3) did not provide satisfactory results. Table 1 provides a summary of the conditions at which the maximum level of detemplation was achieved for each zeolite type considered in this study.

These optimum conditions differ for each zeolite type, and were obtained through the screening of the above mentioned parameters (T, time, H_2O_2 amount, [Fe^{n+}]). As an example, the complete results of the optimisation of the conditions for Fenton detemplation of ZSM-5 materials are reported in Table 1. Figure 1 summarises graphically the maximum detemplation efficiency achieved by Fenton chemistry for each zeolite (data from Table 1), as determined by elemental analysis.

These data are complemented by the TGA and DTGA profiles of the raw and Fenton detemplated materials under study (Figure 2). The TGA profiles of the Fenton detemplated Beta zeolites (Figure 2A) display a pronounced weight loss at *ca.* 100 ^{0}C due to water desorption and a secondary weight loss at *ca.* 350 ^{0}C due to the release of NH_4^+ groups [27]. In the case of the calcined materials, the second weight loss is not observed. As a reference, the raw materials displayed three major weight losses: at T < 200 ^{0}C

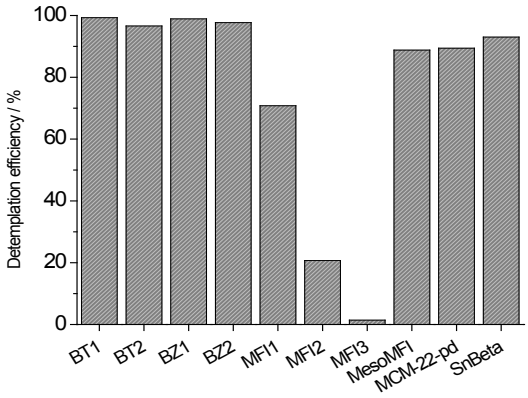

Figure 1. Summary of the detemplation efficiency (η^C) for the studied zeolites.

due to physisorbed water and *ca.* 430 ^{0}C and 530 ^{0}C due to the template decomposition [27]. These results show that a high degree of detemplation was achieved for the Beta zeolites, with virtually complete template removal for the Beta frameworks containing Al (Table 1, entries 1-12). According to the literature, the presence of Al in the zeolite framework substituting Si atoms confers additional thermal stability to the templating cations due to the stronger interaction with the negatively charged framework [72,73]. However, for the studied Beta zeolites the Fenton conditions required to remove the template were not strongly affected by the Si/Al ratio. This can be explained by considering also the role of the hydrophilicity of the zeolite, which increases with increasing amount of Al in the zeolite framework [74]. A higher hydrophilicity is expected to be beneficial for the Fenton detemplation, because it favours the approach of the OH radicals to the template, thus facilitating the decomposition of the template. As a consequence, when the Fenton detemplation conditions were the same, Beta zeolites with lower Al content achieve similar but slightly lower detemplation degree (Table 1, entries 6 and 12) compared to their counterpart with higher Al content (Table 1, entry 9). In agreement with this observation, a slightly lower degree of detemplation (93%) was achieved for the more hydrophobic Sn-Beta (Table 1, entries 28-30).

Table 1. CHN elemental analysis (*wt.*%) of the materials under study. The reaction time was 24 hours in all the Fenton detemplation experiments, except for SnBeta (48 hours).

	Material	Si/Al ratio	Fenton detemplation conditions			Elemental analysis / *wt.* %				% of Fe adsorbed from Fenton	η^C (%)[d]	Thermal treatment´s conditions	Supplier's code
			H_2O_2 / mL/g_{zeo}	T / °C	[Fe] / ppm	C	H	N	Fe				
1	BT1-*raw*	-				10.37	2.12	1.62	-	-	0.0	-	HSZ930A
2	BT1-*C*	12[a]				0.00	0.32	0.00	0.01	-	100.0	550 °C (6h)	
3	BT1-*f*	12[a]	30	70	30	0.07	1.33	1.34	0.10	75	99.3	-	
4	BT2-*raw*	-				10.55	2.42	1.64	-	-	0.0	-	HSZ940A
5	BT2-*C*	18[a]				0.03	0.80	0.00	0.02	-	99.7	550 °C (6h)	
6	BT2-*f*	18[a]	50	90	10	0.35	1.27	1.17	0.12	98	96.6	-	
7	BZ1-*raw*	-				10.9	2.38	1.79	-	-	0.0	-	CP806E
8	BZ1-*C*	11[a]				0.03	1.06	0.00	0.03	-	99.8	550 °C (6h)	
9	BZ1-*f*	11[a]	50	90	10	0.12	1.49	1.53	0.08	45	98.9	-	
10	BZ2-*raw*	-				9.63	2.16	1.54	-	-	0.0	-	CP806C
11	BZ2-*C*	18[a]				0.02	0.64	0.00	0.03	-	99.8	550 °C (6h)	
12	BZ2-*f*	17[a]	50	90	10	0.22	1.17	0.08	0.08	60	97.7	-	
13	MFI1-*raw*	-				3.84	0.89	1.98	-	-	0.0	-	CBV5510G
14	MFI1-*C*	27[a]				0.05	0.27	0.00	0.03	-	98.6	550 °C (6h)	
15	MFI1-*f*	27[a]	50	90	10	1.12	0.65	0.81	n.a.	n.a.	70.8	-	
16	MFI2-*raw*	-				7.30	1.56	0.78	-	-	0.0	-	CBV8010

	Material	Si/Al ratio	Fenton detemplation conditions			Elemental analysis / *wt.* %				% of Fe adsorbed from Fenton	η^C (%)[d]	Thermal treatment´s conditions	Supplier's code
			H_2O_2 / mL/g_{zeo}	T / °C	[Fe] / ppm	C	H	N	Fe				
17	MFI2-*C*	41[a]				0.06	0.33	0.00	0.02	-	99.1	550 °C (6h)	
18	MFI2-*f*	-	15	80	60	5.79	1.30	0.72	-	-	20.7	-	
19	MFI3-*raw*	-				7.42	1.72	0.79	-	-	0.0	-	CBV2801
20	MFI3-*C*	49[a]				0.05	0.14	0.00	0.02	-	99.3	550 °C (6h)	
21	MFI3-*f*	48[a]	100	80	30	7.31	1.66	0.83	n.a.	n.a	1.4	-	
22	MesoMFI-*raw*	n.a.				60.71	2.38	1.53	-	-	0.0	-	[85]
23	MesoMFI-*C*	35[b]				1.57	0.49	0.00	0.07	-	97.4	550 °C (6h)	
24	MesoMFI-*f*		90	90	10	6.82	1.56	0.85			88.8	-	
24a	MesoMFI-*fNA*	32	90	90	10	-	-	-	0.90	100	100.0	NH_4NO_3 exchange & 400 °C (6h)	
25	MCM-22-pd-*raw*	-				31.57	6.09	2.43	-	-	0.0	-	Section 2.2.1
26	MCM-22-pd -*C*	13[a]				0.26	0.98	0.00	-	-	99.2	550 °C (6h)	
27	MCM-22-pd -*f*		90	90	10	3.34	1.29	1.07			89.4	-	
27a	MCM-22-pd-*fA*	13	90	90	10	-	-	-	0.74	73	100.0	400 °C (6h)	
28	SnBeta-*raw*	125[c]				11.89	2.48	1.82	-	-	0.0	-	[54]
29	SnBeta-*C*	149[a]				0.04	0.06	0.00	0.00	-	99.6	550 °C (6h)	
30	SnBeta-*f*	142[a]	90	90	30	0.84	0.66	0.11	0.37	99	93.0	-	

[a] Si/Al ratio (or Sn/Si ratio in the case of SnBeta) from ICP-AES analysis. [c] Si/Sn ratio provided by the supplier. [d] determined by elemental analysis of C. n.a.: not analysed.

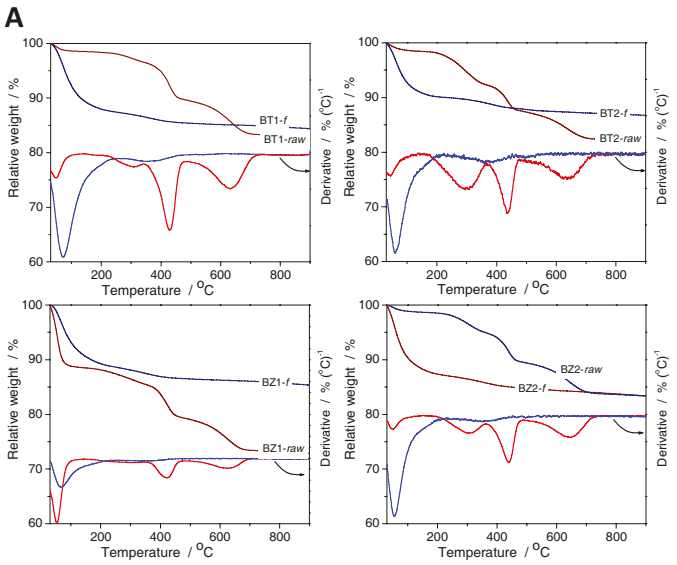

Figure 2A. TGA/DTGA comparison of Fenton detemplated zeolites (blue line) and the parent materials (red line). The treatment conditions are given in Table 1.

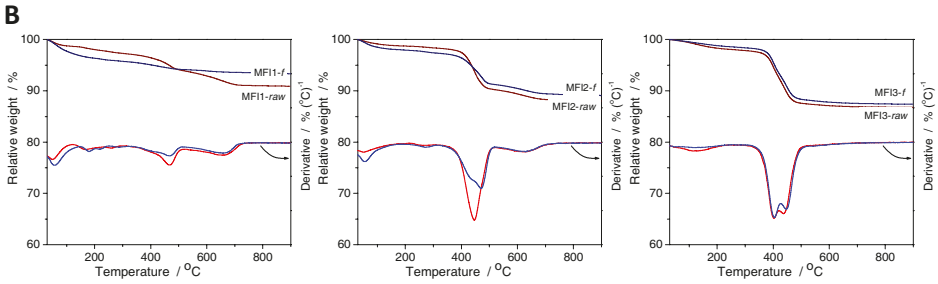

Figure 2B. TGA/DTGA comparison of Fenton detemplated zeolites (blue line) and the parent materials (red line). The treatment conditions are given in Table 1.

The Fenton detemplation was significantly less efficient with the ZSM-5 [MFI] zeolites, even under relatively harsh conditions (e.g. high concentration of Fe^{n+} and amount of H_2O_2, see Table 1, entries 15, 18 and 21, and Table 2 for a more detailed overview). The lower efficiency of the Fenton approach for the zeolites is confirmed by the very similar TGA profiles of the raw and Fenton samples (Fig. 2B). In both cases, the weight loss at T < 200 °C is due to removal of physisorbed water, the weight

loss at T = 400-450 ^{0}C is assigned to the decomposition of the template (tetraprophylammonium, TPA^{+}) and the last signal at T > 600 ^{0}C is due to the combustion of coke produced during the template decomposition (only for MFI1 and MFI2).

Additionally, a shift of the second DTGA peak for MFI with decreasing Al loadings, from ca. 450 to 400 ^{0}C, was observed. This shift indicates a change in the stability of the template occluded in the zeolitic pores, which increases when the interaction template-framework is stronger. As mentioned above, the presence of Al in the framework leads to a partially negatively charged framework, which enhances the strength of the interaction with the templating cations. Therefore, the lower the Si/Al ratio in the ZSM-5 series, the higher the decomposition temperature of the template [72,73]. This shift is almost negligible for Beta zeolites (Figure 2A), indicating a weaker interaction between template and framework. This is in agreement with the opposite trend in the degree of detemplation as a function of the Al content observed for the ZSM-5 and Beta zeolites. The higher difficulty in removing the template from zeolite ZSM-5 compared to zeolite Beta is attributed to the smaller pore openings of the former (10-MR vs. 12-MR); to the higher tortuosity of its 3D-network implying a twisted disposition of the template (tetrapropylammonium, TPA^{+}); to the longer hydrophobic chains in TPA^{+} compared to the template in Beta (tetraethyl ammonium, TEA^{+}); and to the stronger interaction between the template and the inorganic framework compared to that in zeolite Beta [13,75-77]. The size of the zeolite primary particles can also play a role in the efficiency of the Fenton detemplation. SEM analysis (Figure 3) shows that MFI1 and MFI2 have an analogous particle size (around 0.4 μm) while the particle size is noticeably larger for MFI3 (1.1 μm). This can contribute to explain the extremely low degree of Fenton detemplation of the latter material (Table 1, entry 21).

The Fenton detemplation of MesoMFI led to a much higher efficiency in template removal (89 %, see entry 24 in Table 1) compared to that discussed above for the conventional MFI zeolites. This difference is ascribed to the efficient removal of the carbon black used to attain the mesoporosity,

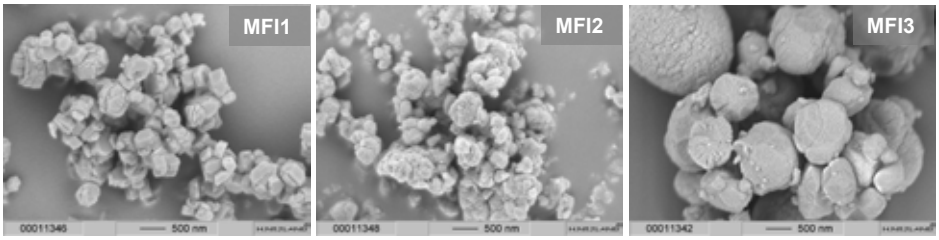

Figure 3. SEM images of the three ZSM-5 zeolites prior to detemplation.

whereas the removal of TPA^+ used for the creation of the MFI micropores is expected to be incomplete. The DTGA profile of the parent material, MesoMFI-*raw* (Fig. 2C), shows a main decomposition peak with maximum at around 650 °C, which is attributed to the decomposition of the carbon black used as template for the mesopores, whereas no peak related to the decomposition of the micropore-template (TPA^+) could be observed. This means that the mass of the TPA^+ is difficult to discern from the large contribution of carbon black whose weight loss covers the range from *ca.* 120 to 630°C. After Fenton detemplation (MesoMFI-*f*), no peak was observed around 650 °C in the DTGA profile, proving the complete removal of the carbon template. This was also confirmed by naked eye observation, as an off-white sample was obtained. On the other hand, a broad peak corresponding to the TPA^+ decomposition was observed between 400 and 500 °C, confirming the incomplete removal of the micropore-template [72]. Once the major fraction of the carbon-containing species was removed by Fenton detemplation, it was possible to remove the residual TPA^+ (as shown by TGA, see Fig. 2C) by a thermal treatment at significantly lower temperature (400 °C; procedure described in section 2.2.5) compared to the conventional calcination (550 °C) [78]. This combination of Fenton and relatively mild thermal techniques is a straightforward and attractive choice as it avoids the structural stress caused by the steam produced when the carbon black is thermally decomposed.

MCM-22-pd was prepared employing three organic molecules: C_{16}TEABr and TPAOH, which are responsible for the delamination of the

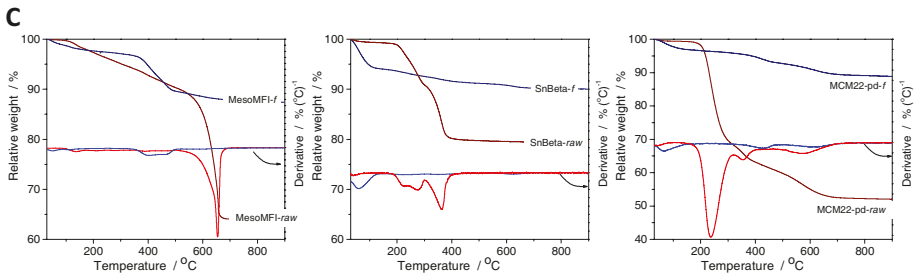

Figure 2C. TGA/DTGA comparison of Fenton detemplated zeolites (blue line) and the parent materials (red line). The treatment conditions are given in Table 1.

material, and HMI, which leads to the creation of the microporosity. The voids between layers of the delaminated MCM-22-pd are in the mesopore range. Weight losses observed in the TGA for the raw MCM-22-pd cover a broad range of temperatures [79]. The weight loss at T < 200 °C, is associated to water desorption. At temperature in the range 200-400 °C, the HMI in the interlayer voids is decomposed, followed by the HMI located within the layers at temperatures ranging from 400 to 500 ^{0}C, and finally, by HMI molecules occluded in the smaller micropores present within the layers at temperatures between 500 ^{0}C and 700 ^{0}C. Weight losses at higher temperatures, as it was pointed out for Beta and MFI zeolites, are related to the combustion of residues (e.g. coke). When Fenton detemplation was applied, 90 *wt.*% of the carbon was removed. The remaining carbon decomposes over a wide range of temperatures according to the TGA/DTGA pattern (Figure 2C). The TGA profile of MCM-22-pd-f only shows two weight losses: one due to water desorption (T < 200 ^{0}C) and a broad one between 400-500 ^{0}C, related to remaining, hardly accessible HMI molecules located within the layers. Also for this material the combination of Fenton detemplation with a relatively mild thermal treatment at 400°C (compared to the conventional calcination temperature at 550°C [62,67]) was efficient to fully remove the organic residues, as proven by TGA (Table 1, entries 24a and 27a).

Table 2. Experimental optimisation of MFI under different Fenton conditions. The Fe amount was determined by ICP-AES and the level of detemplation by TGA and CHN elemental analysis.

Material	Fenton detemplation conditions				Elemental analysis / *wt.* %				% Detemplation[a,b]
	H_2O_2 amount / mL/g zeolite	T / °C	[Fe] / ppm	Reaction time / h	C	H	N	Fe	
MFI1-*a*	30	70	30	24					66[a]
MFI1-*b*	30	70	30	52					65[a]
MFI1-*c*	30	80	30	24					53[a]
MFI1-*d*	100	80	30	24				0.34	52[a]
MFI1-*e*	15	80	60	24	1.12	0.65	0.81		74[a]/71[b]
MFI2-*a*	30	70	30	24					11[a]
MFI2-*b*	30	70	30	52					6[a]
MFI2-*c*	30	80	30	24					9[a]
MFI2-*d*	100	80	30	24					17[a]/21[b]
MFI2-*e*	15	80	60	24	5.79	1.30	0.72		5[a]
MFI3-*a*	30	70	30	24					1[a]
MFI3-*b*	30	70	30	52					0[a]
MFI3-*c*	30	80	30	24	7.31	1.66	0.83		1/1.4[b]
MFI3-*d*	100	80	30	24				0.10	1[a]
MFI3-*e*	15	80	60	24					0[a]

The pH was controlled to 4 before the reaction was started. [a]: measured by TGA. [b]: measured by elemental analysis.

4.3.2. MATERIAL PROPERTIES

An expected asset of Fenton detemplation compared to calcination is the lower impact on the structure of the zeolitic material. To investigate whether the physicochemical features of the studied zeolites were preserved upon Fenton detemplation, the structure, composition, texture and Al-coordination of the materials were analysed and compared to those of the calcined counterparts.

The degree of structure preservation upon detemplation was studied by X-ray diffraction (Figure 4). The characteristic diffraction pattern for each structure (BEA, MFI, and delaminated MWW) was observed for all the seven materials under study, both for the calcined and Fenton detemplated

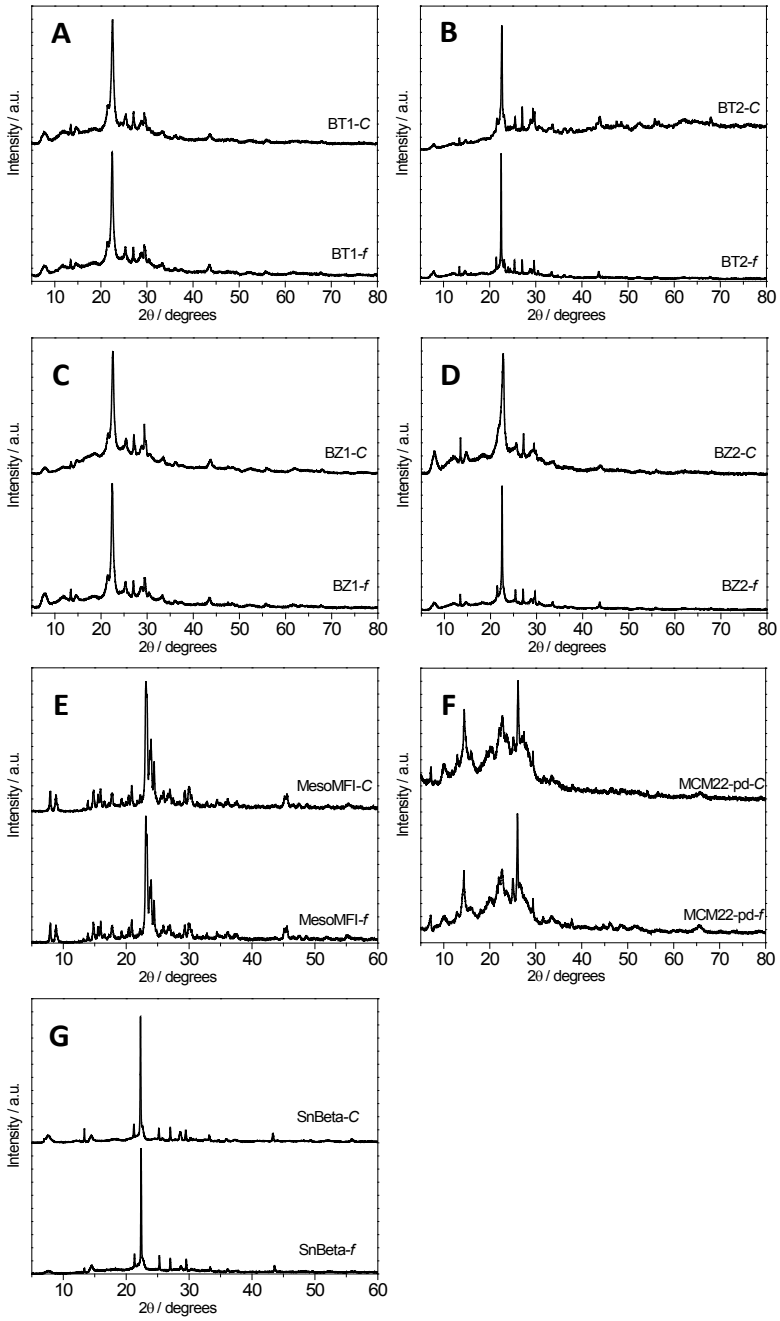

Figure 4. XRD of the Fenton detemplated materials under study compared to the calcined material. A) BT1; B) BT2; C) BZ1; D) BZ2; E) MesoMFI; F) MCM-22-pd; and G) SnBeta.

zeolites. The analogous intensity of the diffraction peaks of the materials obtained with the two approaches indicates a similar degree of crystallinity. As the pH during Fenton detemplation is acidic, dealumination might occur [80]. However, the Si/Al and Si/Sn ratio were not altered by Fenton detemplation (Table 1), which indicates that the conditions were sufficiently mild as to avoid removal of the metal atoms from the framework.

Fenton detemplation implies the use of an aqueous Fe^{3+}/Fe^{2+} solution. These iron cations can be adsorbed on the zeolites during Fenton detemplation. The amount of Fe present in the zeolites that underwent Fenton detemplation was determined by ICP-AES and compared to the Fe content of the calcined materials. Notably, traces of Fe were found in all the calcined materials (Table 1, *-C* named materials). This Fe might have been introduced as impurity in the aluminium source used during the synthesis and/or from the synthesis process itself (reactor, mixer, etc.). As anticipated, the Fe content in the Fenton detemplated materials was higher due to adsorption of Fe^{n+} from the solution. The Fe content and the fraction of Fe adsorbed from the solution (calculated using eq. 2) are detailed in Table 1 (*-f* materials). Although a significant fraction of the Fe employed was adsorbed (from a minimum of 45% to complete adsorption), the Fe content was below 1 *wt.*% for all materials. The exchange of Fe cations in the zeolites can influence their catalytic properties as it can affect the type, number and strength of active sites. For this reason, he Fe concentration was kept as low as possible in the Fenton treatments used in this work. On the other hand, it should be noted that for some applications, such as the abatement of nitrous oxide, the presence of Fe is desirable [26,81].

The textural properties of the materials such as surface area, pore volume and particles agglomeration were studied by means of argon physisorption (Table 3 and Figure 5). For the characterisation of microporous materials, this technique is preferred to nitrogen physisorption, because the quadrupolar moment of the nitrogen molecule leads to less accurate discrimination between pore sizes [82]. For all studied samples, the isotherms of the calcined and Fenton counterparts had a comparable shape,

in agreement with the structure preservation exposed by the XRD patterns. In the cases in which the template removal by the Fenton approach had an efficiency ≥ 99% (*i.e.* for BT1 and BZ1), the surface area and pore volume of the obtained zeolite are significantly higher compared to those of the calcined counterpart (Table 3). Although no structural differences were observed by XRD, this result shows that if complete detemplation is obtained with the Fenton treatment, the textural properties of the material are preserved better than in the material obtained by calcination. The Beta zeolites BT1 and BZ1 show isotherms of type IV with H3 hysteresis loop at $0.5<p/p^{o}<0.8$ for BT1, and at $p/p^{o}>0.7$ for BZ1. This profile is characteristic of nano-sized zeolites with multilayer adsorption and capillary condensation in the mesopore range [83], which is associated to interparticle voids [84]. Similarly, both BT2 and BZ2 display type I isotherm, characteristic of microporous materials, but slightly approaching a type IV for BZ2-*f* due to a small H3 hysteresis loop at high pressures ($p/p^{o}>0.3$). Contrarily to what observed for BT1 and BZ1, the zeolites BT2 and BZ2 obtained by Fenton detemplation (Table 3, entries 4 and 8) present a lower micropore area and volume compared to the calcined samples (Table 3, entries 3 and 7). This is due to the small amounts of residual carbon in these materials (0.35 and 0.22 *wt.*%, respectively, see Table 1). It is worth noting that for all four Beta zeolites, the external surface area was higher for the materials obtained by Fenton detemplation compared to the calcined counterparts (Table 3), which suggests that calcination causes aggregation of the zeolite particles with consequent loss of external surface area. Sn-Beta displays a type I isotherm, characteristic of microporous materials and very similar to that of BT2. The Fenton detemplated Sn-Beta zeolite displays significantly lower surface area compared to the calcined counterpart (Table 3 and Figure 5). Based on the elemental analysis, there was no carbon residue in SnBeta-f, nor Sn-leaching (as determined via ICP-AES of the liquid phase obtained from the Fenton reaction). Further studies are necessary to clarify the origin of the deterioration of the textural properties of Sn-Beta-f. The Ar physisorption isotherms of MesoMFI-*f* and MCM-22-pd-*f* are characterised by

Table 3. Summary of the porosity parameters calculated from argon physisorption isotherms.

Entry	Material	S_{BET}; m^2/g	S_μ; m^2/g	External Surface Area (S_{BET}-S_μ; m^2/g)	V_T; m^3/g	V_μ; cm^3/g
1	BT1-*C*	566	248	318	0.508	0.150
2	BT1-*f*	628	286	342	0.562	0.170
3	BT2-*C*	558	406	152	0.289	0.182
4	BT2-*f*	506	277	229	0.265	0.115
5	BZ1-*C*	562	266	296	0.787	0.111
6	BZ1-*f*	646	282	364	0.872	0.116
7	BZ2-*C*	574	397	177	0.324	0.177
8	BZ2-*f*	597	301	296	0.385	0.128
9	MesoMFI-*CNA*	368	271	97	0.403	0.107
10	MesoMFI-*f*	101	33	68	0.349	0.016
11	MesoMFI-*fNA*	374	276	98	0.421	0.109
12	MCM-22-pd-*C*[a]	556	19	537	0.441	0.064
13	MCM-22-pd -*f*[a]	312	11	302	0.312	0.030
14	MCM-22-pd -*fA*[a]	356	30	326	0.381	0.0002
15	SnBeta-*C*	546	380	166	0.300	0.171
16	SnBeta-*f*	383	289	95	0.261	0.131

[a]: NLDFT was used for the calculations; the *t*-plot approach was unable to detect micropores.

low adsorption at low relative pressures, due to the presence of residual template blocking the micropores (*vide supra*). MesoMFI displays an isotherm of type IV with and H3 hysteresis loop sharply defined in the range p/p_o>0.8 as it was described in the synthesis literature of this material [85]. A relatively mild calcination step at 400°C was applied to remove the residual template from the micropores of MesoMFI-*f* and MCM-22-pd-*f*. MesoMFI-*fNA* displayed similar yet slightly higher surface area and pore volume compared to the calcined material, confirming that Fenton detemplation coupled with calcination at 400°C leads to efficient detemplation of the material. Low-pressure high-resolution Ar (LPHR-Ar) had to be applied to MCM-22-pd in order to detect the micropore contribution. This technique provides high resolution analysis in the microporosity range, being especially suitable when the amount of microporous is very little compared to the overall porosity. MCM-22-pd shows a type IV isotherm with an H4

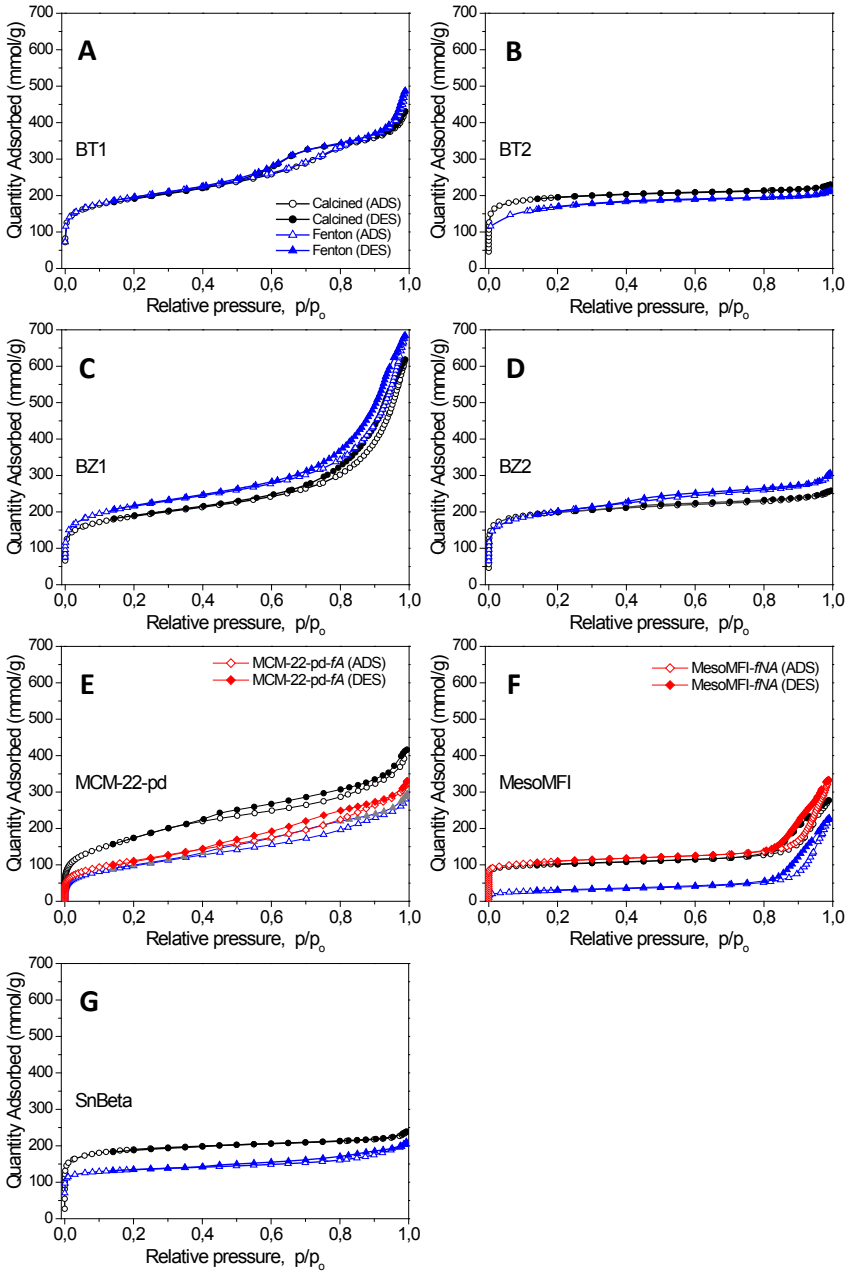

Figure 5. Argon physisorption isotherms at -186 °C of the Fenton detemplated materials under study compared to the calcined materials. In the case of MesoMFI and MCM-22-pd, the isotherm of the Fenton detemplated materials treated thermally are also presented. The data for BT1 were reported previously [71] and are presented here for comparison.

hysteresis loop, which corresponds to partially delaminated materials with slit-like voids in the mesopore range. It must be noted that the calcined material, MCM-22-pd-*C*, has a relatively lower fraction of mesopore volume (85% of total pore volume) compared to the typically reported values (96%) [86], which indicates a lower layer expansion (and this is the reason for which this material was denoted as 'partially delaminated'). The additional thermal treatment at 400°C to MCM-22-pd-*f*A increased the surface area and pore volume but the textural properties were still inferior compared to MCM-22-pd-*C* (Table 3, entries 12 and 14). This difference is tentatively ascribed to condensation between layers, which might have occurred under these conditions.

The presence of Al substituting Si in tetrahedral sites of zeolites generates Brønsted acidity if H^+ are the counter-ions balancing the charge difference between Al and Si. This feature is crucial for the application of zeolites as solid acid catalysts [87]. Since the detemplation process can cause removal of Al atoms from the zeolite framework it is important to characterise the coordination of Al atoms in the studied aluminosilicate zeolites by ^{27}Al-NMR (Figure 6). The spectra of the raw materials showed a single peak at *ca.* 56 ppm corresponding to the tetrahedrally coordinated framework aluminium atoms (Al_{tetra}) [39]. Upon calcination, a second peak belonging to octahedrally coordinated extra-framework aluminium species (EFAL) appears at *ca.* 0 ppm [35] for all materials but MesoMFI (due to the high stability of the large MFI crystals [85]). Additionally, the calcined H-Beta zeolites displayed a broad shoulder of the Al_{tetra} signal, which is assigned to pentacoordinated Al (Al_{penta}). EFAl sites arise from the distortion of tetrahedrically coordinated Al sites when stress is applied to the framework. For example, the high temperatures applied during calcination combined with the generation of steam due to the decomposition of the organics can lead to the extraction of some Al atoms from the framework with generation of extra-framework species such as $Al(OH)^{2+}$, $Al(OH)_2^+$, $Al(OH)_3$, AlO(OH) and Al_2O_3 [88]. Remarkably, the Fenton detemplation hardly affected the coordination of Al as shown by the

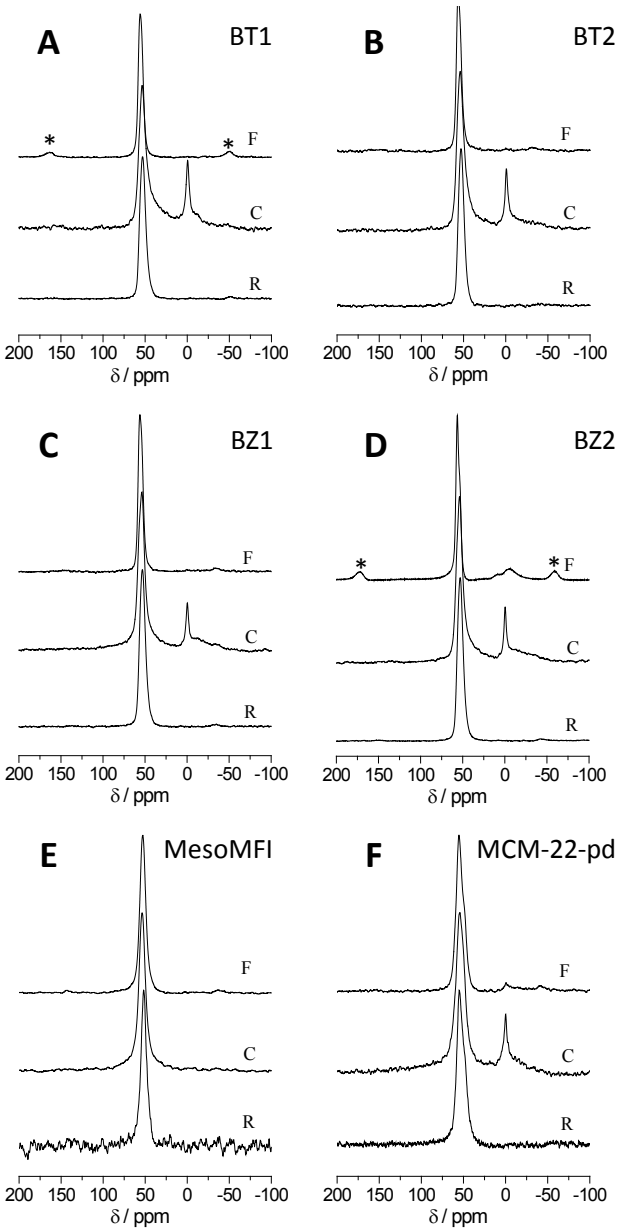

Figure 6. ^{27}Al MAS NMR of the Fenton detemplated materials under study compared to the raw and calcined counterparts. (* denotes spinning side bands).

absence of any additional peak besides the original single resonance of the framework aluminium (Al_{tetra}). Only for BZ2, and to a lesser extent for MCM-22-pd, a weak signal was observed in the range attributed to octahedrally coordinated aluminium. The results of the characterisation by ^{27}Al-NMR prove that Fenton detemplation is much more suitable for preserving the tetrahedrally coordinated framework Al compared to template removal by calcination. This is an important feature in view of the catalytic application of these zeolites, as it allows preserving most of the Brønsted acid sites.

4.4. CONCLUSIONS

Fenton detemplation is an environmentally friendly approach applicable to different zeolitic structures. Physicochemical features including the nature of the template, the channel size, pore accessibility, template-framework interaction, particle size and Si/Al ratio were found to influence the detemplation process leading to different efficiency in removing the template. High efficiency was observed in removing the template used in the synthesis of BEA zeolites (TEA^+), whereas the Fenton approach proved less effective for detemplating MFI zeolites (TPA^+ as template). Fenton detemplation was also successfully applied to remove the carbon black used to generate a mesoporous structure (MesoMFI) and the CTABr used as delaminating agent for layered zeolites (MCM-22-pd). For the last two materials, the complete removal of the carbon-containing species from the micropores could be achieved with a relatively mild thermal treatment at 400°C.

Importantly, the employed Fenton approach allowed detemplation of the studied materials without damaging their structure and without affecting the coordination of the tetrahedrally coordinated Al sites. These features are particularly attractive in view of catalytic application of the zeolites and can pave the road towards industrial application of Fenton detemplation in the manufacture of zeolites.

4.5. ACKNOWLEDGEMENTS

The authors are thankful for the financial support from the Nederlandse Organisatie voor Wetenschappelijk Onderzoek (NWO) under the project VIDI 10284. Shell, DSM, Norit, Zeolyst and Topsoe are acknowledged for the kind supply of materials. Prof. N. Nishiyama (Osaka) is acknowledged for sharing ideas on the MCM-22 synthesis. We thank: Dr. K. Djanashvili from the TU Delft for her support in the Al-NMR measurements; J. Baas from the Solid State Materials, E. Polushkin and J. Velde from the University of Groningen for their support in the XRD, SEM and elemental analysis measurements, respectively.

4.6. REFERENCES

[1] M.E. Davis, Nature. 417 (2002) 813-821.

[2] A. Corma, J. Catal. 216 (2003) 298-312.

[3] W. Vermeiren, J. Gilson, Top. Catal. 52 (2009) 1131-1161.

[4] Zeolites and Ordered Porous Solids: Fundamentals and Applications, First edition, Editorial Universitat Politècnica de València, 2011.

[5] J. Perez-Ramirez, C.H. Christensen, K. Egeblad, C.H. Christensen, J.C. Groen, Chem. Soc. Rev. 37 (2008) 2530-2542.

[6] Handbook of Heterogeneous Catalysis, (2004), Wiley-VCH, Weinheim, 1999.

[7] C. Baerlocher, L.B. McCusker, D.H. Olson, Atlas of Zeolite Framework Types, Sixth Revised Edition, Elsevier, 2007.

[8] R. Xu, W. Pang, J. Yu, Q. Huo, J. Chen, Anonymous Chemistry of Zeolites and Related Porous Materials. Synthesis and Structures, John Wiley & Sons, (Asia), 2007, pp. 39.

[9] J. Cejka, A. Corma, S. Zones (Eds.), Zeolites and Catalysis: Synthesis, Reactions and Applications, Wiley-VCH, Weinheim, 2010, pp. 67.

[10] C.S. Cundy, P.A. Cox, Chem. Rev. 103 (2003) 663-701.

[11] V. Valtchev, G. Majano, S. Mintova, J. Perez-Ramirez, Chem. Soc. Rev. 42 (2013) 263-290.

[12] J. Cejka, H. van Bekkum, A. Corma, F. Schueth, Introduction to Zeolite Science and Practice, 3rd Revised Edition, Stud. Surf. Catal. 168, Elsevier, Amsterdam, 2007.

[13] R. Xu, W. Pang, J. Yu, Q. Huo, J. Chen, Chemistry of Zeolites and Related Porous Materials. Synthesis and Structures, John Wiley & Sons, (Asia), 2007.

[14] H.A. Aleksandrov, C. Aquino, F. Babonneau, D. Bégin, J.A. van Bokhoven, J. Bronić, M.A. Carreon, J. Čejka, M.H.J.M. de Croon, T. Devic, J. Dong, A.M. Doyle, C. Fernandez-Martin, F. Gaslain, V.V. Guliants, K.I. Hadjiivanov, M. Jaber, A. Jankowska, T.A. Jelić, V. Kaučič, S. Kowalak, M.V. Landau, B. Lebeau, M. Ledoux, C.M. Lew, Y. Liu, R.F. Lobo, N.Z. Logar, B. Louis, D.J. Macquarrie, G. Mali, T. Maschmeyer, M. Mazaj, J. Miehé-Brendlé, M.J.M. Mies, B. Mihailova, S. Mintova, I. Naydenova, T.M. Nenoff, N.N. Tušar, P.S. Petkov, G.P. Petrova, C. Pham-Huu, P. Pina, G.D. Pirngruber, E.V. Rebrov, N. Ren, A. Ristić, J. Santamaría, W. Schmidt, J.C.

Schouten, C. Serre, B. Subotić, M. Sun, Y. Tang, V. Toal, L. Tosheva, M. Urbiztondo, V. Valtchev, G.N. Vayssilov, A. Vinu, L. Vradman, A. Walcarius, J. Wang, Y. Yan, Y. Zhang, Ordered Porous Solids, Elsevier, Amsterdam, 2009.

[15] E.R. Geus, H. Vanbekkum, Zeolites. 15 (1995) 333-341.

[16] M. Milanesio, G. Artioli, A.F. Gualtieri, L. Palin, C. Lamberti, J. Am. Chem. Soc. 125 (2003) 14549-14558.

[17] C. Minchev, H. Weyda, V. Minkov, V. Penchev, H. Lechert, J. Therm. Anal. Calorim. 37 (1991) 573-582.

[18] A. Corma, V. Fornes, M. Navarro, J. Pérez-Pariente, J. Catal. 148 (1994) 569-574.

[19] E. Lami, F. Fajula, D. Anglerot, T. Courieres, Microporous Mater. 1 (1993) 237-245.

[20] O. Kresnawahjuesa, D.H. Olson, R.J. Gorte, G.H. Kuhl, Micropor. Mesopor. Mat. 51 (2002) 175-188.

[21] J. Kuhn, M. Motegh, J. Gross, F. Kapteijn, Micropor. Mesopor. Mat. 120 (2009).

[22] J. Kuhn, J. Gascon, J. Gross, F. Kapteijn, Micropor. Mesopor. Mat. 120 (2009) 12-18.

[23] M. El Roz, L. Lakiss, V. Valtchev, S. Mintova, F. Thibault-Starzyk, Micropor. Mesopor. Mat. 158 (2012) 148-154.

[24] A.N. Parikh, A. Navrotsky, Q.H. Li, C.K. Yee, M.L. Amweg, A. Corma, Micropor. Mesopor. Mat. 76 (2004) 17-22.

[25] Q.H. Li, M.L. Amweg, C.K. Yee, A. Navrotsky, A.N. Parikh, Micropor. Mesopor. Mat. 87 (2005) 45-51.

[26] I. Melian-Cabrera, F. Kapteijn, J.A. Moulijn, Chem. Commun. (2005) 2178-2180.

[27] I. Melian-Cabrera, F. Kapteijn, J.A. Moulijn, Chem. Commun. (2005) 2744-2746.

[28] I. Melián-Cabrera, A.H. Osman, E.R.H. van Eck, A.P.M. Kentgens, E. Polushkin, F. Kapteijn, J.A. Moulijn, Stud. Surf. Sci. Catal., 170 (2007), 648-654.

[29] I.V. Melián-Cabrera, J.A. Moulijn, in: A. Cybulski, J.A. Moulijn, A. Stankiewicz (Eds.), Novel Concepts in Catalysis and Chemical Reactors: Improving the Efficiency for the Future, Wiley, Weinheim, 2010.

[30] L.L. Perez, M.J. Ortiz-Iniesta, Z. Zhang, I. Agirrezabal-Telleria, M. Santes, H.J. Heeres, I. Melian-Cabrera, J. Mater. Chem. 1 (2013) 4747-4753.

[31] E. Neyens, J. Baeyens, J. Hazard. Mater. 98 (2003) 33-50.

[32] W.Z. Tang, Physicochemical Treatment of Hazardous Wastes, CRC Press LLC, Florida, 2004.

[33] J.J. Pignatello, E. Oliveros, A. MacKay, Crit. Rev. Environ. Sci. Technol. 36 (2006) 1-84.

[34] I. Melian-Cabrera, S. Espinosa, F.J. Garcia-Montelogo, F. Kapteijn, J.A. Moulijn, Chem. Commun. (2005) 1525-1527.

[35] J. Perezpariente, J. Sanz, V. Fornes, A. Corma, J. Catal. 124 (1990) 217-223.

[36] A. Omegna, M. Vasic, J. van Bokhoven, G. Pirngruber, R. Prins, Phys. Chem. Chem. Phys. 6 (2004) 447-452.

[37] Y.F. Chu, J.P. McWilliams, US 4916097 (1990).

[38] C.Y. Yeh, X. Gao, W.E. Cormier, M. Pasquale, US 2004/0014592 A1 (2004).

[39] E. Bourgeat-Lami, P. Massiani, F. Direnzo, P. Espiau, F. Fajula, T. Courieres, Appl. Catal. 72 (1991) 139-152.

[40] T. Koranyi, J. Nagy, J. Phys. Chem. B. 109 (2005) 15791-15797.

[41] J.C. Jansen, E.J. Creyghton, S.L. Njo, H. vanKoningsveld, H. vanBekkum, Catal. Today. 38 (1997) 205-212.

[42] P.A. Wright, W.Z. Zhou, J. Perez-Pariente, M. Arranz, J. Am. Chem. Soc. 127 (2005) 494-495.

[43] A. Simon-Masseron, J.P. Marques, J.M. Lopes, F.R. Ribeiro, I. Gener, M. Guisnet, App. Catal. A-Gen. 316 (2007) 75-82.

[44] L. Fernandes, J. Monteiro, E. Sousa-Aguiar, A. Martinez, A. Corma, J. Catal. 177 (1998) 363-377.

[45] M.A. Arribas, A. Martinez, Catal. Today. 65 (2001) 117-122.

[46] M. Bregolato, V. Bolis, C. Busco, P. Ugliengo, S. Bordiga, F. Cavani, N. Ballarini, L. Maselli, S. Passeri, I. Rossetti, L. Forni, J. Catal. 245 (2007) 285-300.

[47] J. Das, Y.S. Bhat, A.B. Halgeri, Catal. Lett. 23 (1994) 161-168.

[48] J. Cejka, B. Wichterlova, Catal. Rev. 44 (2002) 375-421.

[49] A. Corma, A. Martinez, P.A. Arroyo, J.L.F. Monteiro, E.F. SousaAguiar, Appl. Catal. A-Gen. 142 (1996) 139-150.

[50] G. Bellussi, G. Pazzuconi, C. Perego, G. Girotti, G. Terzoni, J. Catal. 157 (1995) 227-234.

[51] R. Srivastava, N. Iwasa, S. Fujita, M. Arai, Catal. Lett. 130 (2009) 655-663.

[52] A.E.W. Beers, J.A. van Bokhoven, K.M. de Lathouder, F. Kapteijn, J.A. Moulijn, J. Catal. 218 (2003) 239-248.

[53] A. Corma, L. Nemeth, M. Renz, S. Valencia, Nature. 412 (2001) 423-425.

[54] M.S. Holm, S. Saravanamurugan, E. Taarning, Science. 328 (2010) 602-605.

[55] L. Young, S. Butter, W. Kaeding, J. Catal. 76 (1982) 418-432.

[56] N. Rahimi, R. Karimzadeh, Appl. Catal. A-Gen. 398 (2011) 1-17.

[57] G. Mirth, J. Cejka, J.A. Lercher, J. Catal. 139 (1993) 24-33.

[58] K. Egeblad, C.H. Christensen, M. Kustova, C.H. Christensen, Chem. Mat. 20 (2008) 946-960.

[59] A. Corma, V. Fornes, J.M. Guil, S. Pergher, T.L.M. Maesen, J.G. Buglass, Micropor. Mesopor. Mat. 38 (2000) 301-309.

[60] K. Na, M. Choi, W. Park, Y. Sakamoto, O. Terasaki, R. Ryoo, J. Am. Chem. Soc. 132 (2010) 4169-4177.

[61] L. Xu, H. Xing, S. Wu, J. Guan, M.J. Jia, Q. Kan, Bull. Mater. Sci. 34 (2011) 1605-1610.

[62] S. Inagaki, H. Imai, S. Tsujiuchi, H. Yakushiji, T. Yokoi, T. Tatsumi, Micropor. Mesopor. Mat. 142 (2011) 354-362.

[63] J. Wang, X. Tu, W. Hua, Y. Yue, Z. Gao, Micropor. Mesopor. Mat. 142 (2011) 82-90.

[64] S. Inagaki, K. Kamino, E. Kikuchi, M. Matsukata, Appl. Catal. A-Gen. 318 (2007) 22-27.

[65] W. Fan, S. Wei, T. Yokoi, S. Inagaki, J. Li, J. Wang, J.N. Kondo, T. Tatsumi, J. Catal. 266 (2009) 268-278.

[66] W.J. Roth, J. Cejka, Catal. Sci. Technol. 1 (2011) 43-53.

[67] Y. Wu, X. Ren, Y. Lu, J. Wang, Micropor. Mesopor. Mat. 112 (2008) 138-146.

[68] Micromeritics Instruments Corporation, Micromeritics 2420, Operation Manual, Micromeritics Instruments Corporation, USA.

[69] R.J. Watts, M.D. Udell, P.A. Rauch, S.W. Leung, Hazard. Waste Hazard. Mater. 7 (1990) 335-345.

[70] C. Walling, Acc. Chem. Res. 8 (1975) 125-131.

[71] M.J. Ortiz-Iniesta, I.V. Melián-Cabrera, J. Micropor. Mesopor. Mat 206 (2015) 58-66.

[72] L.M. Parker, D.M. Bibby, J.E. Patterson, Zeolites. 4 (1984) 168-174.

[73] M. Soulard, S. Bilger, H. Kessler, J. Guth, Zeolites. 7 (1987) 463-470.

[74] L. Shirazi, E. Jamshidi, M.R. Ghasemi, Cryst. Res. Technol. 43 (2008) 1300-1306.

[75] R. Gougeon, L. Delmotte, D. Le Nouen, Z. Gabelica, Micropor. Mesopor. Mat. 26 (1998) 143-151.

[76] D.P. Serrano, J. Aguado, G. Morales, J.M. Rodriguez, A. Peral, M. Thommes, J.D. Epping, B.F. Chmelka, Chem. Mater. 21 (2009) 641-654.

[77] International Zeolite Association (IZA). 2014 (2014).

[78] C.H. Christensen, I. Schmidt, A. Carlsson, K. Johannsen, K. Herbst, J. Am. Chem. Soc. 127 (2005) 8098-8102.

[79] P. Frontera, F. Testa, R. Aiello, S. Candamano, J.B. Nagy, Micropor. Mesopor. Mat. 106 (2007) 107-114.

[80] H.K. Beyer, in: H.G. Karge, J. Weitkamp, P. Anderson (Eds.), Molecular Sieves Vol. 1, Post-Synthesis Modifications I, Springer, Berlin-Heidelberg, 2002, pp. 203.

[81] A.H. Oygarden, J. Perez-Ramirez, Appl. Catal. B-Environ. 65 (2006) 163-167.

[82] J.C. Groen, L.A.A. Peffer, J. Perez-Ramirez, Micropor. Mesopor. Mat. 60 (2003) 1-17.

[83] K.S.W. Sing, D.H. Everet, R.A.W. Haul, L. Moscou, R.A. Pieroti, J. Rouquerol, T.

Siemieniewska, Pure Appl. Chem. 57 (1985) 603-619.

[84] M.A. Camblor, A. Corma, S. Valencia, Micropor. Mesopor. Mat. 25 (1998) 59-74.

[85] C.J.H. Jacobsen, C. Madsen, J. Houzvicka, I. Schmidt, A. Carlsson, J. Am. Chem. Soc. 122 (2000) 7116-7117.

[86] A. Corma, A. Martinez, V. Martinez-Soria, J. Catal. 200 (2001) 259-269.

[87] J.A. van Bokhoven, in: V. Valtchev, S. Mintova, M. Tsapatsis (Eds.), Ordered Porous Solids, Elsevier, Amsterdam, 2009, pp. 651-668.

[88] P.P. Pescarmona, K.P.F. Janssen, C. Delaet, C. Stroobants, K. Houthoofd, A. Philippaerts, C. De Jonghe, J.S. Paul, P.A. Jacobs, B.F. Sels, Green Chem. 12 (2010) 1083-1089.

5

Acidic and catalytic properties of a mildly-detemplated microcrystalline NH_4-Beta zeolite

ABSTRACT

Microcrystalline commercial NH_4-Beta zeolite (Si/Al=13.5) was detemplated by Fenton methodology, employing H_2O_2 and Fe cations, and the results were compared with a standard detemplation by calcination. The materials were analysed by TGA, CHN elemental analysis, ICP, XRD, N_2/(LPHR-)Ar physisorption, FTIR, py-IR, NH_3-TPD, and ^{27}Al MAS MQ NMR. Upon Fenton detemplation, the original tetrahedral aluminium species were unaffected and no extra-framework aluminium (EFAl) species were formed (^{27}Al MAS MQ NMR), in contrast to the calcination protocol. Subsequent activation to prepare the H-form of the zeolite was performed by a mild thermal treatment at 350 °C (compared to 550 °C for calcination). The catalytic properties of the various Beta zeolite samples were determined for a model reaction, *viz.* the catalytic cracking of low-density polyethylene (LDPE). Beta zeolite prepared using Fenton methodology showed better catalytic performance compared with calcined Beta zeolite samples and other commercial catalysts, such as ZSM-5 and H-USY, as shown by a lower initiation temperature for LDPE cracking. These findings are rationalised by a higher Brønsted acidity and pore volume of the Fenton detemplated samples compared to the calcined counterpart.

Keywords: beta zeolite; template removal; mild oxidation; calcination; acidity preservation; Brønsted and Lewis sites; catalytic cracking of LDPE.

5.1. INTRODUCTION

Zeolites are used in large amounts as catalysts in the refining and petrochemical industry [1-7]. In addition, new applications have been found in emerging areas like environmental protection and medical diagnosis [8-10]. Their high stability, acidity, shape selectivity and tunability of properties for the desired application make zeolites very versatile materials [11]. The development of novel synthesis routes and post-synthesis treatments has been extensively investigated in the last decades. A major breakthrough was the use of organic amines as templates (or structural directing agents, SDA) instead of inorganic bases [12,13]. The most commonly used SDA's are amines and organic quaternary ammonium cations [14-20]. The introduction of organic bases in zeolite synthesis resulted in a large expansion in the number of microporous materials such as ZSM-5 (MFI), ZSM-11 (MEL), Beta (BEA) and alumina-phosphates [5,21,22].

The removal of the template after synthesis is of great importance to realise the desired product properties. Various protocols for template removal have been developed and can be divided into destructive (thermal and chemical approaches) and non-destructive methods aiming at template recovery. Most strategies are limited to mesoporous or large pore size materials [23] and very few examples can be found for microporous zeolites [24].

Removal of the template by thermal calcination requires high temperatures and the use of air to remove the organic template. This process is highly exothermal and is known to lead to structural damage [25-30]. Template removal by a reaction at mild conditions is considered an attractive alternative. The most commonly used reagents are ozone [31], hydrogen peroxide in combination with a metal catalyst ($Fe^{III/II}$, Fenton chemistry) [32-38], ammonia (at medium temperatures to remove tetramethylammonium cations (TMA^+) [39]), and strong acids (e.g. HCl in methanol [40] and acetic acid). Fenton chemistry is considered a very attractive approach for the detemplation of zeolites due to the mild temperatures required [41].

Beta zeolite is a zeolite with a large 3D structure with cavities and strong acidity. As such, it has found widespread applications in industry [42-44]: examples in the refining and petrochemical industry are hydrocracking [45], hydro-isomerization of alkanes [46,47], synthesis of surfactants [48], catalytic cracking [3,7,8,49,50], methylation of phenols [51], alkylation [52-55] and acylation [56,57]. Beta zeolite is known for its high thermal sensitivity and calcination is known to lead to the formation of extra-framework aluminium (EFAl) species, which decreases the amount of Brønsted sites [25,58-60] especially in the case of small sized crystals [61]. Therefore, Beta zeolite is a perfect candidate to study detemplation protocols under mild conditions. A number of studies have been reported in the literature for the detemplation of Beta zeolite. Jones *et al.* studied solvent extraction as an alternative for calcination and achieved a 48% SDA removal using aqueous acetic acid [62]. The amount of SDA remaining in the structure mirrors the Al content in the zeolite, which implies the presence of strong TEA-Al interactions. For improvement, Gauti *et al.* functionalised Beta nanoparticles prior to solvent extraction [63]. This procedure led to a template removal of 60%, though dealumination occurred to a significant extent. We have previously shown that quantitative template removal from the ammonium Beta zeolite is possible without affecting the framework structure using Fenton detemplation with hydrogen peroxide, and Fe cations as the catalyst [64]. Here, we present a detailed characterisation study of the Beta zeolites obtained by Fenton detemplation followed by a subsequent thermal treatment to obtain the zeolite in the H-form. The morphological and acidic properties of the resulting zeolites were determined and compared, and the use of the materials as catalysts for the cracking of LDPE was investigated. In this application, acidity and pore distribution are the most relevant parameters [65]. A TGA instrument was used with that purpose, as it is a simple, fast and reliable alternative to analise the LDPE cracking at small scale.

5.2. EXPERIMENTAL SECTION

5.2.1. MATERIALS

Hydrogen peroxide (30 *wt.* % and stabilised), nitric acid (65 *wt.* %, pro analyses) and ammonia solution (25 *wt.* %, pro analyses) were purchased from Merck. Fe(III)-nitrate nonahydrate (98 % metal basis) and ammonium Fe(III)-oxalate trihydrate (pure) were supplied by Riedel-de-Haën. Al-nitrate nonahydrate (98 %) was purchased from Sigma-Aldrich. Low--density polyethylene used for the cracking experiments was provided by DSM. Template-containing Beta zeolite in ammonium-form (abbreviated as BT-*raw* throughout this chapter, see Table 1) with a Si/Al ratio of *ca.* 13.5 (mol/mol, according to the supplier) was acquired from TOSOH Corporation (HSZ930A).

5.2.2. DETEMPLATION PROTOCOLS

CALCINATION

Calcination was carried out in a box furnace (LT9/11 Nabertherm), using porcelain crucibles of different shapes and volumes to screen possible bed effects. The external diameter and height of the crucibles together with the sample weights are provided in Table 1. The samples were typically heated from 30 to 550 °C at 10 °C /min and held at 550 °C for 6 h.

STANDARD DETEMPLATION PROTOCOL

In a typical experiment, BT-*raw* (0.5 g) was mixed with 30% H_2O_2 (15 mL) and stirred until the formation of a homogeneous suspension. Then, a certain amount (65 µL) of a standard Fe solution (5 g Fe(III)-nitrate in 100 ml of deionised water) was added to obtain an Fe concentration of 30 ppm. The

pH of the slurry was adjusted to 4 by adding a dilute HNO_3 solution (0.4 M). The suspension was stirred at 70 °C for 24 h under continuous stirring and refluxing. The solid was separated by centrifugation, washed with demineralised water twice and dried overnight at 80 °C in an oven.

5.2.3. ACTIVATION OF THE CATALYSTS

The Fenton-detemplated material (BT-*f*) is obtained in the NH_4-form. Conversion to the H^+ form was performed using a thermal treatment. Various temperatures (300 to 550 °C) and batch/dwell times (3 or 6 h) were screened to determine the optimum conditions (highest conversion at lowest severity). The activation process was monitored by following the NH_4 band of the materials with IR spectroscopy.

Table 1. Overview of zeolite samples used in this study, including abbreviation scheme.

Zeolite type	Material	Treatments[3]	Si/Al ratio
Beta	BT-*raw*	As-received (templated)	13.5[1]
	BT- *C1*	Calcination at 550 °C; 6 h in a crucible 100/10; 2 g. Muffle oven	13.1[2]
	BT- *C2*	Calcination at 550 °C; 6 h in a crucible 20/25; 2 g. Muffle oven	-
	BT- *C3*	Calcination at 550 °C; 6 h in a crucible 70/5; 0.07 g. Tubular oven under dry air	-
	BT-*f*	Fenton-derived material	12.6[2]
	BT-*fA1*	Fenton detemplation and thermal activation at 350 °C, 6 h in a crucible 100/10; 2 g. Muffle oven	-
	BT-*fA2*	Fenton detemplation and thermal activation at 350 °C, 6h in a crucible 20/25; 2 g. Muffle oven	-
	BT-*fA3*	Fenton detemplation and thermal activation at 350 °C, 6h in a crucible 70/5; 0.07 g. Tubular oven under dry air	-
	BT-*fC1*	Fenton detemplation and thermal activation at 550 °C, 6h in a crucible 100/10; 2 g. Muffle oven	12.0[2]
ZSM-5	MFI27-C	Calcination at 550 °C; 6 h in a crucible 100/10; 2 g. Muffle oven	13.5[1]
	MFI55-*C*	Calcination at 550 °C; 6 h in a crucible 100/10; 2 g. Muffle oven	27.5[1]
USY	USY	None	15[1]

[1] According to the supplier; [2] Measured by ICP. [3]For the calcination treatments the crucible dimensions are detailed as: internal diameter/deepness (mm/mm); sample amount (g); type of oven used.

5.2.4. CHARACTERISATION

The template content of the zeolites was determined by thermogravimetric analysis (TGA) in a Mettler-Toledo (TGA/SDTA851e) analyser using a flow of synthetic air of 100 ml/min (STP). Typically, around 5-10 mg of sample were loaded in an α-Al_2O_3 (70 µL) crucible and the temperature was increased from 30 to 900 °C at 10 °C/min. The TGA curve for the zeolite was obtained by subtracting the curve for an empty crucible from that of the sample.

To confirm the TGA data, the elemental composition of the samples was determined using CHN elemental analyses (EuroVector 3000 CHNS). All analyses were done in duplicate to check sample homogeneity. For all samples, the standard deviation was below 2%. Acetanilide (99.9 %) was used as external standard.

Induced Coupled Plasma (ICP-OES) analyses were carried out to determine the Si/Al ratio and the concentration of residual Fe in the sample. For this, a known amount of solid sample was dissolved in a 6 *wt.*% HF solution overnight to ensure full dissolution. The liquid concentration was determined using a Perkin-Elmer (Optima 7000 DV) instrument. A blank 6 *wt.*% HF solution was measured and used as reference.

Powder X-ray diffraction (XRD) measurements were acquired using a Bruker D8 powder X-ray diffractometer using CuKα radiation (λ=1.54056 Å). The spectra were recorded with a step size of 0.02° with 3 seconds accumulation time, in the 2θ angle range of 2 to 60°.

Textural analyses were carried out by Ar physisorption at -186 °C on a Micromeritics ASAP 2420 analyser and ASAP 2020 for Low-Pressure High Resolution (LPHR) measurements. Prior to the measurements, the solid samples were degassed under vacuum at 300 °C for 12 h; Fenton-derived materials were degassed at 200 °C during 10 h. The surface area was calculated by BET method (S_{BET}). The single-point pore volume (V_T) was estimated from the amount adsorbed at a relative pressure of 0.972 in the desorption branch, as well as using the Horvath-Kawazoe model [66]. The micropore size distributions (PSD) were calculated using the Horvath–Kawazoe model

applied to the adsorption branch of the isotherm. The full isotherm reconstruction (cumulative pore volume) was done using a non-local DFT kernel [67]; NLDFT micropore volume ($V_{\mu p}^{NLDFT}$) was estimated for pores ≤10 Å.

The skeletal density was determined by helium pycnometry. The measurements were performed in an AcuPic 1340 instrument at room temperature. The sample (1 ml) was placed in the sample chamber and evacuated 5 times prior to each measurement to remove adsorbed molecules. Subsequently, each sample was measured 10 times. The standard deviation for each analysis was determined.

^{27}Al magic angle spinning nuclear magnetic resonance (MAS-NMR) measurements were conducted on a Bruker Avance-400 spectrometer using a 4 mm zirconium holder, applying spinning frequency of 11 kHz at 298 K. The ^{27}Al MAS NMR spectra were obtained at 104.201 MHz, with acquisition delay of 1 s and acquisition time of 0.08 s., typically 4000 scans were collected. The spectra were referenced with respect to 1.0 M aqueous solution of $Al(NO_3)_3$ set at δ= 0 ppm.

NH_3-TPD experiments were carried out using a Micromeritics AutoChem II system equipped with a thermal conductivity detector. The sample (*ca.* 60 mg) was pretreated by heating it up to 500 °C in a He flow (50 ml/min STP) at 10 °C/min. Subsequently, the sample was cooled to 120 °C at a similar cooling rate, and then exposed to NH_3 in He (1 *vol.* %, 25 ml/min STP) for 30 min. Subsequently, a flow of He (25 ml/min STP) was passed through the reactor for 60 min to remove weakly adsorbed NH_3 from the sample surface. After baseline stabilisation, the desorption of NH_3 was monitored in the range of 120-1000 °C using a heating rate of 10 °C/min. Acid site density values are given as arbitrary units due to a baseline offset at high temperature. Blank measurements in the absent of NH_3 but using the same temperature program were carried out for each material in order to discern between NH_3 and other adsorbed molecules.

For in situ FTIR studies, the zeolites were pressed into thin self-supporting wafers (2 cm^2, 15 mg). The wafers were placed into an IR quartz cell allowing heating of the sample as well as the introduction of known

quantities of one or more gases. The catalysts were activated under vacuum (10^{-6} Torr) by slow heating (2 °C/min) to 450 °C and maintaining the sample for 1 h at 450 °C. The spectra were recorded at room temperature using a Nicolet Nexus spectrometer with a MCT detector (opening 50, 128 scans, and an optical resolution 4 cm^{-1}). For the study of the sample acidity, the zeolite wafer was exposed to pyridine vapours at a pressure of 1 Torr for 15 min at 150 °C. Spectra were recorded after evacuation for 5 min at the required desorption temperature (25-450 °C). Band intensities were corrected for slight differences in sample weight and bands areas were calculated by fitting the spectral profiles with a Gaussian-Lorentzian function using IR OMNIC software. The concentration of the Brønsted and Lewis acid sites were calculated from the integrated area of the PyH^+ and PyL bands (1546 and 1456 at 1448 cm^{-1}, respectively) using the values of the molar extinction coefficients of these bands (1.13 and 1.28 cm/μmol^{-1}, respectively) [68].

5.2.5. CATALYTIC LDPE PYROLYSIS EXPERIMENTS

For the catalytic pyrolysis of LDPE, a Mettler Toledo TGA/SDTA851e microbalance equipped with a sample robot (34-position) was employed. The polymer (LDPE) was first ground and sieved to particle sizes lower than 0.3 mm. Then, a ratio of 75:25 polymer to catalyst was well mixed in an agate mortar and poured into the α-Al_2O_3 crucibles (70 µl). The pyrolysis was carried out under a nitrogen flow (ca. 80 mL/min) with a heating rate of 5 °C/min. For the isothermal conversion experiments (at 275, 300, 325 and 350 °C), a heating rate of 50 °C/min and a 2 h dwell time was used, with polymer to catalyst wt. ratios of 75:25 and 95:5. Further pyrolysis experiments were performed with different heating rates (5, 10, 15, 20, 25, 35 and 50 °C/min) from 30 to 600 °C using a polymer to catalyst wt. ratio of 75 to 25. The polymer (LDPE) decomposition rate was followed by the weight losses. The data were corrected for weight loss related to adsorbed water on the zeolite (30-200 °C). The amount of coke formed was considered to be

negligible for simplification. The heat flow was not corrected for the presence of the catalyst [69,70].

The Ozawa method [71-73] was used to calculate the apparent activation energy, which is especially suitable for weight-loss reactions on heating, such as thermal degradation of polymers. The E_a^{app} was calculated from the slope of the plot log ϕ versus 1/T, using the equation:

$$\frac{d(\log\phi)}{d(1/T)} = -0.4567\frac{E_a^{app}}{R} \qquad (1)$$

where ϕ is the heating rate (K/min); T is the temperature (K); and R is the ideal gas constant (8.314 J/mol K). The E_a^{app} was calculated for several conversions (α = 0.05, 0.1, 0.2, 0.3, 0.4, 0.5, 0.6, 0.8, 0.9 and 0.95, with α being the conversion).

The TGA experiments at dynamic temperatures were repeated at least twice. About half of the experiments were repeated between 4 and 8 times. The deviation for these experiments was calculated as an average relative deviation using eq. 2:

$$ARD(\%) = \frac{100}{N}\sum_{i=1}^{N}\left|\frac{x_i^{\exp} - x_{av,i}}{x_{av,i}}\right| \qquad (2)$$

where $x_i^{\exp}$ and $x_{av,i}$ are the experimental values of the variable (temperature) and average values of the temperature, respectively, and i = number of data points for each experiment. These calculations resulted in an ARD(%) between 0.0007 and 0.19.

Likewise, the catalyst regeneration studies were performed using a Mettler Toledo TGA/SDTA851e microbalance for the catalysts BT-*C1* and BT-*fA1*. All the cycles were performed according to the procedure described above for the isothermal conversion experiments (heating rate of 50 °C/min; 2 h dwell time at 275, 300, 325 or 350 °C; polymer to catalyst weight ratio of 75 to 25). The conversion values were determined after a 1 or 2 h dwell time

at the targeted temperature (275, 300, 325 or 350 °C). Between the cycles, the catalyst was regenerated under air at 550 °C for 1 h in the same crucible. Subsequently, the catalyst was recovered from the crucible, weighted and mixed with the appropriate amount of fresh polymer (75:25 *wt.* ratio). This procedure was repeated for every cycle.

5.3. RESULTS AND DISCUSSION

5.3.1. PROPERTIES OF THE CATALYSTS

STRUCTURE AND COMPOSITION

The Beta-zeolite used in this study, in the NH_4^+ form and containing a template, was subjected to both thermal and Fenton detemplation protocols. Subsequently, the Fenton detemplated zeolite was (mildly) calcined at various conditions to obtain the H^+ form of the zeolite. An overview of the samples used in this study is given in Table 1, including the abbreviations used for the various zeolites at different stages.

The as-received material (BT-*raw*) was characterised by XRD and the typical diffractions for a Beta zeolite are present at the expected 2 theta value. The XRD profile of the parent Beta zeolite sample shows a combination of sharp and broad diffractions peaks as a result of the intergrowth of the A and B polymorphs (Figure 1). Additionally, the XRD patterns for one of the calcined (BT-*C1*) samples, the Fenton detemplated sample (BT-*f*) and an activated Fenton detemplated sample (BT-*fA1*) are given in Figure 1. No significant change was observed in the diffraction patterns, indicating that the structure of the Beta zeolite samples is preserved by the various detemplation strategies.

The template content of the detemplated materials was determined by TGA and elemental analysis. TGA and DTGA profiles (Supplementary material, Figure A.1) show a weight loss when heating up the samples to

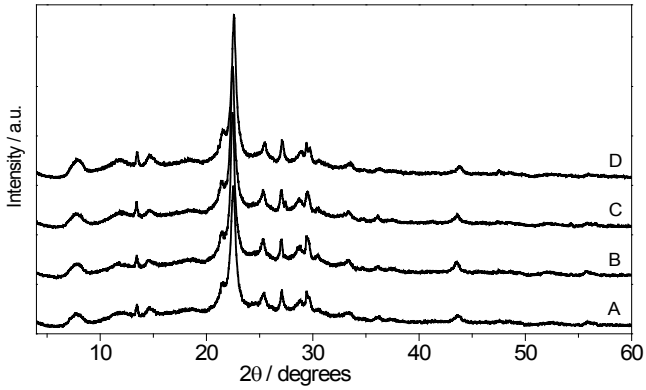

Figure 1. X-Ray diffraction spectra for Beta zeolites after different treatments: a) BT-*raw*; b) BT-*C1*; c) BT-*f*; d) BT-*fA1*.

about 200 °C, due to the presence of adsorbed water. For the Fenton detemplated material (BT-*f*), a small but clear weight loss peak at about 375 °C is present, which can be ascribed to the presence of adsorbed small organic molecules formed during template decomposition. Thus, the TGA data indicate that template removal is quantitative for all samples.

Table 2. CHN elemental analysis of raw and detemplated Beta zeolites.

Sample code	N%	C%	H%
BT-*raw*	1.62	10.37	2.12
BT- *C1*	0	0	0.32
BT-*f*	1.34	0.07	1.33

To further confirm this statement, CHN elemental analysis of the starting and detemplated materials was performed (Table 2). After mild template removal by the Fenton approach, the carbon content was lower than 0.1 *wt.*%, which is in agreement with the TGA profiles and suggests close to quantitative template removal, in agreement with literature data [32,38].

Due to the acidic media applied during the Fenton detemplation process, dealumination may take place. However, elemental analysis (ICP-OES)

revealed negligible variation in the Si/Al ratio (13.0 and 12.6 for BT-*C1* and BT-*f*, respectively, see Table 1), indicating that dealumination is not occurring to a significant extent. In addition, the Fe content for various samples was measured. Sample BT-*C1,* obtained by calcination only, has an iron content of 0.01 *wt.*%, likely due to inclusion of Fe during zeolite synthesis, e.g. from reactor walls and/or the presence of some Fe residues in the reagents. The Fenton detemplated sample BT-*f* contains 0.1 *wt.*% of Fe, which corresponds to 74% of the Fe intake in the detemplation protocol.

TEXTURAL PROPERTIES

To determine the textural properties of the various materials, porosity measurements were performed using low-pressure high-resolution Ar physisorption (LPHR-Ar) at -186 °C. Argon was used as it is known to give less specific interactions with the pore walls resulting in higher quality data compared to nitrogen. The isotherms of various representative samples (BT-*C1*, BT-*f,* BT-*fA1* and BT-*fC1*) are provided in Figure 2. The *t*-plot and NLDFT approximations were used to determine the surface area and pore volume, respectively (Table 3). The observed type IV isotherms with H3 hysteresis loop correspond to a typical nano-sized Beta zeolite [61,74-77].

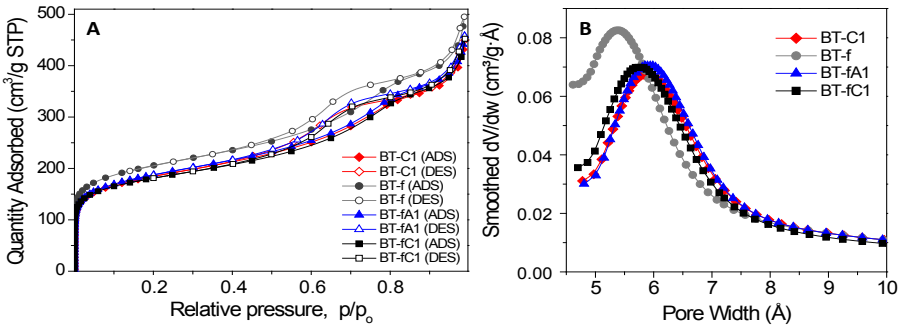

Figure 2. A) Low-Pressure High-Resolution Argon (LDHR Ar) physisorption isotherms. B) Pore size distributions are based on the H-K model [91].

The profiles are indicative for multilayer adsorption with capillary condensation in the interparticle voids having size in the mesopore range. In the micropore region ($p/p^o < 0.3$), the Fenton detemplated sample (BT-*f)* shows higher adsorption levels than the calcined sample: the micropore surface area is 13% higher and the micropore volume is 12% higher than in the calcined counterpart (BT-*C1)*. However, after activation (conversion of NH_4^+ to H^+) of the Fenton detemplated material by mild calcination (BT-*fA1*), the micropore surface area and the pore volume are closer to the values for the directly calcined sample (BT-*C1).* By using the calcination conditions after Fenton detemplation, BT-*fC1* was obtained, which shows a reduced porosity compared to the other materials. The BET surface area of the Fenton detemplated material (BT-*f)* is by far the highest among all samples (628 m^2/g, see Table 3). After activation at 350 or 550 °C, the BET decreased to 576 and 552 m^2/g, respectively, which are close to the calcined sample BT-*C1* (566 m^2/g). The larger BET surface area of BT-*f* is due to both micro- and mesopore contributions (Table 3). When the Fenton detemplated sample is calcined at extreme conditions (BT-*fC1*), particularly the external surface area is reduced considerably, probably due to aggregation of the zeolite particles. Pore volume data show the same trends found for the BET surface area. The micropore size distribution, determined using the Horvath-Kawasoe model, shows that the maximum value for BT-*f* is shifted to a smaller pore diameter compared to the other samples (Figure 2B). This small shift is due to the presence of larger ammonium groups (NH_4^+) instead of small protons (H^+), leading to a slight narrowing of the pores.

Table 3. Porosity values for the various Beta zeolite samples.

Material	S_{BET} m^2/g	S_μ^{t-plot} m^2/g	S_{MESO}^{t-plot} m^2/g	V_T cm^3/g	V_μ^{t-plot} cm^3/g	V_{MESO}^{t-plot} cm^3/g
BT- *C1*	566	248	318	0.508	0.150	0.358
BT-*f*	628	286	342	0.562	0.170	0.392
BT-*fA1*	576	243	332	0.522	0.152	0.370
BT-*fC1*	552	258	240	0.510	0.148	0.362

The mesopore size distribution according to the BJH model shows a main peak centred at *ca.* 60 Å, with comparable intensity, for all samples (Figure 3). The lowest intensity was observed for to BT-*C1,* which is likely related to particle agglomeration due to the harsher thermal treatment.

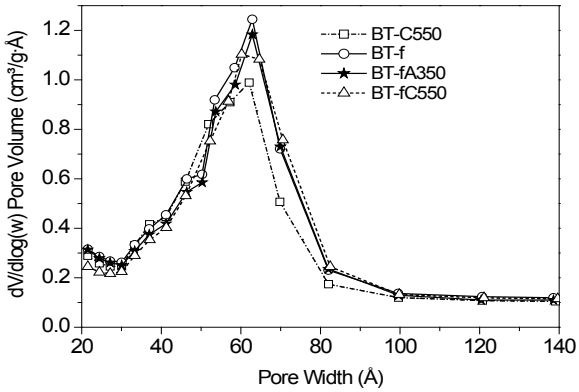

Figure 3. BJH-PSD of the desorption branch at LPHR-Ar of the materials under study.

SOLID STATE AL-NMR MEASUREMENTS: INSIGHT IN AL-COORDINATION

To gain insight in the framework structure and particularly the relatively amounts of Al species with different coordination modes, four of the samples were measured using solid state NMR. The ^{27}Al MQ-MAS NMR spectra are provided in Figure 4.

BT-*f* shows a single peak at about $\delta = 50$ ppm, related to the presence of tetra-coordinated framework aluminium. The spectrum is virtually equal to that of the starting zeolite containing the template (BT-*raw*), indicating that Fenton detemplation does not lead to major changes in the Al coordination. Instead, the thermally treated BT-*C1* and BT-*fA1* samples show an additional peak at about $\delta = 0$ ppm, associated with extra-framework aluminium (EFAl) [26]. The formation of EFAl stems from the harsh thermal treatment [61]. Additionally, a shoulder at about $\delta = 25$ ppm is observed for BT-*C1*, related to the presence of penta-coordinated Al [26]. In order to compare the effects

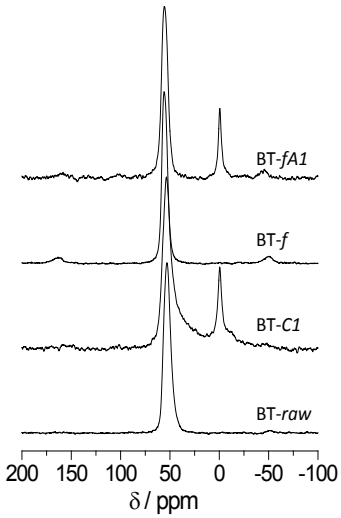

Figure 4. 1D Al-NMR spectra.

of the different calcination/activation procedures and conditions (Table 1), the peaks in the ^{27}Al MQ-MAS NMR spectra were integrated (Table 4). For the calcined/activated materials, between 15 and 25% of the Al is present as extra-framework aluminium. It is worth noticing that there is not a significant difference between the samples obtained after Fenton detemplation at different conditions (A1 to A3). The bed height during the calcination step seems to affect the relative amount of the various Al coordinations and the material calcined in the deep (C2) bed led to an increase in the EFAl (10%) compared to a sample obtained at similar conditions in a shallow bed (C1). This behaviour can be related to higher contact time with the steam formed during calcination experienced by the sample in a deep bed.

Additional information on the coordination of Al was obtained by 2D-^{27}Al spin-echo MQ-MAS NMR for BT-*raw* (a) and BT-*f* (b) (Figure 5). Both samples show only a single peak corresponding to tetrahedrally coordinated framework-aluminium atoms, in line with the 1D Al NMR measurements.

Table 4. Al-NMR calculations for octahedrally (AlOh) and tetrahedrally (AlTh) coordinated Aluminium from Al-NMR; and decomposition temperature of a 5 *wt*.% (T5) and a 50 *wt*.% (T50) of LDPE under thermal and catalytic conditions.

Material	Al^{Th} (%)	Al^{Oh} (%)		T5 (°C)	T50 (°C)	1st Decomp. peak[1] (°C)	2nd Decomp. peak[2] (°C)
LDPE	-	-	-	418	462	464	-
BT-*raw*	100	0	-	-	-	-	-
BT- *C1*	84	16	0.19	247	321	272	388
BT- *C2*	77	23	0.31	244	315	278	351
BT- *C3*	85	15	0.18	237	311	267	351
BT-*f*	100	0	-	266	314	307	381
BT-*fA1*	83	17	0.20	233	306	302	394
BT-*fA2*	84	14	0.16	242	313	264	351
BT-*fA3*	85	15	0.18	237	312	256	351
BT-*fC1*	-	-	-	248	315	282	349
MFI27-*C*	-	-	-	312	374	383	-
MFI55-*C*	-	-	-	328	404	392	423
USY	-	-	-	239	328	294	364

Al^{Oh}: Al octahedrically coordinated (EFAl); Al^{Th}: Al tetrahedrally coordinated. [1] and [2]: First and second decomposition peak extracted from DTGA profiles, respectivelly.

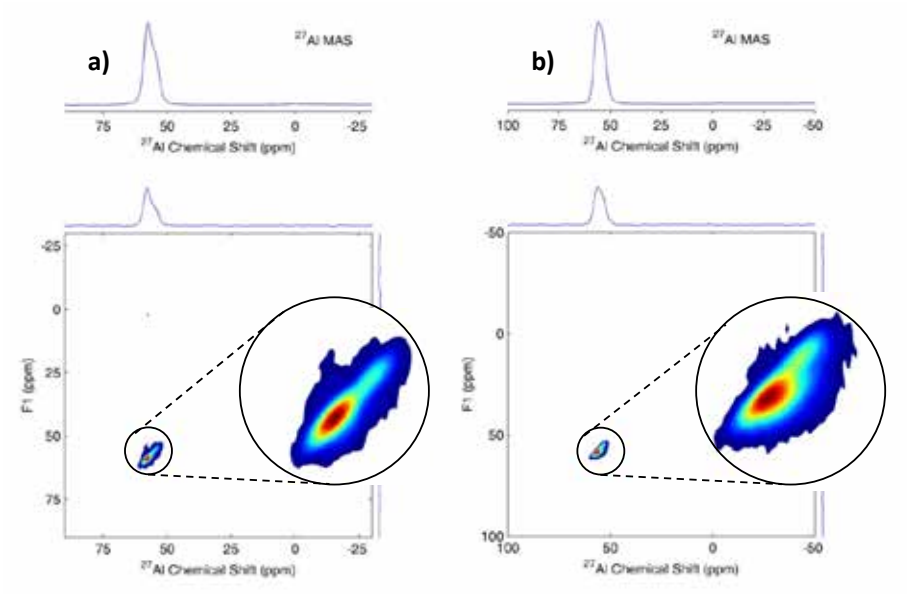

Figure 5. Al coordination via ^{27}Al MQ NMR of: (a) BT- *raw*, and (b) BT-*f*.

ACIDIC PROPERTIES

To gain insight in the acidity of the samples, pyridine adsorption and desorption FTIR and NH_3-TPD studies were performed. FTIR studies, including those in the absence of pyridine, after pyridine adsorption and after subsequent pyridine desorption, were performed for selected samples.

The IR spectra of the neat, dehydrated samples show three characteristic OH bands in the 3800-3400 cm^{-1} range (Figure 6). These bands are associated with different silanol groups. The most intense band is observed at 3746 cm^{-1}, assigned to silanol groups on the external surface [78]. A second band at 3610 cm^{-1} is due to the presence of bridging hydroxyl groups (Si-(OH)-Al) [78]. A relatively weak band is present at 3784 cm^{-1}, commonly assigned to Al-OH groups in which Al atoms are tricoordinated (Al atoms linked to the framework by two oxygen atoms [79]). The intensity of the four bands is distinctly different for the four samples and provides valuable information on the effect of various detemplating procedures on the amounts of Si-OH and Al-OH groups. The peak at 3610 cm^{-1} is by far more intense for the Fenton detemplated sample BT-*f* and BT-*fA1* than for the calcined sample. This indicates a higher amount of bridging hydroxyl groups between Si and Al for the Fenton samples. After calcination of the Fenton detemplated sample, BT-*fC1*, the intensity of this band is reduced considerably and actually the spectrum shows close similarities with that of the calcined sample, BT-*C1*.

After pyridine adsorption (spectra recorded in the whole range after exposing the samples to pyridine at 150 °C, not shown here), the bands associated to Al-OH (3784 cm^{-1}) and Si-OH (3746 cm^{-1}) groups disappeared almost completely. The disappearance of the OH bands at 3610 cm^{-1} (Figure 6) shows the acid nature of the bridging OH groups [78]. The presence of two small peaks in the silanol region shows that a part of silanols interacts with pyridine. These acidic silanols groups are attached to amorphous silica alumina debris (3746 cm^{-1}) or located at the vicinity of EFAL Lewis sites (3733 cm^{-1}) whereas the non-acidic OH groups correspond to framework terminal silanols or to extra-framework silanol groups located far from Lewis acid sites [78].

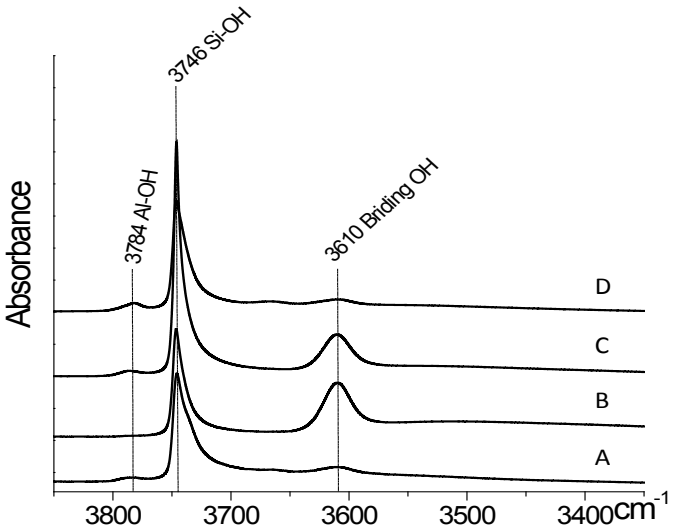

Figure 6. IR spectra (OH region, 3800- 3400 cm^{-1}) of various samples: A) BT-*C1*; B) BT-*f*; C) BT-*fA1*; D) BT-*fC1*. Before analyses, the samples were activated under vacuum (10^{-6} Torr) by slow heating (2°C/min) up to 450 °C and 1 h at 450 °C.

The 1400-1700 cm^{-1} region of the spectra after pyridine adsorption at 150 °C is of particularly interest as it contains characteristic IR bands of pyridine interacting with the Brønsted and Lewis acid sites of the zeolite (Figure 7). The spectra reveal the characteristic set of bands for pyridine adsorbed on Beta zeolites [80] *viz.* i): two bands at 1637 and 1546 cm^{-1}, assigned to the pyridinium ion (PyH^+) and indicative for Brønsted acid sites ii) two bands at 1622 and 1456 cm^{-1} and two bands at 1613 and 1448 cm^{-1}, assigned to pyridine bound to Lewis acid sites (PyL1 and PyL2, respectively). PyL2 associated bands are almost absent at adsorption conditions. However, they were more visible in a desorption step at elevated temperatures (100-400 °C), though only for the Fenton treated materials (graphs not presented here). At last, a peak at 1491 cm^{-1} is present in all samples, which is a superposition of signals of adsorbed species on Lewis and Brønsted acid sites.

A quantitative study of the concentration of Brønsted and Lewis acid sites was performed based on the integrated intensities of the PyH^+ and PyL bands (respectively, 1546 cm^{-1} and 1456 cm^{-1} (PyL1) and 1448 cm^{-1} (PyL2)).

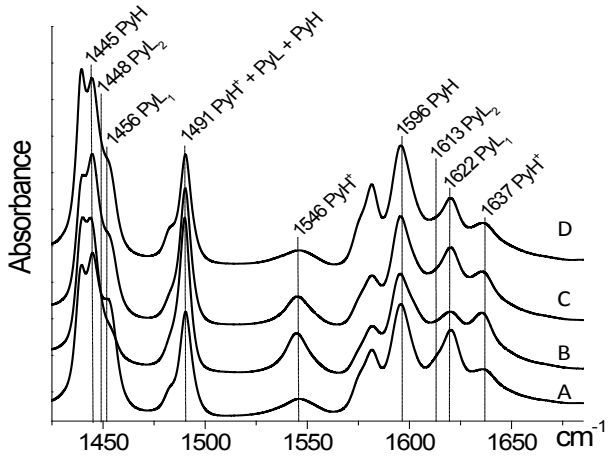

Figure 7. FTIR spectra after pyridine adsorption (150 °C): A) BT-*C1*; B) BT-*f*; C) BT-*fA1*; and D) BT-*fC1*.

The concentration of Brønsted and Lewis acid sites for the four samples versus the pyridine desorption temperature are presented in Figure 8.

Remarkably, the Fenton detemplated sample BT-*f* show a high level of Brønsted acid sites. This is not expected as this sample is not activated and the zeolite is in the ammonia form. However, the pyridine adsorption--desorption studies were preceded by an activation step by heating the samples at 450 °C under vacuum. It is anticipated that this procedure results in the formation of the H-form of the zeolite and this explains indeed the high Brønsted acidity of this sample. As such, the reported Brønsted acidity of the BT-*f* sample is not the intrinsic activity.

The activated Fenton detemplated sample BT-*fA1* also shows a high level of Brønsted acid sites compared to the calcined samples. In contrast, the Lewis acid site concentration is considerably lower for this Fenton detemplated sample, indicating that the amount of EFAl species is reduced. These findings are in line with the Al-NMR studies, showing lower amounts of EFAl for the Fenton detemplated samples (*vide supra*). Thus, Fenton detemplation leads to a Beta zeolite with a higher Brønsted acidity and lower Lewis acidity when compared to calcination.

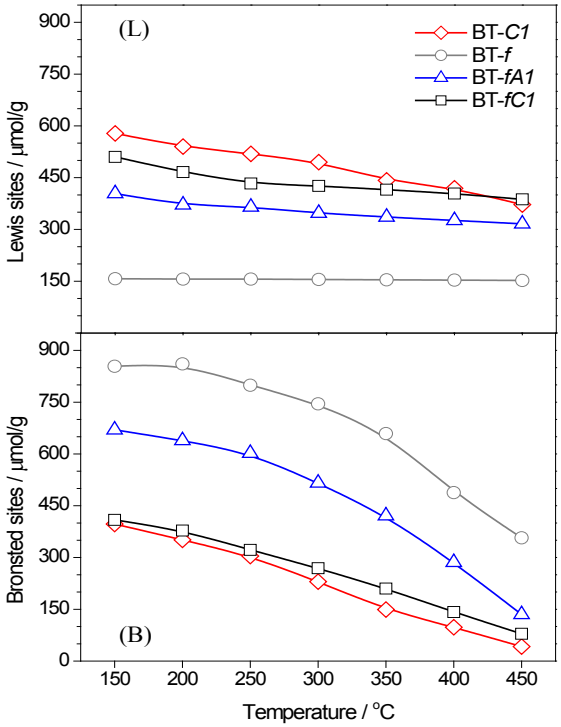

Figure 8. Concentration of Brønsted (B) and Lewis (L) acid sites in the samples versus the temperature from pyridine desorption studies.

The presence of Fe cations on the Fenton detemplated materials may also affect the acidic properties of the materials and has to be taken into account. Their presence will likely contribute to the acidity, though this aspect is not covered in more detail in this article [81-83].

The NH_3-TPD profiles and total acidity calculations (a.u./g) for the various Beta zeolite samples are provided in Figure 9 and Table 5. All profiles exhibit two main desorption peaks at temperatures below 500 °C. The first peak (210-232 °C) is the most intense for all samples. A second peak is present at around 365 °C, which is indicative for the presence of stronger acidic sites.

Quantification of the total acidity was performed by integration of the peaks. The highest total acidity (1420 a.u/g) was found for BT-*f*, which is actually 46% higher than the directly calcined sample (BT-*C1)* and indicates that

the Fenton detemplated sample contains more acidic sites than the calcined one. These findings are in line with the pyridine FT-IR studies and a good correlation between the Brønsted acidity as measured by FT-IR and the total acidity by NH_3-TPD was observed for the samples BT-*fA1*, BT-*fC1* and BT-*C1*.

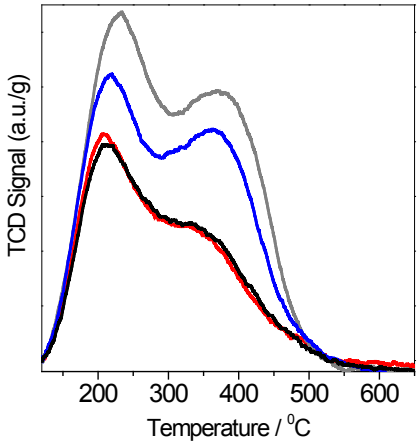

Figure 9. NH_3-TPD profiles of selected Beta zeolites (Table 1). BT-*C1* (red); BT-*f* (grey); BT-*fA1*(blue); and BT-*fC1* (black).

Table 5. Total acidity (NH_3-TPD) and density (He-pycnometry) of various materials

Material	Total Acidity; (a.u./g)	Density (g/cm^3)
BT- *raw*	-	1.934 ± 0.003
BT- *C1*	767	2.161 ± 0.006
BT-*f*	1420	1.735 ± 0.007
BT-fA1	1161	1.864 ± 0.0004
BT-*fC1*	759	2.169 ± 0.008

5.3.2. CATALYTIC PERFORMANCE: CATALYTIC CRACKING OF LDPE

5.3.2.1 INTRODUCTION

In the previous section, it was shown that the Fenton detemplated materials possess higher Brønsted acidity as well as high pore volumes compared to the calcined counterparts and as such could be of particular interest for Brønsted acid catalysed reactions involving large molecules. We have selected the catalytic cracking of low density polyethylene (LDPE) as a model reaction. This reaction was chosen as it is known to be catalysed by zeolites [84-86] and is sensitive to the textural properties of zeolites. Additionally, it has the advantage that it can be performed on mg scale in a TGA device in a high-throughput mode.

Catalytic performance was tested for all the samples prepared in this study (Table 1). For comparison, experiments with ZSM-5 and USY (properties are described in Table 1) were also performed under the same conditions. TGA experiments were carried out either in an isothermal or non-isothermal mode (see experimental section for details). For all the non-isothermal cases, a catalyst loading of 25 *wt.*% and a heating rate of 5 °C/min was used. The amount of coke formed during reaction was calculated by heating the catalyst after reaction in the TGA up to 900 °C under air.

Some illustrative TGA profiles are given in Figure 10. For the thermal decomposition of LDPE only a single peak was observed at 464°C. This value is close to the value reported by Saha et al. (475 °C) [87]. Upon catalytic cracking, LDPE starts to decompose at about 225-275 °C, depending on the catalyst, and complete conversion is observed after heating up to 400 °C. The derivative of the weight loss curve is also provided; it clearly shows two peaks due to polymer cracking to yield lower molecular weight compounds: one between 250 and 300 °C and another at around 350 °C. The exact position of the peaks is a function of the catalyst.

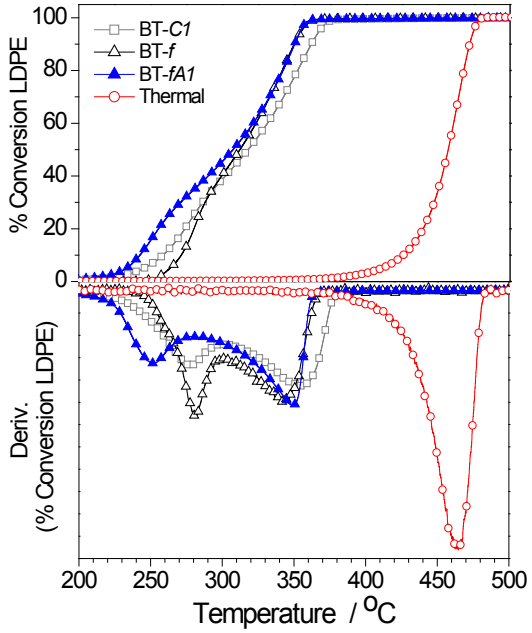

Figure 10. Conversion curves and derivative for the catalytic cracking of LDPE (heating rate of 5 °C/min).

5.3.2.2 SCREENING EXPERIMENTS

To compare the performance of the various catalysts, two process variables were considered *viz* i) the position of the main peaks in the derivative of the weight loss curves and ii) the temperatures required for 5 and 50 *wt.*% LDPE conversion (abbreviated as T5 and T50, respectively). The results are compiled in Table 4, whereas the conversion curves are provided in the Supplementary Information (Figure A.3).

Fenton activated materials (BT-*fA1,2,3*) showed lower T5 and T50 values than their calcined counterparts (BT-*C1,2,3*). The lowest T5 value was found for BT-*fA1* (233°C), which is 180 °C lower than for the thermal decomposition of LDPE. Notably, BT-*C3* calcined under dry air conditions displayed similar LDPE-decomposition temperatures as BT-*fA1,2,3*. This suggests that the formation of steam during catalyst synthesis has a negative effect on catalyst performance. The amount of steam formed is dramatically reduced when

using a Fenton protocol compared to calcination in air and as such has a positive effect on performance. Also of interest is the observation that the "non-activated" BT-*f* is catalytically active and actually its performance is close to that observed for the mildly activated counterpart BT-*fA1*, the only exception being the T5 value, which is 33 °C higher. These data imply that the activation (conversion of the ammonia form to the active H^+ form) can take place *in-situ*. This is also illustrated in Figure 10. At the start, the activity of the Fenton detemplated sample is inferior and a lower weight loss than for the activated samples was observed. However, above 280 °C, it becomes more active than BT-*C1* and shows a similar weight loss profile as BT-*fA1*. Thus, 280 °C seems about the minimum temperature to activate the Fenton detemplated sample.

5.3.2.3 RELATIONS BETWEEN CATALYTIC ACTIVITY AND CATALYST PROPERTIES

Data analyses shows that there is a relation between catalytic performance and the porosity of the samples. This is illustrated in Figure 11. Here, both the intraparticle microporosity and the interparticle voids in the mesopore range of the samples are plotted versus the T5 and T50. A trend is visible: the catalyst performance is considerably improved for catalysts with large micro- and mesopore volume. These findings can be rationalised by considering the mechanism of the reaction. It is most likely that the initial long polymer chains are broken at the external surface of the zeolite, followed by reaction of the oligomers in the more internal acid sites, as was pointed out in the literature [86]. Thus, catalysts with higher meso- and micropore volume seem preferred. These findings are in line by research reported by Bonilla et *al.* [88]. These authors found that the introduction of mesoporosity improves catalytic performance, rationalised by considering that diffusion limitations, particularly of importance for larger molecules like polymer fragments, can be alleviated in larger pores.

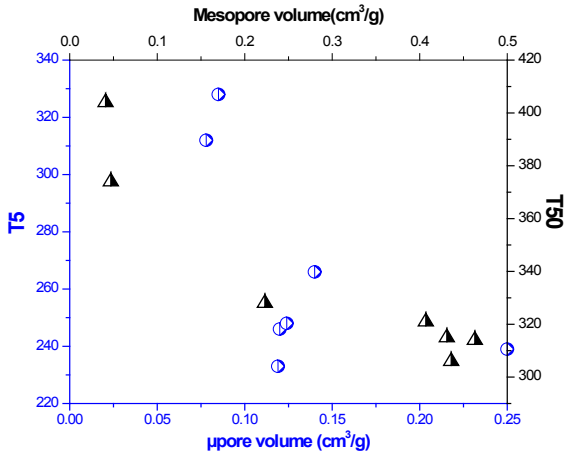

Figure 11. T5 and T50 values for the catalytic decomposition of LDPE versus the micro- and meso-pore volume of the catalysts.

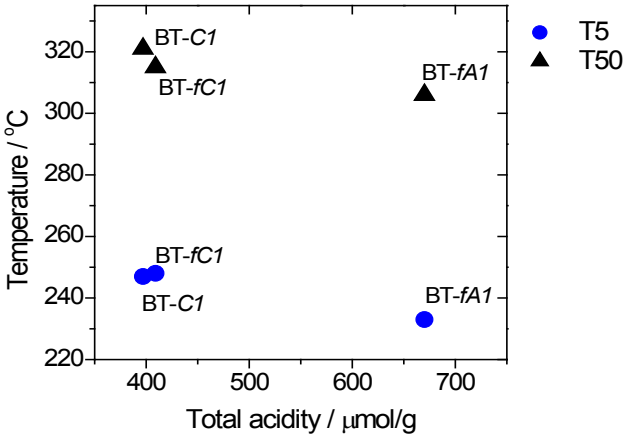

Figure 12. Concentration of Brønsted acid sites (py-IR, 150 °C pyridine desorption temperature) of the catalysts versus T5 and T50 values for the catalytic decomposition of LDPE.

In addition, there also appears to be a relation between the Brønsted acidity as measured by pyridine FT-IR and catalyst performance. This is illustrated in Figure 12, where the T50 value is plotted against the Brønsted acidity as determined at 150°C. A clear trend is visible, with a higher Brønsted acidity of a sample leading to better catalytic performance, *viz.*

lower T50 values. Thus, both the textural properties and particularly the pore volume (Figure 11) as well as the total acidity (Figure 12) affect catalytic performance. Catalysts with a high pore volume and acidity are preferred, in line with the proposed reaction pathway for the catalytic cracking of LDPE. Therefore, the Fenton detemplated and subsequently mildly activated samples perform best as they show the highest acidity in combination with the largest pore volumes.

5.3.2.4 COMPARISON OF CATALYTIC PERFORMANCE WITH OTHER ZEOLITES

When comparing the performance of the different types of zeolites, the best performance was obtained using the Beta and the H-USY zeolite type (Table 4 and Supplementary Information, Figure A.3B.). However, H-USY has the tendency of yielding a larger amount of coke (about 10 *wt.*%) compared to Beta (about 6 *wt.*%), likely due to the larger pore sizes of USY [84]. Performance of H-ZSM-5 (MFI27-*C* and MFI55-*C*) was considerably worse and for instance the T50 value was *ca.* 50 °C higher than for the others. The difference is even more pronounced when considering the T5 and the first decomposition peak.

5.3.2.5 EXTENDED STUDIES WITH SELECTED CATALYSTS

An extended study of the behaviour of BT-*C1*, BT-*fA1* and BT-*fC1* was carried out by performing experiments on the degradation of LDPE in an isothermal mode. These three materials were selected to gain insights in the effects of the combination of a mild pre-detemplation (Fenton) followed by a thermal treatment (BT-*fA1* at 350°C and BT-*fC1* at 550°C); or a single but harsher thermal treatment (BT-*C1* at 550°C). The isothermal experiments were performed at 275, 300, 325 and 350 °C for 2 h under nitrogen using

a heating rate of 50 °C/min. Additionally, two polymer to catalyst wt. ratios were applied (75:25 and 95:5). The conversions after one and two hours of reaction are collected in Table 6.

The results reveal an exceptional performance of BT-*fA1* at low temperatures (275 and 300 °C), with ca. 5 *wt.*% higher conversions compared to the other catalysts. However, at higher temperatures (325 and 350°C) the conversions are comparable for all the catalyst with a variation between 1-2 *wt.*%.

Table 6. Results for the catalytic cracking of LDPE at isothermal conversion using BT-*C1*, BT-*fA1* and BT-*fC1*.

Catalyst	Polymer:Catalyst ratio	Temperature (°C)	α (%) at 1 h	α (%) at 2 h
BT- *C1*	75:25	275	57.8	66.4
		300	78.7	86.0
		325	95.8	96.0
		350	96.5	96.4
	95:5	275	57.2	66.2
		300	80.4	88.4
		325	98.1	98.5
		350	98.5	98.5
BT-*fA1*	75:25	275	60.8	70.2
		300	86.6	92.4
		325	94.9	95.2
		350	95.6	95.8
BT-*fC1*	75:25	275	57.0	68.0
		300	79.6	87.2
		325	96.7	97.4
		350	97.6	97.6

Apparently, the Fenton detemplated catalyst is the most active catalyst at low temperature. A possible explanation is the highest BET surface area and pore volume (including mesopores) for this catalyst, which facilitates the catalytic cracking reaction (*vide infra*), though its larger Brønsted acidity likely also plays a role (*vide supra*) [84].

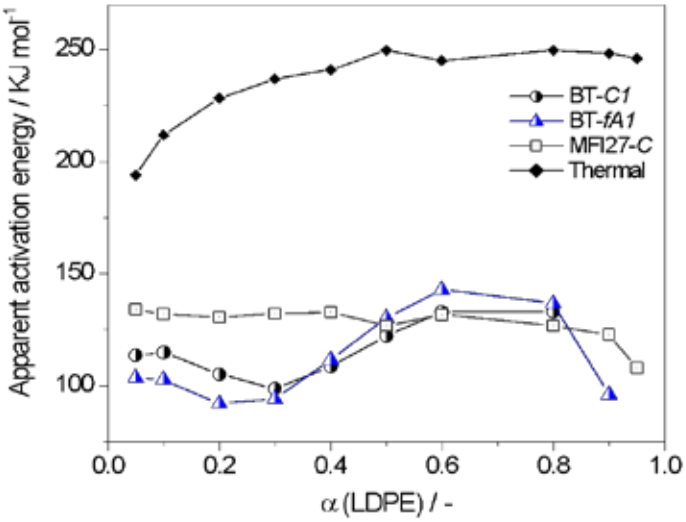

Figure 13. Apparent activation energy versus conversion of LDPE for various catalysts under non-isothermal conditions.

The results obtained for BT-*C1* show that a lower catalyst loading leads to slightly higher conversions. Though counter-intuitively, it has been reported before in the literature [89].

5.3.2.6 EXPERIMENTS WITH SELECTED CATALYSTS AT DIFFERENT HEATING RATES

Finally, a kinetic study was performed to determine the apparent activation energy for various catalysts (BT-*C1*, BT-*fA1*, MF27-*C*) using the Ozawa method (eq.1) [71,72] For this purpose, the samples were heated from 30 to 600 °C with different heating rates (5, 10, 15, 20, 25, 35 and 50 °C/min). The apparent activation energy (E_a^{app}) was calculated at the same conversion levels for each catalyst (Figure A.4), which is a requirement for the Ozawa method. Plots of the E_a^{app} versus the conversion of LDPE for the thermal and catalytic decomposition of LDPE are given in Figure 13. The apparent activation energies are a function of the conversion, indicating a complex

reaction mechanism involving various reactions. For the thermal cracking of LDPE, the activation energy increased till about 50 *wt.*% conversion and then remained constant at a value of about 250 kJ/mol. This value is slightly higher than reported in the literature for LDPE (180-200 kJ/mol). These differences may be due to differences in relevant properties of the LDPE used, like molecular weight and branching levels.

The apparent activation energies are considerably reduced when using the three catalysts and all are below 150 kJ/mol, indicative for considerable catalytic activity. Qualitatively, the profiles for the activation energy versus the conversion are similar for both Beta zeolites (BT-*C1* and BT-*fA1*). The E_a^{app} decreases in the range $5 < \alpha < 0.3$, increases in the range $0.3 < \alpha < 0.6$ and then decreases again. These trends are in line with a complex reaction mechanism. According to the literature, four-steps can be discriminated (1) thermal degradation; (2-3) catalytic cracking of heavy fragments to give liquids and/or gas, (4) cyclisation to form aromatics [90]. All steps have different activation energies and this is likely the reason for the profiles provided in Figure 13.

The profiles for the two Beta catalysts show some peculiar features. The activation energy for BT-*fA1* is lower than for BT-*C1* when α is smaller than 0.4. This suggests that the performance of BT-*fA1* is better in the initial stage of the reaction than for the calcined counterpart. A possible explanation is a better accessibility of the acid sites during the cracking stage of the reaction, which is in line with the higher mesoporosity found for this catalyst (Section 5.3.1.2). However, at higher conversions, the calcined catalyst shows lower apparent activation energies. Without detailed studies on product compositions versus conversion rates (e.g. by TGA-MS), it is not possible to explain this observation.

A different apparent activation energy versus conversion plot was observed for MFI27-*C*. Here, the E_a^{app} was almost constant during the reaction, with a small decrease at higher conversions ($\alpha > 0.6$). In addition, the activation energy, particularly at the start of the reaction, is higher than for the Beta catalysts, indicative for lower catalyst activity for the ZSM-5 catalyst.

These differences may have their origin in the fact that the cavities of ZSM-5 zeolite ({[100] 10 5.1 × 5.5 <-> [010] 10 5.3 × 5.6}***) are smaller than the cavities of Beta zeolite ({<100> 12 6.6 × 6.7** <-> [001] 12 5.6 × 5.6*}). As such, cracking of the LDPE in the initial stage of the reaction is expected to be more facile due to lower levels of diffusion limitations.

5.3.2.7 CATALYST REGENERATION STUDIES

It is well known that the cracking of LDPE leads to coke formation on the catalysts and that a regeneration step is required to reactivate the catalyst to extend catalyst life time. An established regeneration protocol involves calcination of the used zeolite under air at temperatures above 400 °C. This procedure was also explored for catalysts BT-*C1* and BT-*fA1*. It involved heating up a mixture of polymer and catalyst (75:25 *wt.*% ratio) to a pre-set temperature (275 and 300°C) at a heating rate of 50 °C/min. The reaction temperature was kept at this value for either 1 or 2 h. Subsequently, the catalyst was regenerated under air at 550 °C for 1 h, isolated and used for a second (and subsequent) catalytic experiment (see experimental section for more details).

The results for the one and two hour experiments for BT-*C1* and BT-*fA1* are shown in Figure 14. The highest conversion was again achieved for the Fenton detemplated sample BT-*fA1*. The LDPE conversion for the Fenton detemplated sample is a function of the number of catalyst recycles and decreases after successive recycles. In contrast, the activity of the calcined catalyst (BT-C1) is about constant. After 5 cycles, the conversion of BT-*fA1* was equal to that for its calcined counterpart, BT-*C1*. It suggests that upon regeneration, the textural properties change and actually become close to those for the calcined counterpart. These findings suggest that Fenton de-templated catalysts are best used for catalytic conversions where catalysts degradation and thus the need for regeneration is less of an issue than for catalytic cracking reactions (e.g. low temperature liquid phase conversion).

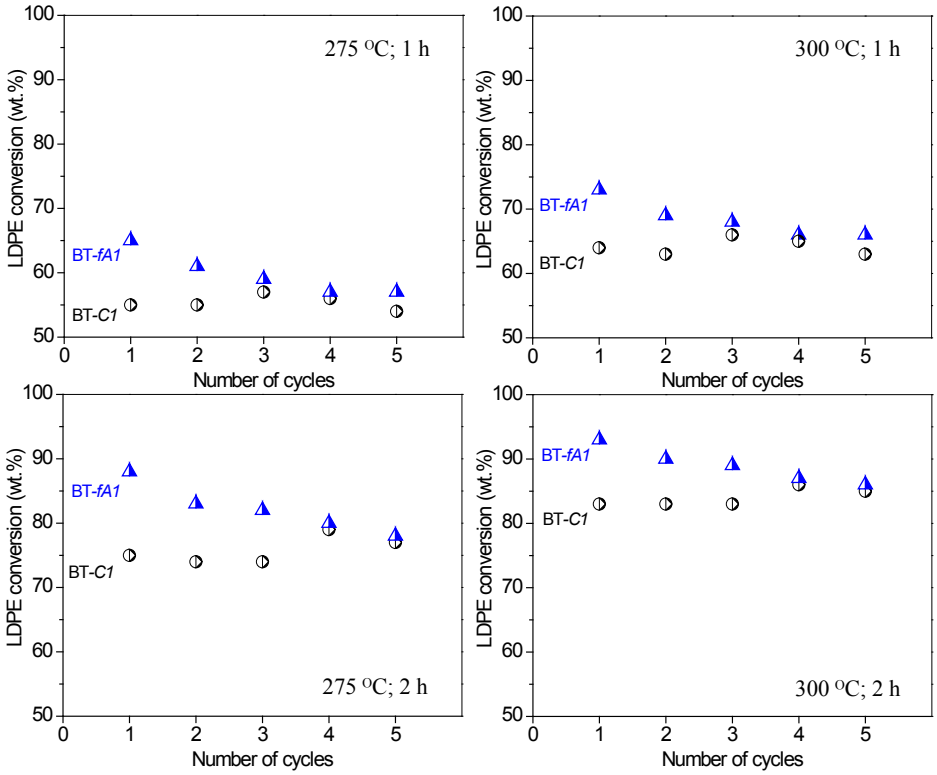

Figure 14. Conversion of LDPE versus number of catalyst recycles for BT-*C1* and BT-*fA1* at different temperatures (275 and 300 °C) and times (1 and 2 h)

5.4. CONCLUSIONS

We reported the synthesis and properties of a Fenton detemplated (BT-*f1)* and mildly activated Beta zeolite (BT-*fA1*). For the Fenton- detemplated zeolite sample in the acidic form (BT-*fA1)*, it was shown that particularly the Brønsted acidity, as measured by pyridine FT-IR studies (670 μmol/g at 150 °C), and the total pore volume (0.522 cm^3/g) are considerably higher than for its calcined counterpart (BT-*C1,* 397 μmol/g and 0.508 cm^3/g). The catalytic performance of the samples was determined using a model reaction, *viz.* the catalytic cracking of LDPE and the results were compared to other zeolites (H-USY, H-ZSM-5). It was shown that BT-*fA1* gave the best

catalytic performance in terms of decomposition temperature compared to H-USY, H, ZSM-5 and its calcined counterpart (BT-*C1*).

Catalyst regeneration studies after LDPE cracking by oxidation using air at elevated temperatures show that the performance decreases with the number of catalytic cycles and that the performance becomes equal to the values observed for the calcined counterpart. As such, the favourable textural properties of the Fenton detemplated samples are lost upon recycling. These findings indicate that the Fenton detemplated catalysts are more suitable for catalytic reactions operating under milder conditions, such as low temperature liquid phase reactions.

5.5. ACKNOWLEDGEMENTS

The authors are thankful for the financial support from the Nederlandse Organisatie voor Wetenschappelijk Onderzoek (NWO) under the project VIDI 10284. TOSOH Corporation is acknowledged for the kind supply of materials. We thank to J. Baas; J. van der Velde and Prof. Dr. J.C. Hummelen from the University of Groningen for their support in the XRD, elemental analysis and FT-IR measurements, respectively.

5.6. REFERENCES

[1] International Zeolite Association (IZA) (2014).

[2] D.W. Breck, Zeolite Molecular Sieves, Structure, Chemistry and Use, John Wiley & Sons, New York, London, Toronto 1974, pp. 636.

[3] J. Weitkamp, L. Puppe, Catalysis and Zeolites, Fundamentals and Applications, Springer, Berlin, 1999.

[4] J. Cejka, H. van Bekkum, A. Corma, F. Schueth, Introduction to Zeolite Science and Practice, 3rd Revised Edition, Stud. Surf. Catal. 168, Elsevier, Amsterdam, 2007.

[5] R. Xu, W. Pang, J. Yu, Q. Huo, J. Chen, Chemistry of Zeolites and Related Porous Materials. Synthesis and Structures, John Wiley & Sons, (Asia), 2007.

[6] V. Valtchev, S. Mintova, M. Tsapatsis, Ordered Porous Solids: Recent Advances and Prospects, Elsevier, Amsterdam, 2009.

[7] J. Cejka, A. Corma, S. Zones (Eds.), Zeolites and Catalysis: Synthesis, Reactions and Applications, Wiley-VCH, Weinheim, 2010.

[8] M.E. Davis, Nature. 417 (2002) 813-821.

[9] W. Vermeiren, J.-. Gilson, Top. Catal. 52 (2009) 1131-1161.

[10] A. Corma, J. Catal. 216 (2003) 298-312.

[11] Handbook of Heterogeneous Catalysis, (2004), Wiley-VCH, Weinheim, 1999.

[12] R.M. Barrer, Zeolites. 1 (1981) 130-140.

[13] C.S. Cundy, P.A. Cox, Chem. Rev. 103 (2003) 663-701.

[14] J. Cejka, A. Corma, S. Zones (Eds.), Zeolites and Catalysis: Synthesis, Reactions and Applications, Wiley-VCH, Weinheim, 2010, pp. 67.

[15] A. Burton, S. Zones, S. Elomari, Curr. Opin. Colloid Interface Sci. 10 (2005) 211-219.

[16] A. Jackowski, S.I. Zones, S. Hwang, A.W. Burton, J. Am. Chem. Soc. 131 (2009) 1092-1100.

[17] R. Castaneda, A. Corma, V. Fornes, F. Rey, J. Rius, J. Am. Chem. Soc. 125 (2003) 7820-7821.

[18] A. Corma, F. Rey, J. Rius, M. Sabater, S. Valencia, Nature. 431 (2004) 287-290.

[19] A. Corma, M.J. Diaz-Cabanas, J. Luis Jorda, C. Martinez, M. Moliner, Nature. 443 (2006) 842-845.

[20] R. Xu, W. Pang, J. Yu, Q. Huo, J. Chen, Chemistry of Zeolites and Related Porous Materials. Synthesis and Structures, John Wiley & Sons, (Asia), 2007, pp. 39.

[21] N.D. Hould, R.F. Lobo, Chem. Mater. 20 (2008) 5807-5815.

[22] IZA Synthesis Commission (2014).

[23] J. Patarin, Angew. Chem. Int. Edit. 43 (2004) 3878-3880.

[24] H. Lee, S. Zones, M. Davis, Nature. 425 (2003) 385-388.

[25] A. Omegna, M. Vasic, J. van Bokhoven, G. Pirngruber, R. Prins, Phys. Chem. Chem. Phys. 6 (2004) 447-452.

[26] E. Bourgeat-Lami, P. Massiani, F. Direnzo, P. Espiau, F. Fajula, T. Courieres, Appl. Catal. 72 (1991) 139-152.

[27] T. Koranyi, J. Nagy, J. Phys. Chem. B. 109 (2005) 15791-15797.

[28] I. Kiricsi, C. Flego, G. Pazzuconi, W. Parker, R. Millini, C. Perego, G. Bellussi, J. Phys. Chem. 98 (1994) 4627-4634.

[29] P.J. Kunkeler, B.J. Zuurdeeg, J.C. van der Waal, J.A. van Bokhoven, D.C. Koningsberger, H. van Bekkum, J. Catal. 180 (1998) 234-244.

[30] J.A. van Bokhoven, D.C. Koningsberger, P. Kunkeler, H. van Bekkum, A.P.M. Kentgens, J. Am. Chem. Soc. 122 (2000) 12842-12847.

[31] J. Kuhn, M. Motegh, J. Gross, F. Kapteijn, Micropor. Mesopor. Mat. 120 (2009) 12-18.

[32] I. Melian-Cabrera, F. Kapteijn, J.A. Moulijn, Chem. Commun. (2005) 2744-2746.

[33] Y. Liu, J. Xu, L. He, Y. Cao, H. He, D. Zhao, J. Zhuang, K. Fan, J. Phys. Chem. C. 112 (2008) 16575-16583.

[34] H. Xing, Y. Zhang, M. Jia, S. Wu, H. Wang, J. Guan, L. Xu, T. Wu, Q. Kan, Catal. Commun. 9 (2008) 234-238.

[35] L.L. Perez, M.J. Ortiz-Iniesta, Z. Zhang, I. Agirrezabal-Telleria, M. Santes, H.J. Heeres, I. Melian-Cabrera, J. Mater. Chem. A. 1 (2013) 4747-4753.

[36] Z. Zhang, D.L. Santangelo, G. ten Brink, B.J. Kooi, J.A. Moulijn, I. Melián-Cabrera, Mater. Lett. 131 (2014) 186-189.

[37] I. Melian-Cabrera, F. Kapteijn, J.A. Moulijn, Catal. Today. 110 (2005) 255-263.

[38] I. Melian-Cabrera, F. Kapteijn, J.A. Moulijn, Chem. Commun. (2005) 2178-2180.

[39] O. Kresnawahjuesa, D.H. Olson, R.J. Gorte, G.H. Kuhl, Micropor. Mesopor. Mat. 51 (2002) 175-188.

[40] P.B. Malla, S. Komarneni, Zeolites. 15 (1995) 324-332.

[41] W.Z. Tang, Physicochemical Treatment of Hazardous Wastes, CRC Press LLC, Florida, 2004.

[42] J.C. Jansen, E.J. Creyghton, S.L. Njo, H. vanKoningsveld, H. vanBekkum, Catal. Today. 38 (1997) 205-212.

[43] P.A. Wright, W.Z. Zhou, J. Perez-Pariente, M. Arranz, J. Am. Chem. Soc. 127 (2005) 494-495.

[44] A. Simon-Masseron, J.P. Marques, J.M. Lopes, F.R. Ribeiro, I. Gener, M. Guisnet, Appl. Catal. A-Gen. 316 (2007) 75-82.

[45] M.A. Camblor, A. Corma, A. Martinez, V. Martinez-Soria, S. Valencia, J. Catal. 179 (1998) 537-547.

[46] L. Fernandes, J. Monteiro, E. Sousa-Aguiar, A. Martinez, A. Corma, J. Catal. 177 (1998) 363-377.

[47] M.A. Arribas, A. Martinez, Catal. Today. 65 (2001) 117-122.

[48] M.A. Camblor, A. Corma, S. Iborra, S. Miquel, J. Primo, S. Valencia, J. Catal. 172 (1997) 76-84.

[49] Y.S. Tao, H. Kanoh, L. Abrams, K. Kaneko, Chem. Rev. 106 (2006) 896-910.

[50] L. Tosheva, V.P. Valtchev, Chem. Mater. 17 (2005) 2494-2513.

[51] M. Bregolato, V. Bolis, C. Busco, P. Ugliengo, S. Bordiga, F. Cavani, N. Ballarini, L. Maselli, S. Passeri, I. Rossetti, L. Forni, J. Catal. 245 (2007) 285-300.

[52] J. Das, Y.S. Bhat, A.B. Halgeri, Catal. Lett. 23 (1994) 161-168.

[53] J. Cejka, B. Wichterlova, Catal. Rev. 44 (2002) 375-421.

[54] A. Corma, A. Martinez, P.A. Arroyo, J.L.F. Monteiro, E.F. SousaAguiar, Appl. Catal. A-Gen. 142 (1996) 139-150.

[55] G. Bellussi, G. Pazzuconi, C. Perego, G. Girotti, G. Terzoni, J. Catal. 157 (1995) 227-234.

[56] R. Srivastava, N. Iwasa, S. Fujita, M. Arai, Catal. Lett. 130 (2009) 655-663.

[57] A.E.W. Beers, J.A. van Bokhoven, K.M. de Lathouder, F. Kapteijn, J.A. Moulijn, J. Catal. 218 (2003) 239-248.

[58] A. Corma, V. Fornes, M. Navarro, J. Pérez-Pariente, J. Catal. 148 (1994) 569-574.

[59] Y.F. Chu, J.P. McWilliams, US 4916097 (1990).

[60] C.Y. Yeh, X. Gao, W.E. Cormier, M. Pasquale, US 2004/0014592 A1 (2004).

[61] M.A. Camblor, A. Corma, S. Valencia, Micropor. Mesopor. Mat. 25 (1998) 59-74.

[62] C.W. Jones, K. Tsuji, T. Takewaki, L.W. Beck, M.E. Davis, Micropor. Mesopor. Mat. 48 (2001) 57-64.

[63] B. Gautier, M. Smaihi, New J. Chem. 28 (2004) 457-461.

[64] I. Melian-Cabrera, F. Kapteijn, J.A. Moulijn, Chem. Commun. (2005) 2744-2746.

[65] J. Perez-Ramirez, S. Abello, A. Bonilla, J.C. Groen, Adv. Funct. Mater. 19 (2009) 164-172.

[66] A. Saito, H.C. Foley, Microporous Mater. 3 (1995).

[67] Micromeritics Instruments Corporation, Micromeritics V3.04 1994-2008, ASAP 2020, (2008).

[68] M. Guisnet, P. Ayrault, C. Coutanceau, M.F. Alvarez, J. Datka, J. Chem. Soc. Farad. T. 93 (1997) 1661-1665.

[69] A. Coelho, I.M. Fonseca, I. Matos, M.M. Marques, A.M. Botelho do Rego, M.A.N.D.A. Lemos, F. Lemos, Appl. Catal. A-Gen. 374 (2010) 170-179.

[70] A. Coelho, L. Costa, M.d.M. Marques, I. Fonseca, M.A. Lemos, F. Lemos, Reaction Kinetics Mechanisms and Catalysis. 99 (2010) 5-15.

[71] T. OZAWA, Bull. Chem. Soc. Jpn. 38 (1965) 1881.

[72] B. Saha, A.K. Ghoshal, Thermochim. Acta. 453 (2007) 120-127.

[73] T. Hatakeyama, Z. Liu, Handbook of Thermal Analysis, John Wiley & sons, 1998, pp. 42.

[74] P. Prokesova-Fojokova, S. Mintova, J. Cejka, N. Zilkova, A. Zukal, Micropor. Mesopor. Mat. 92 (2006) 154-160.

[75] L. Wang, Z. Zhang, C. Yin, Z. Shan, F. Xiao, Micropor. Mesopor. Mat. 131 (2010) 58-67.

[76] J.C. Groen, L.A.A. Peffer, J. Perez-Ramirez, Micropor. Mesopor. Mat. 60 (2003) 1-17.

[77] K.S.W. Sing, D.H. Everet, R.A.W. Haul, L. Moscou, R.A. Pieroti, J. Rouquerol, T. Siemieniewska, Pure. Appl. Chem. 57 (1985) 603-619.

[78] A. Janin, M. Maache, J. Lavalley, J. Joly, F. Raatz, N. Szydlowski, Zeolites. 11 (1991) 391-396.

[79] A. Vimont, F. Thibault-Starzyk, J. Lavalley, J. Phys. Chem. B. 104 (2000) 286-291.

[80] T. Barzetti, E. Selli, D. Moscotti, L. Forni, J. Chem. Soc. -Faraday Trans. 92 (1996) 1401-1407.

[81] G.D. Pirngruber, in: V. Valtchev, S. Mintova, M. Tsapatsis (Eds.), Ordered Porous Solids, Elsevier, Amsterdam, 2009, pp. 749-771.

[82] A.H. Oygarden, J. Perez-Ramirez, Appl. Catal. B-Environ. 65 (2006) 163-167.

[83] I. Melian-Cabrera, F. Kapteijn, J.A. Moulijn, Catal. Today. 110 (2005).

[84] J. Agullo, N. Kumar, D. Berenguer, D. Kubicka, A. Marcilla, A. Gomez, T. Salmi, D.Y. Murzin, Kinet. Catal. 48 (2007) 535-540.

[85] D.P. Serrano, J. Aguado, J.M. Escola, ACS Catalysis. 2 (2012) 1924-1941.

[86] A. Corma, A.V. Orchilles, Micropor. Mesopor. Mat. 35-6 (2000) 21-30.

[87] B. Saha, A.K. Ghoshal, Thermochimica Acta. 453 (2007) 120-127.

[88] A. Bonilla, D. Baudouin, J. Perez-Ramirez, J. Catal. 265 (2009) 170-180.

[89] A. Coelho, L. Costa, M.M. Marques, I.M. Fonseca, M.A.N.D.A. Lemos, F. Lemos, Appl. Catal. A-Gen. 413 (2012) 183-191.

[90] K. Takuma, Y. Uemichi, A. Ayame, Appl. Catal. A-Gen. 192 (2000) 273-280.

[91] M. Kruk, M. Jaroniec, Chem. Mat. 13 (2001) 3169-3183.

5.7. SUPPLEMENTARY INFORMATION

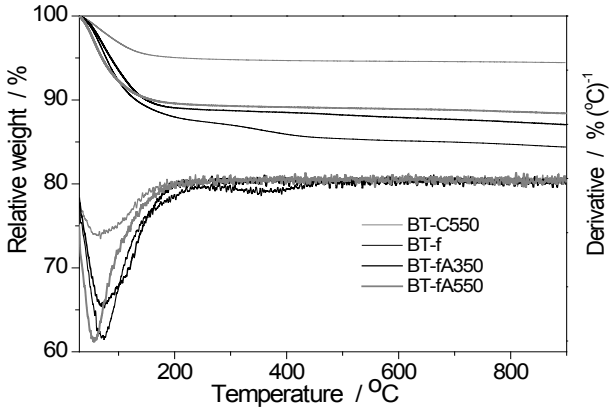

Figure A.1. TGA and DTGA of the detemplated materials.

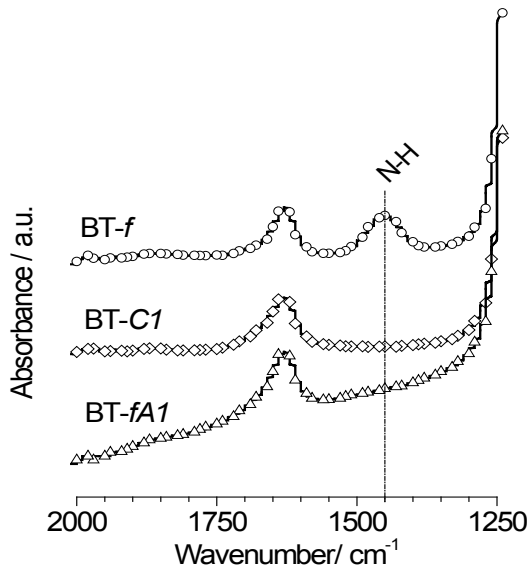

Figure A.2. FT-IR study to determine optimum activation conditions for BT-*f* by comparing the N-H band (centred at 1600 cm^{-1}). The Fenton detemplated (BT-*f*), calcined (BT-*C1*) and Fenton activated material (BT-*fA1*) are shown for comparison.

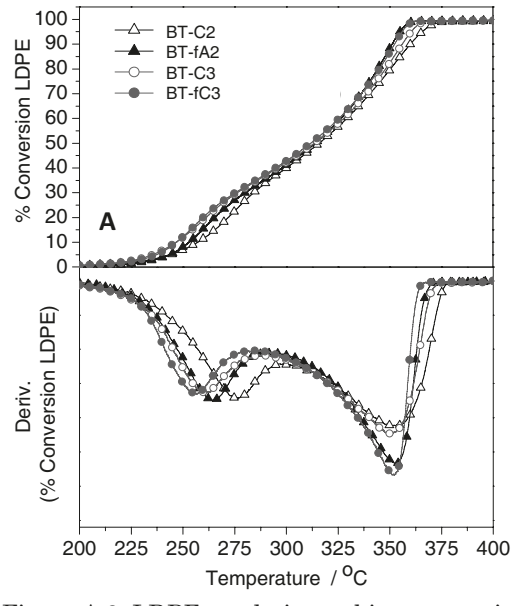

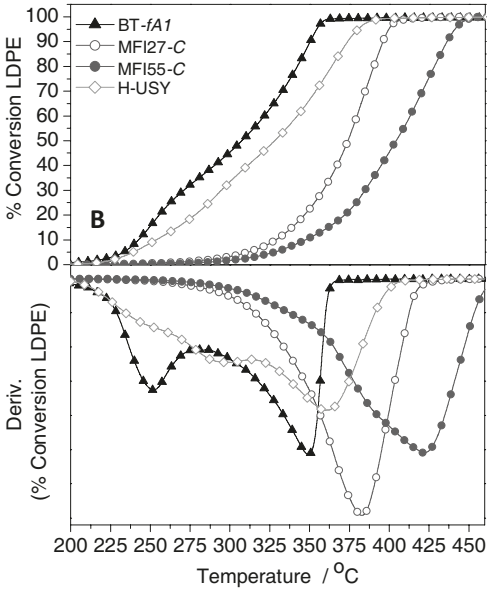

Figure A.3. LDPE catalytic cracking conversion curves and derivatives under non-isothermal conditions. Heating rate of 5°C/min. A) BT-*C2*, BT-*fA2*, BT-*C3*, and BT-*fC3*; B) BT-*fA1*, MFI27-*C*, MFI55-*C*, H-USY are represented.

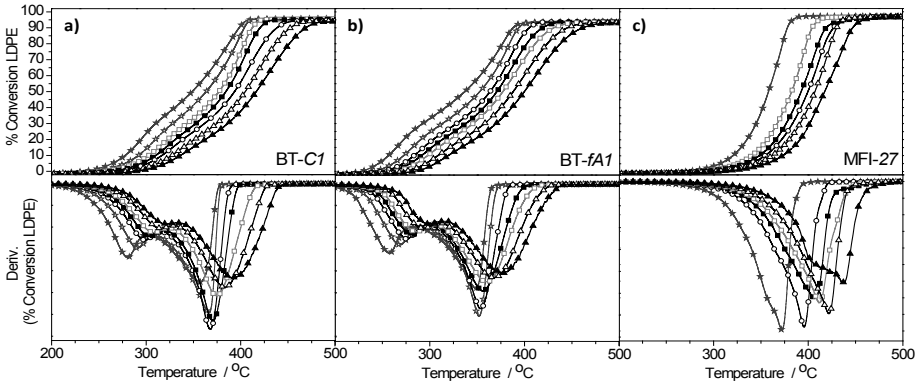

Figure A.4. Non-isothermal conversion curves and their derivatives with different heating rates: 5, 10 15, 20, 25, 35 and 50 °C/min (curves from left to right, respectively). a) BT-*C1*; b) BT-*fA1*; c) MFI27-*C*.

Summary / Samenvatting / Resumen

SUMMARY

Zeolites have a very wide application range, including the use as catalysts. Actually, zeolites constitute a large portion of the solid catalysts used to date in industry. The successful introduction of zeolites in the catalysis arena was due to their favourable properties such as high stability (thermal, hydrothermal and mechanical), ion-exchange capacity, shape selective character, high catalytic activity and its potential to act as a host for advanced catalysts. Recently, zeolites have also been introduced in emerging areas such catalytic biomass conversions, pollution abatement, energy saving devices and sensors. The major challenge nowadays is the fine-tuning of these materials to a specific application, either by direct synthesis or by a combination with post-synthesis treatments. An overview of the use of zeolites, zeolite synthesis, and post treatment methods is given in *Chapter 1*.

A new zeolite activation procedure after synthesis is reported in *Chapter 2*. Conventionally, two calcination steps are used: one to remove the template and a second one to obtain the zeolite in the acidic form. We investigated a direct activation route, which consists of a Na^+ NH_4-exchange on the as-synthesised zeolite before removing the organic template. A subsequent calcination step leads to combined template removal and the creation of Brønsted acid sites, and as such, one calcination step is avoided. The structural, textural and acidic properties of materials were determined for this new route and were shown to be comparable to those obtained with the conventional method. The new methodology was shown to be suitable for microcrystalline zeolites, though was not effective for crystalline MFI zeolite types.

The subsequent chapters of this thesis are dealing with zeolite detemplation using a Fenton protocol. The main objective is to determine the scope, advantages and limitations of the detemplation of zeolites using this methodology. Relevant properties of the materials were determined and compared to their calcined counterparts.

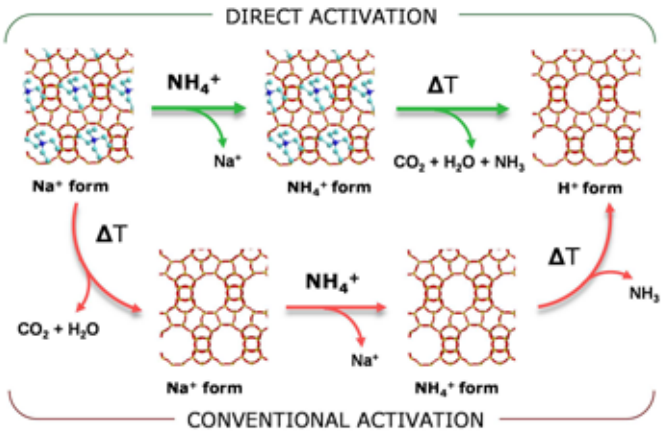

Figure S.1. Zeolite activation protocols; conventional (bottom) and proposed direct activation route for microcrystalline zeolites (top).

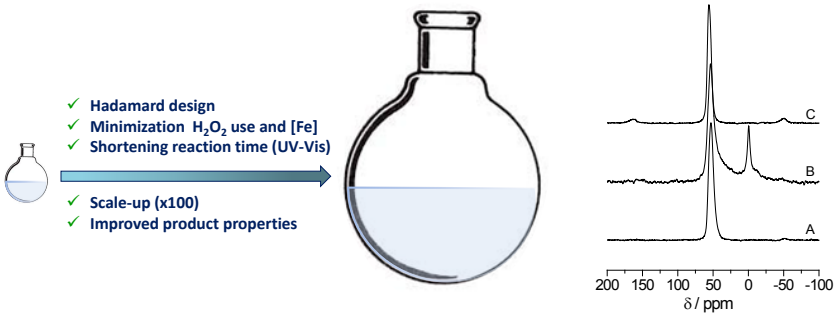

Figure S.2. Graphical abstract of the contents of Chapter 3 (left) and ^{27}Al MAS NMR spectra for the raw material (**A**), calcined (**B**) and scaled-up Fenton detemplated (**C,** right).

Microcrystalline Beta zeolite detemplation based on Fenton chemistry was studied in *Chapter 3*. The main objective was to minimise the use of hydrogen peroxide and the iron catalyst to make the concept industrially more attractive. In addition, optimised experiments were also performed on a somewhat larger scale (100 times) to gain insights in scale–up issues. Relevant material properties of the zeolites obtained using the optimised Fenton protocols for small and larger scale were shown to be essentially similar. The Fenton detemplated material showed similar Si/Al and XRD patterns when

compared to the calcined counterpart. However, textural characteristics differ considerably and full preservation of the tetrahedral Al species was observed for the Fenton detemplated samples (Figure S.2. right).

The suitability of Fenton detemplation as an environmental friendly detemplation method was studied for relevant microporous and mesoporous zeolites such as BEA, MFI, mesoporous MFI, MWW derivatives, and Sn-containing BEA (*Chapter 4*). The influence of the Si/Al ratio and crystallite size was studied for MFI and BEA zeolites (Si/Al = 25, 40 and 140 for MFI; Si/Al = 12.5 and 19 for BEA). Although a high Si/Al ratio seems to hinder the template removal, a high detemplation degree (> 90%) was achieved for BEA zeolites including a Sn-containing BEA (Sn-Beta). An overview of results is given in Figure S.3. In the case of carbon-templated mesoporous ZSM-5 (MesoMFI) and MWW derivatives (partially delaminated MCM-22), Fenton detemplation had to be combined with a mild thermal treatment (400 ^{0}C instead of 550 ^{0}C) to obtain quantitative template removal. Structural and textural properties show that the Fenton protocol allows template removal without damaging the structure and without affecting the amount of tetrahedrally coordinated Al sites. The results indicate that the Fenton detemplation protocol has potential to be used as an environmental friendly detemplation method for the industrial manufacture of zeolites.

Chapter 5 is centred on the detemplation/activation of microcrystalline commercial NH_4-Beta zeolite (Si/Al=13.5) and the subsequent use these materials for the catalytic cracking of low-density polyethylene (LDPE). The as-received material was detemplated using a standard Fenton detemplation protocol and subsequently activated by a mild thermal treatment at 350°C (BT-*fA1*) to prepare the H-form of the zeolite. Analysis shows that particularly the Brønsted acidity (Figure S.4. left), and the total pore volume for BT-*fA1* are considerably higher than for its calcined counterpart. This proved to be beneficial for the catalytic cracking of LDPE (Figure S.4. right). The results were compared to other zeolites (H-USY, H-ZSM-5) and its calcined counterpart (BT-C1) and it was shown that BT-fA1 gives the best catalytic performance.

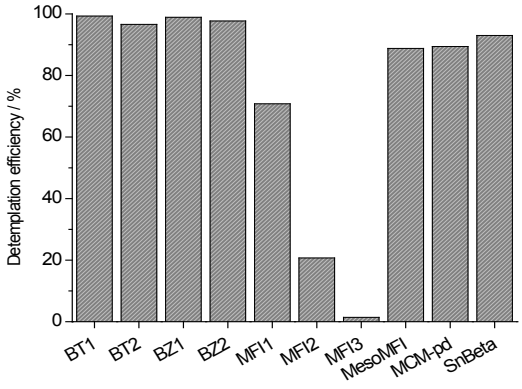

Figure S.3. Summary of the detemplation efficiency for the studied zeolites.

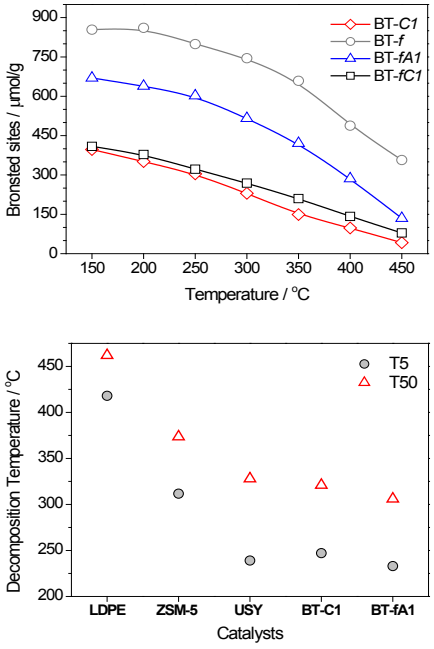

Figure S.4. Concentration of Brønsted acid sites in the samples versus the temperature from pyridine desorption studies (left) and decomposition temperature for 5 and 50 *wt.*% LDPE, (T5 and T5, respectively, right).

Catalyst regeneration studies after LDPE cracking by oxidation using air at elevated temperatures show that the performance decreases with the number of catalytic cycles and that the performance becomes equal to the values observed for the calcined counterpart. As such, the favourable textural properties of the Fenton detemplated samples are lost upon recycling. These findings indicate that the Fenton detemplated catalysts are likely more suitable for catalytic reactions at milder conditions, such as low temperature liquid phase reactions.

SAMENVATTING

Zeolieten worden op grote schaal toegepast, in het bijzonder als katalysatoren voor de chemische industrie. Het succes van zeolieten is vooral te danken aan hun gunstige eigenschappen zoals hoge stabiliteit (thermisch, hydro-thermisch en mechanisch) en goede activiteit en selectiviteit profielen voor een groot aantal chemische omzettingen. Zeolieten zijn ook recentelijk geïntroduceerd in nieuwe onderzoek gebieden zoals de katalytische conversie van biomassa, afval verwerking technologie, energiebesparende apparaten en sensoren. De voornaamste uitdagingen in de zeoliet synthese zijn het bepalen en afstemmen van de materiaal en katalytische eigenschappen voor een geselecteerde toepassing. Dit kan door een goede keuze van de uitgangsmaterialen maar ook door aanpassingen aan de synthese en nabehandeling stappen. Een overzicht van het gebruik van zeolieten, de syntheseroutes naar zeolieten en nabehandeling stappen worden besproken in *Hoofdstuk 1*.

In *Hoofdstuk 2* wordt een nieuwe procedure beschreven om een zeoliet na synthese te activeren. Normaal gesproken worden hiervoor twee calcinatie stappen gebruikt. In de eerste stap wordt de organische mal ("template") verwijderd, de tweede wordt gebruikt om de zeoliet in de zure vorm om te zetten. We hebben een directe activatie route onderzocht (Figuur S.1). Hierbij wordt eerst, via ionenwisseling, Na^+ vervangen voor NH_4^+ en daarna wordt de organische mal verwijderd door middel van een calcinatie stap waarbij ook Br**ønsted zu**re groepen worden ge**ïntroduceerd**. Met deze nieuwe procedure kan een calcinatie stap worden vermeden. De structuur, textuur en zure eigenschappen van de materialen gemaakt volgens de nieuwe procedure zijn bepaald en het bleek dat ze vergelijkbaar zijn met die van de materialen gemaakt volgens de conventionele methode. De nieuwe methodologie is geschikt voor micro kristallijne zeolieten, maar bleek niet effectief te zijn voor kristallijne MFI type zeolieten.

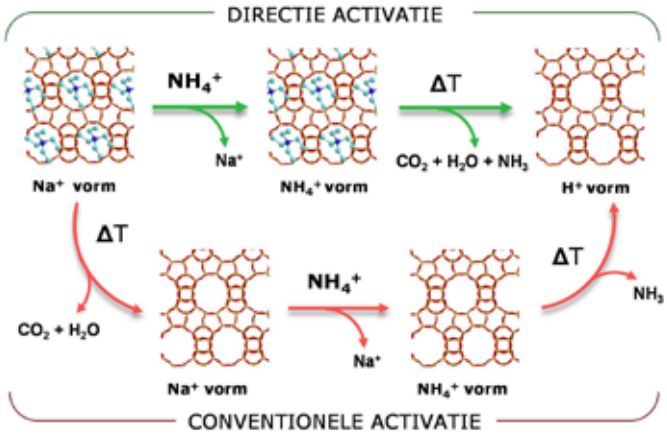

Figuur S.1. Zeoliet activatie: conventionele (beneden) en verbeterde activatie route (boven)

De volgende hoofdstukken van deze dissertatie beschrijven het verwijderen van de organische mal in zeolieten door middel van een zogenaamd Fenton protocol. Dit is een alternatief voor een calcinatie stap. De voornaamste doelen waren het bepalen van het toepassingsbereik en het identificeren van voor- en nadelen van deze Fenton methode. Voor een aantal zeolieten zijn de relevante eigenschappen na het verwijderen van de organische mal bepaald en vergeleken met die van de gecalcineerde tegenhangers.

Het gebruik van Fenton technologie om de organische mal te verwijderen uit micro kristallijne Beta zeolieten is beschreven in *Hoofdstuk 3* (Figuur S.2). Het voornaamste doel was om het gebruik van waterstof peroxide en de ijzer katalysator te minimaliseren zodat het concept aantrekkelijker wordt voor industriële toepassing. Daarnaast zijn er experimenten uitgevoe rd op grotere schaal (100 maal t.o.v. de eerste inleidende experimenten) om inzichten te krijgen in opschaal problemen. Relevante materiaal eigenschappen van de zeolieten gemaakt op kleine en grotere schaal zijn bepaald en er waren geen noemenswaardige verschillen te zien. Daarnaast zijn ook de eigenschappen van de gemaakte zeolieten vergeleken met de gecalcineerde versies. De Si/Al ratio en de XRD patronen vertoonden geen verschillen. Echter vooral de coördinatie van de Al atomen in

de zeolieten verschilde aanzienlijk. Voor materialen gemaakt met Fenton technologie was de hoeveelheid tetraedrisch aluminium vergelijkbaar met die van de zeoliet voor het verwijderen van de mal, terwijl een duidelijke afname werd waargenomen voor de gecalcineerde versie (Figuur S.2. rechts).

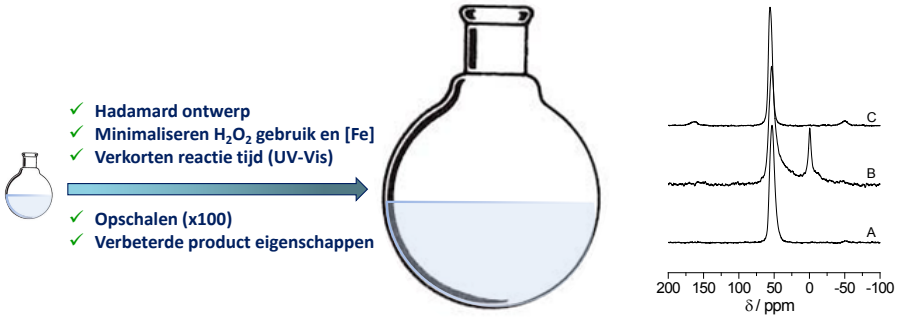

Figuur S.2. Grafische weergave van Hoofdstuk 3 (links) en Al MAS NMR spectra van de zeoliet als ontvangen (A), gecalcineerd (B) en na verwijdering van de mal met het opgeschaalde Fenton protocol (C, rechts)

Het gebruik van de Fenton methode voor het verwijderen van de mal voor relevante micro- en meso poreuze zeolieten zoals BEA, MFI, meso poreus MFI, MWW afgeleiden en een Sn bevattende BEA wordt beschreven in *Hoofdstuk 4*. Een overzicht van de resultaten is gegeven in Figuur S.3. De invloed van de Si/Al ratio en kristal grootte is onderzocht voor de MFI en BEA zeolieten (Si/Al = 25, 40 en 140 voor MFI; Si/Al = 12.5 en 19 voor BEA). Het bleek dat 90% van de organische mal verwijderd kan worden met de Fenton methode. In het geval van meso poreus ZSM-5 (MesoMFI) en MWW afgeleiden (gedeeltelijke gedelamineerde MCM-22) moet het Fenton protocol gecombineerd worden met een milde thermische behandeling (400 in plaats van 550°C) om de mal volledig te verwijderen. Analyses laten zien dat het mogelijk is om de mal te verwijderen zonder de zeoliet structuur te beschadigen en de hoeveelheid tetraedrische gecoördineerde Al te beïnvloeden. De resultaten laten zien dat de Fenton methode breed toepasbaar is en voordelen heeft ten opzichte van de calcinatie methode.

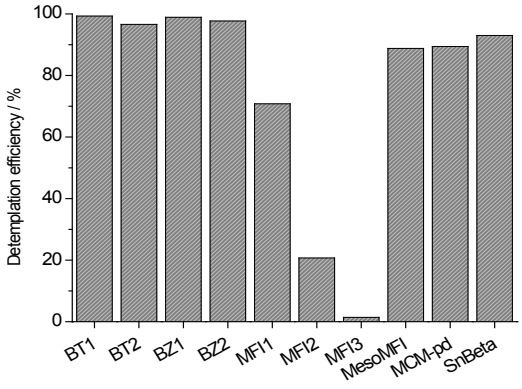

Figuur S.3. Resultaten voor template verwijdering met het Fenton protocol

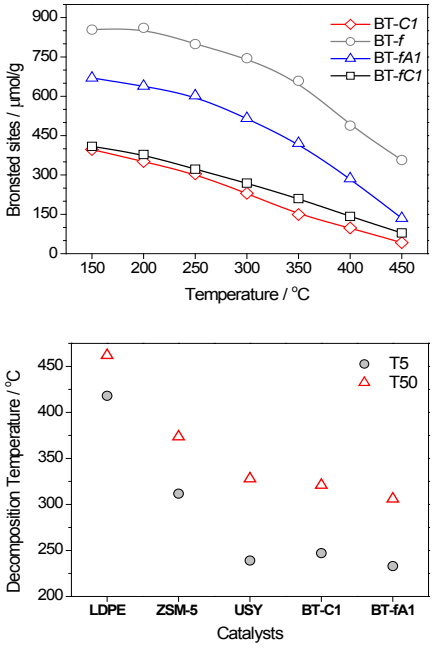

Figuur S.4. Concentratie van Brønsted zure sites versus de temperatuur voor verschillende materialen links) en de ontleding temperatuur voor 5 en 50 *wt.*% LDPE omzetting (T5 en T50, respectievelijk, rechts)

In *Hoofdstuk 5* wordt onderzoek beschreven naar het verwijderen van de organische mal en het activeren van een micro kristallijne NH_4-Beta zeoliet. De katalytische eigenschappen van de verkregen materialen zijn bepaald met een model reactie en wel het katalytische kraken van polyethyleen (LDPE). De organische mal werd verwijderd met een standaard Fenton protocol, gevolgd door een milde thermische behandeling bij 350 °C (BT-*fA1*) om de H-vorm van de zeoliet te verkrijgen. Analyse laat zien dat vooral de Brønsted zuurgraad (Figuur S.4. links), en de totale porie volume hoger zijn dan voor de gecalcineerde versie. Dit bleek zeer gunstig te zijn voor de katalytische eigenschappen (Figuur S.4. rechts). De resultaten werden vergeleken met andere zeolieten (H-USY, H-ZSM-5) en de gecalcineerde tegenhanger (BT-*C1*). Een Fenton behandeling gevolgd door een milde thermische activering (zeoliet BT-*fA1)* geeft een materiaal met de beste katalytische eigenschappen.

Katalysator regeneratie studies door middel van oxidatie met lucht bij verhoogde temperatuur laten zien dat de katalytische activiteit afneemt na een aantal katalytische cycli en vergelijkbaar wordt met die van de gecalcineerde tegenhanger. Het lijkt er dus op dat tijdens het recyclen de gunstige textuur eigenschappen verloren gaan van de materialen waar de mal met Fenton technologie is verwijderd. Uit deze resultaten blijkt dat Fenton behandelde katalysatoren waarschijnlijk betere kandidaten zijn voor katalytische reacties bij mildere condities zoals lage temperatuur vloeistof fase reacties.

RESUMEN

Las zeolitas poseen un amplio campo de aplicación, incluyendo su uso como catalizadores. En la actualidad, las zeolitas constituyen una gran parte de los catalizadores sólidos usados en la industria. Su satisfactoria introducción en el campo de la catálisis fue debido a cualidades como: alta estabilidad (térmica, hidrotérmica y mecánica), capacidad para intercambiar iones, selectividad de forma, alta actividad catalítica (presencia de sitios activos) y potencial para actuar como soporte (host) de catalizadores avanzados. Recientemente, las zeolitas también se han introducido en áreas de interés emergente como la conversión catalítica de biomasa, reducción de la contaminación, dispositivos para el ahorro de energía y sensores. De ahí que uno de los retos sea el ajuste preciso de estos materiales a una aplicación específica mediante síntesis directa o por combinación con tratamientos post-sintéticos. En el *Capítulo 1* se hace un resumen general del uso, síntesis y tratamientos post-sintéticos de las zeolitas.

En el *Capítulo* 2 se presenta un nuevo protocolo para la activación de zeolitas tras su síntesis. De manera convencional, ésta tiene lugar a través de dos calcinaciones: una para eliminar el template (molde orgánico) y otra para liberar los sitios ácidos. En este trabajo se propone una ruta para la activación directa, consistente en el intercambio sódico-amónico de los sólidos tal cual se obtienen de la síntesis, sin previa eliminación del template. Un sólo paso de calcinación posterior sirve para quemar el template orgánico, a la vez que crear los sitios Brønsted ácidos, evitando una calcinación. Las propiedades estructurales, texturales y ácidas de los materiales obtenidos mediante esta nueva ruta son, en general, bastante comparables a los obtenidos por el método convencional. Esta nueva ruta (activación directa) se adapta a zeolitas microcristalinas, aunque no resulta efectivo para el tipo MFI.

Los capítulos siguientes afrontan la aplicabilidad de la química Fenton para descomponer el template orgánico de los materiales zeolíticos. El principal objetivo es determinar el alcance, ventajas y limitaciones de la eliminación del template (*detemplationn*) usando este método. Se han determinado

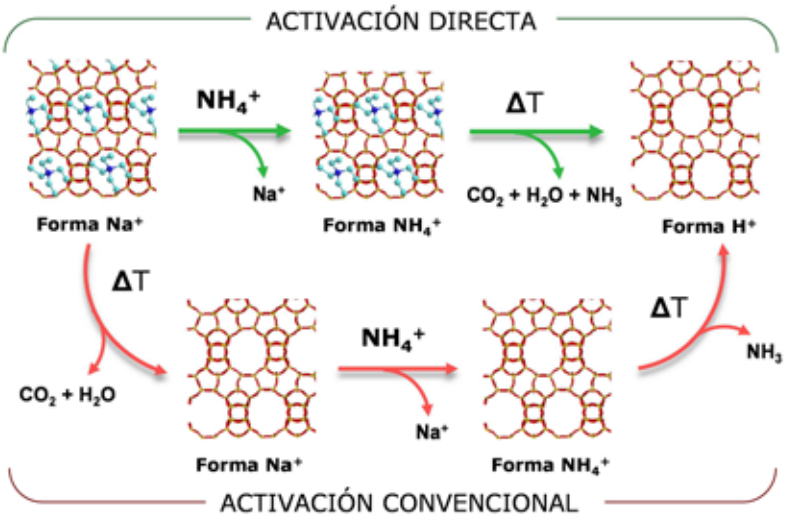

Figura S.1. Rutas para la activación de zeolitas: convencional (abajo) y método directo propuesto (arriba) para zeolitas microcristalinas.

y evaluado propiedades relevantes de los materiales tomando como referencia a sus homólogos calcinados.

La eliminación del template en la zeolita Beta microcristalina usando Fenton se describe en el *Capítulo 3*. El objetivo principal ha sido minimizar al máximo el uso de peróxido de hidrógeno (H_2O_2) y del catalizador de hierro para hacerlo más atractivo industrialmente. De manera complementaria, los experimentos optimizados se llevaron a cabo aumentanto la escala (hasta 100 veces) con la finalidad de profundizar en la comprensión de posibles problemas de escalado. En cuanto a las propiedades del material final, utilizando el protocolo optimizado para pequeña y gran escala, son esencialmente iguales. Por otra parte, el material Fenton escalado muestra una relación Si/Al y espectros de Rayos X comparables a su hom**ólogo calcinado,** mientras difiere considerablemente en las propiedades texturales y la preservación total de las especias de Al tetraédricamente coordinado (Figura S.2. derecha).

Se ha estudiado la idoniedad del método Fenton para descomponer el template orgánico como un método respetuoso con el medio ambiente para zeolitas microporosas y mesoporosas relevantes como BEA, MFI,

Figura S.2. Extracto gráfico del *Capítulo 3* (izquierda) y espectros ^{27}Al MAS NMR del material inicial (**A**), calcinado (**B**) y escalado Fenton (**C,** derecha).

MFI mesoporoso, derivados de MWW, y BEA sustituida con Sn (*Capítulo 4*). La influencia de la relación Si/Al y el tamaño de los cristales se ha estudiado para zeolitas de tipo MFI y BEA (Si/Al = 25, 40 y 140 para MFI; Si/Al = 12.5 y 19 para BEA). Si bien el alto valor de la relación Si/Al ratio parece dificultar la eliminación del template; se consiguió un alto grado de eliminación del template para las zeolitas de tipo BEA (> 90%) incluyendo la sustituida con Sn (Sn-Beta). En la Figura S.3. se presenta un resumen general de los resultados. En el caso de la zeolita ZSM-5 mesoporosa sintetizada usando carbón (MesoMFI) y los derivados del tipo MWW (MCM-22 parcialmente delaminada), el protocolo Fenton se ha tenido que combinar con un tratamienton térmico suave (400 ^{0}C en lugar de 550 ^{0}C) para obtener una eliminación cuantitativa del template. Las propiedades estructurales y texturales muestran que el protocolo Fenton ha permitido eliminar el template sin dañar la structura de las zeolitas y sin afectar a la cantidad de Al tetraédricamente coordinado. Los resultados indican que el protocolo Fenton para eliminar el template tiene un gran potencial como método respetuoso con el medio ambiente para la fabricación industrial de zeolitas.

El *Capítulo 5* se centra en la eliminación del template/activación de la zeolita comercial microcristalina NH_4-Beta (Si/Al=13.5) y el posterior uso de estos materiales para el cracking catalítico de polietileno de baja densidad (LDPE). El material, tal cual fue recibido, fue detemplado usando el

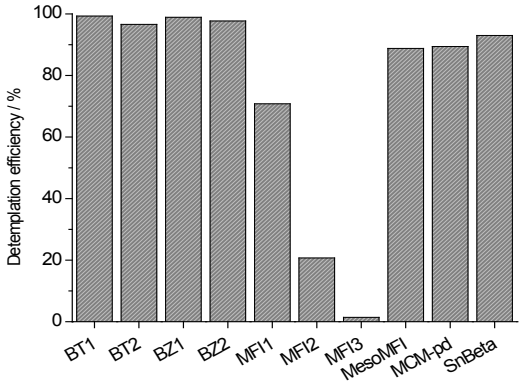

Figura S.3. Resumen de la eficiencia de la eliminación del template para las zeolitas estudiadas.

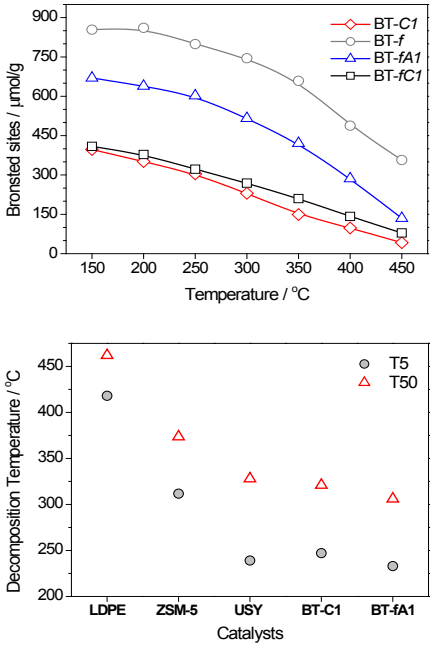

Figura S.4. Concentración de sitios ácidos tipo Brønsted en las muestras versus temperatura en estudios de desorción de piridina (izquierda) y temperatura de descomposición del 5 (T5) y 50% (T50) en peso de LDPE (derecha).

protocolo lo estándar Fenton, seguido de una activación mediante un tratamiento térmico suave a 350°C (BT-*fA1)* para preparar la forma ácida de la zeolita. Los análisis muestran que particularmente la acidez Brønsted (Figura S.4. izquierda) y el volumen total de poros son considerablemente más altas que para su homólogo calcinado, lo que apunta ser beneficioso para en el cracking catalítico de LDPE (Figura S.4. derecha). Los resultados catalíticos se han comparado con otras zeolitas (H-USY, H-ZSM-5) **y su homólogo calcinado** (BT-C1) demostrando que BT-fA1 obtiene el mejor rendimiento catalítico.

Los estudios realizados sobre la regeneración de los catalizadores tras su uso en el cracking de LDPE mediante la oxidación en aire a altas temperaturas muestran un descenso del rendimiento de los catalizadores con el número de ciclos y que tiende a ser similar a los valores observados por el análogo calcinado. Esto puede ser debido a una pérdida de las propiedades texturales favorables de BT-*fA*1 a lo largo de los ciclos de reciclado que sufre el catalizador. Estos hallazgos apuntan a que el campo de aplicación de los catalizadores detemplados usando el método Fenton se ajustan más a reacciones catalíticas que operen en condiciones moderadas, como reacciones en fase líquida a bajas temperaturas.

ACKNOWLEDGEMENTS

It is the time for the: *Hora Finita*! My PhD student period has come to an end and the time to write these acknowledgements comes with it! How to start? Let´s try from the beginning...

When I took the decision of starting a PhD, I was so naïve about it! However, today I can say that it has been the most rewarding experience of my life in all senses. Not even with all the words in the world can I possibly express my gratitude to every single person that I have met in those years, thanks for your support, advices and smiles every single day; without you I would not have been able to overcome it. So, if your name is not directly written here, please don´t feel offended, I keep you in my heart.

First I would like to thank my promotor, prof. Dr. ir, H.J. Heeres for giving me the opportunity of making this amazing journey and for taking over my thesis to bring it to a happy end. Also for being there every time I asked you for help. And, at the same time, to the generous and priceless help of my co-promotor Dr. P.P. Pescarmona, you arrived at the right moment at the right place and gave me back my self-confidence, thanks for your huge effort and time. Prof. Dr. Scherpen, you gave me the strength when I felt lost, thanks.

I also would like to thank Dr. Melián-Cabrera for providing me the opportunity to start my journey in Groningen, enrolling me into his Fenton´s project, thanks!

Special thanks for my reading committee: prof. Dr. F. Picchioni, prof. Dr. D. Murzin, prof. Dr. K. Seshan for reading and evaluating my thesis. Thanks for your valuable comments.

Prof. Dr. F. Picchioni, Francesco grazie mile for being right in the office next door, and supporting me in the hard moments. Sometimes silence says more than words. I should also thank Ton, a.k.a Prof. Dr. A. A. Broekhuis, I have to admit that I was very intimidated the first time I met you in your office! I am really glad for your wise advice and support. Prof. Dr. Beatriz Noheda, your advice and positive energy were priceless.

The financial support of STW, and the valuable suggestions and critical remarks of the user committee were fundamental for the development and improvement of this piece of work. Thanks to all the committee members, Dr.M.S. Rigutto, Dr. H. Foekema, Prof. Dr. J. G. de Vries, Prof. Dr. J. A. Moulijn, Dr. A.A. Winkler for your tireless discussions. And Cora Heesakkers, thanks for your friendliness. The trips to those meetings were unforgettable, I really appreciated them.

Any of the chapters of this thesis would not have been possible without the support and suggestions of a great group of experts in catalyst characterization, although all the material is not included in this thesis. Starting from one of the very first people I met in Groningen, Ing. Jacob Bass, who became also a friend, thanks for your availability 24/7 and patience. In our department, my most truthful gratitude goes to Ing. Jan Henk Marsman and Ing. Leon Rohrbach, you always tried to find a solution to my problems. Ing. Hans van der Velde thanks for your always fruitful and straight forward discussions and trust; Dr. Evgeny Polushkin; Dr. Gert H. ten Brink (for "mastering" me in image processing); Johan Kuipers, thanks for caring about my liquid argon tank! A large part of the conclusions in this thesis would not have been be possible without external collaborations. Dr. Ernst van Eck thanks for hosting me in Nijmegen and allowing me to learn and use your NMR machines, it was a great pleasure and responsibility at the same time, I really enjoyed it. Thanks also to Dr. Kristina Djanashvili (TU Delft) for the NMR measurements and discussions until the very last moment; Dr. Javier Agúndez (CSIC, Madrid) for the Hg-porosimetry; Dr. Karolina Sadowska (Krakow, Poland) for the py-IR measurements; Ruud Hendrikx (TU Delft) for XRF characterization; and Haldor Topsoe, for the samples, meetings and rewarding discussions.

My *hartelijk bedankt* goes to the technical team: Anne Appeldoorn, Marcel de Vries, and Ing. Erwin Wilbers, for your endless patience and because you never lost hope that I would learn Dutch. The little I know it is all thanks to you. Thanks Marya for caring about me, and to all of you for the organization of the labuitjes! That´s something I miss already.

I really appreciated the long discussions about chemistry "and much more" inside and outside our department, particularly at the *borrels*. Since the moment I heard this word, I knew it was going to be useful :). Thanks to the Bernouilli boards for sharing the lounge where we celebrated so many happy and sad moments. It is people who makes a place meaningful, thanks to: Dr. Diego (official translator from Dutch to any language in the world, thanks for proof reading my thesis and being my paranymph, you are simply great!), Dr. Teddy (thanks for your clear and straight forward advices), Dr. Zheng (not enough words for you my dear, you are the best partner I could ever imagine, and thanks for checking this thesis), Dr. Patrizio (my "husband", paranymph, and a great friend), Dr. Lidia (por los momentos compartidos), Dr. Valeriya (what a russian! and what a trip! I have no words neither), Laurens (my youngest officemate, ruining your naïve concept about science was priceless :P), Dr. Arjan (for being the biggest in all senses! ;)), Henk (for the long conversations about modeling and life), Dr. Jan Willem (please never change!), Dr. Gacia (our first postdoc, you were a great mentor ;)), Dr. Shilpa (thanks for the corrections!), Dr. Rajeesh, prof. Dr. María González and prof. Dr. Emi (thanks for sharing your experiences), prof. Dr. Bilal (always with the right answer), MSc. Tom and Akinobu (thanks for all you taught me!), Dr. CB, Dr. Agnes, Dr. Jenny, Ria, Dr. Louis, Angela, Dr. Ilmi, Dr. Iqbal, Dr. Fachri, Dr. Andrew Phua, Dr. Anna Piskun, MSc. Martijn Beljaars, hermanos Araya, Dr. Claudio y Alexandra (congratulations!), MSc. Graham (always with an interesting conversation in his pocket), MSc. Eric, MSc. Karen, MSc. Lucas, MSc. Anton, MSc. Albert, MSc. Hesam, ... and because mixing is always good, I wasn´t able to separate all you by groups, you are all singular and special to me. Some for the warm welcome to Groningen, others for the visits to the "*amigo*," wadlopen, labuitjes, dances, concerts, parties, etc. You all have one thing in common; you gave me a smile, a cheering word, or even a beer! right when I needed it, I am really glad for having the opportunity of meeting you, you were my catalysts: Dr. Tatiana (thanks for being my compass), Dr. Nùria (laatste rondje?), Dr. Santi and Dr. Stefanie (you are unique), Dr. Fátima Pérez, Dr. Sanju, Dr. Johanne (sincere, transparent,

... move your hair! just you), Dr. Julio, Dr. Luca (keep smiling my friend!), (soon) Dr. Begoña (running from anywhere to join a party, and for the lunches until mid-night), Dr. Andrea Scaramucci, Dr. Giulio, Dr. Tano, Dr. Jesús, (tocayo, for the parties shared and to share!), Dr. Filippo and Dr. Dorota, Dr. Cati, Dr. Ralph (my friend from Valladolid, you can´t imagine how much you help me), Dr. Wouter, Dr. Lumi, Dr. Manolo (always trustful), Dr. Alena, Dr. Johan, Dr. Jort, Dr. Sèb (always ready for drinking and eating, just I do!), Dr. Claudia (keep being so sweet), Dr. Valentín and MSc. Puri (finally back!), MSc. Manuela (be optimistic!), Dr. María José, Julio and the loveliest kids in the world, Dr. Sara and MSc. Lucas (congratulations!), Dr. Andreia and Ing. Tiago, Dr. Julia Intemann, Dr. Javier Muñariz, Dr. Jasper, MSc. Silvia Vila, MSc. Lele, Dr. (soon) Raquel (always busy :P), Dr. Thony, Dr. Mathieu, Dr. Ana Rioz, Eli, Dr. Matt, MSc. Marta, Dr. Carlos, MSc. Eduard, Ing. Alex, Dr. Giovanni, MSc. Pablo Ortiz, MSc. Pablo and Sara, Dr. Alberto Rodríguez, MSc. Sergio, MSc. Giulia, Dr. Matea and Chris, Illeana, Dr. Mauricio, Dr. Juan, Dr. Lara, MSc. Mu-Chieh, MSc. Leticia, MSc. Peter, MSc. Ani, Dr. Andrea and MSc. Lucia, Dr. Alicja, Dr. Justina, Dr. Lorenza and Dr. Marta (my body--combat mates), MSc. Alicia Muñoz and Ing. Ryota.

Special thanks for the patience of my officemates: Dr. Zheng (for the mandarins), Dr. Teddy, Dr. Sjoerd, Dr.(soon) Cynthia, prof. Dr. Emi, Ing. Inouk, Dr. Jos and MSc. Laurens. Would you ever imagine I could talk so much?

My flatmates, you were like a family during my period in Groningen, I miss you very much: Dr. Johanne, Dr. María José and Dr. Héctor! I could not be luckier! :)

However, everything would not have been possible without the hold (and boost!) of the wonderful group of people I met at the IER of Albacete: Dr. Rocio, Dr. Joost, Dr. Carlos, Dr. Toño, Dr. Jesús, Ing. Antonio and Ing. Jorge, thank you very much guys!

And coming a bit earlier in time, my university mates, thanks for all the priceless time I shared with you and for the times to share! Dr. Amparo, Dr. Antonio, Dr. Yoana, MSc. Mª Cruz, Dr. Tito, MSc. Helena, Ing. Diana and MSc. Alex (you are the perfect cousin-friend mixture, thanks!).

Family, it is a little word compared to its meaning. I will need more than a book to express all that you gave me and how much I need you. Por cada llamada, noche sin dormir, y los momentos que me he perdido, pero también por las alegrías (que han sido muchas!), lo siento y gracias por seguir ahí, especialmente a vosotros: mama, por las largas conversaciones que siempre se me hacían cortas; papa, por apoyarme en todo y confiar en mí más que yo misma, Juan porque me encanta molestarte, Ing. Óscar J. por tu cordialidad y sencillez, abuelas (Teresa y Delfina), abuelos (Juan V. y Jesús), tíos, tías y primos aunque algunos no me acompañéis físicamente, sé que siempre estáis ahí, cuidando de mí. Likewise my family in-law, thanks for your understanding, encouraging words and support all this time: Charo, Juan and Ana.

Juan, you know this thesis would not have been possible without your endless and untiring support during my time in Groningen and also during the last two years. There is not a map strong enough to split us. Thanks for believing in me and giving me the self-confidence I lost sometimes: *grazie*.

PS: probably you are asking yourselves, why to put Dr., MSc., etc.? Does it make any difference? Probably not, but this is still a scientific publication, and you are my references!

LIST OF PUBLICATIONS

1. **Fenton chemistry-based detemplation of an industrially relevant microcrystalline beta zeolite. Optimisation and scaling-up studies**, M.J. Ortiz-Iniesta, I.V. Melián-Cabrera, Microporous and Mesoporous Materials, 206 (2013) 58-66. DOI: 10.1016/j.micromeso.2014.12.019
2. **Hot-spots during the calcination of MCM-41: A SAXS comparative analysis of a soft mesophase,** L. López Perez, M.J. Ortiz-Iniesta, H.J. Heeres, and I.V. Melián-Cabrera, Materials Letters, 118 (2014) 51-54. DOI: 10.1016/j.matlet.2013.11.091
3. **Direct activation of microcrystalline zeolites**, M.J. Ortiz-Iniesta, H.J. Heeres, I.V. Melián-Cabrera, Microporous and Mesoporous Materials, 171 (2013) 208-214. DOI: 10.1016/j.micromeso.2013.01.006
4. **Detemplation of soft mesoporous silica nanoparticles with structural preservation,** L. López Pérez, M.J. Ortiz Iniesta, Z. Zhang, I. Agirrezabal-Telleria, M. Santes, H. Jan Heeres, Ignacio Melián-Cabrera, Journal of Materials Chemistry A, 1 (2013) 4747. DOI: 10.1039/c3ta01240a

CONFERENCE PROCEEDINGS

1. **Post-synthesis treatments and their effects on MCM-22 derivatives. Properties evaluation and application to the catalytic cracking of low-density polyethylene,** María Jesús Ortiz-Iniesta, Akinobu Yamamoto, Norikazu Nishiyama, Ignacio Melián-Cabrera. Oral contribution. XIII International Materials Research Congress (2014).
2. **Fenton detemplation of zeolites and zeotypes, and their relevant properties evaluation,** M.J. Ortiz-Iniesta, H.J. Heeres, and I. Melián-Cabrera. Oral contribution. British Zeolite Association (BZA), 2014, University of Glasgow, Glasgow (UK).
3. **Structure-performance relations of nano beta zeolites in the catalytic cracking of LDPE**, M.J. Ortiz-Iniesta, E.R.H van Eck, A.P.M. Ketgens, H.J. Heeres, and I. Melián-Cabrera. Poster contribution. XVth The Netherlands' Catalysis and Chemistry Conference (NCCC), 2014, Noordwijkerhout, The Netherlands.
4. **Catalysis at the terrace - Enhancing the external surface of zeolite nano-particles through mild postsynthesis tools and its impact on the catalytic pyrolysis,** M.J. Ortiz-Iniesta, E.R.H van Eck, A.P.M. Ketgens, K. Sadowska, J. Datka, H.J.Heeres, and I. Melián-Cabrera. Oral contribution. XIIIth The Netherlands' Catalysis and Chemistry Conference (NCCC), 2012, Noordwijkerhout, The Netherlands.
5. **NH_4-exchange of zeolites before template removal. A simplified activation protocol with acidity preservation,** M.J. Ortiz-Iniesta, H.J. Heeres, I. Melián-Cabrera. Poster contribution. 5th International FEZA Conference, Valencia, Spain, July 2011.
6. **Application of experimental design to optimisation of the synthesis of PMMA microspheres,** M.J. Ortiz-Iniesta, J. Peña Martínez. Poster contribution. XIII Scientific symposium "Antonio González". University of La Laguna, Spain, October 2009.